2019-04-24

The Convergence of VEGF-Neuropilin and YAP/TAZ Signaling Promotes Stem-Like Traits and DNA Repair in Breast Cancer

Ameer L. Elaimy
University of Massachusetts Medical School

THE CONVERGENCE OF VEGF-NEUROPILIN AND YAP/TAZ SIGNALING PROMOTES STEM-LIKE TRAITS AND DNA REPAIR IN BREAST CANCER

A Dissertation Presented

By

Ameer L. Elaimy

Submitted to the Faculty of the

University of Massachusetts Graduate School of Biomedical Sciences, Worcester

in partial fulfillment of the requirements for the degree of

DOCTOR OF PHILOSOPHY

April, 24th, 2019

(MD/PhD, Cancer Biology)

THE CONVERGENCE OF VEGF-NEUROPILIN AND YAP/TAZ SIGNALING PROMOTES STEM-LIKE TRAITS AND DNA REPAIR IN BREAST CANCER

A Dissertation Presented

By

Ameer L. Elaimy

This work was undertaken in the Graduate School of Biomedical Sciences

(MD/PhD, Cancer Biology)

Under the mentorship of

Arthur M. Mercurio, PhD, Thesis Advisor

Thomas J. Fitzgerald, MD, Member of Committee

Junhao Mao, PhD, Member of Committee

Dohoon Kim, PhD, Member of Committee

Xaralobos Varelas, PhD, External Member of Committee

Dannel Mccollum, PhD, Chair of Committee

Mary Ellen Lane, PhD,

Dean of the Graduate School of Biomedical Sciences

April, 24th, 2019

ACKNOWLEDGMENTS

I would like to express my sincere gratitude to my thesis advisor, Arthur Mercurio, who is both an outstanding scientist and mentor. I attribute my successes during my PhD to the combination of his immense knowledge and experience with his continued support, motivation and patience. I will always be in awe of his tremendous dedication to mentorship, which sets an example of what I hope to become in the future. I am truly grateful not only for his commitment to my development as a physician/scientist, but for his friendship as well.

I am extremely appreciative of the rigorous feedback I always received from Hira Goel. I thank all other members of the Mercurio lab, Caitlin, Melanie, John, Sanjoy and Mandy for their contributions throughout my PhD.

I am thankful to my TRAC for their feedback, availability and support. I am grateful to Dan McCollum for serving as my TRAC chair and for numerous helpful discussions about my PhD work. TJ FitzGerald was instrumental in helping me appreciate the clinical significance of my work and for preparing me for a future career as an oncologist/scientist. Junhao Mao and Dohoon also always provided excellent feedback about my work.

I would also like to thank Dr. Xaralabos Varelas for taking the time to serve as my external examiner and for reviewing my dissertation.

I am forever grateful to my family for their sacrifices and support which have allowed me to pursue a career as a physician/scientist.

ABSTRACT

The role of vascular endothelial growth factor (VEGF) signaling in cancer is well-known in the context of angiogenesis but is also important in the functional regulation of tumor cells themselves. Notably, autocrine VEGF signaling mediated by its co-receptors called neuropilins (NRPs) appears be essential for sustaining the proliferation and survival of cancer stem cells (CSCs), which are implicated in mediating tumor growth, progression and drug resistance. Therefore, the first half of this thesis focuses on the mechanism of VEGF-NRP-mediated support of CSCs. Aberrant activity of the Hippo pathway effector YAP and TAZ are associated with breast CSCs and have been shown to confer stem cell-like properties. I found that VEGF-NRP2 signaling contributes to the activation of YAP/TAZ in various breast cancer cells, which mediates a positive feedback loop that promotes mammosphere formation. VEGF-NRP2 signaling activated the GTPase Rac1, which inhibited the Hippo kinase LATS, which enabled the activity of YAP/TAZ. In complex with the transcription factor TEAD, TAZ then bound and repressed the promoter of the gene encoding the Rac GTPase-activating protein (Rac GAP) β2-chimaerin. By activating GTP hydrolysis, Rac GAPs effectively turn off Rac signaling; hence, YAP/TAZ-mediated repression of β2-chimaerin sustained Rac1 activity in CSCs. Depletion of β2-chimaerin in non-CSCs increased Rac1 activity, YAP/TAZ activation and mammosphere formation. Analysis of breast cancer patients revealed an inverse correlation between β2-chimaerin and TAZ expression in tumors. These findings highlight an unexpected role for β2-chimaerin in a feedforward loop of YAP/TAZ activation and the acquisition of CSC properties.

Given that CSCs have been implicated in therapy resistance and are enriched in triple negative breast cancer (TNBC), which exhibits VEGF-NRP2 signaling, the second half of this thesis focuses on understanding the mechanism by which VEGF-NRP2 contributes to the chemoresistance of TNBC. I discovered that VEGF-NRP2 promote homologous recombination (HR) in *BRCA1* wild-type TNBC cells by contributing to the expression and function of Rad51, an essential enzyme in the HR pathway that mediates efficient DNA double strand break repair. Mechanistically, I found that VEGF-NRP2 stimulates YAP/TAZ-dependent Rad51 expression and that Rad51 is a direct YAP/TAZ-TEAD transcriptional target. I also discovered that VEGF-NRP2-YAP/TAZ signaling contributes to the resistance of TNBC cells to chemotherapy and that Rad51 rescues the defects in DNA repair upon inhibition of either VEGF-NRP2 or YAP/TAZ in response to cisplatin. These findings reveal novel roles for VEGF-NRP2 and YAP/TAZ in DNA repair and they indicate a unified mechanism involving VEGF-NRP2, YAP/TAZ and Rad51 that contributes to resistance to platinum chemotherapy.

In summary, this thesis provides novel insight into the roles of autocrine VEGF-NRP2 signaling in breast CSC function and therapy resistance and provides rationale in inhibiting NRP2 for platinum-resistant tumors that are dependent on YAP/TAZ activation.

TABLE OF CONTENTS

LIST OF TABLES

LIST OF FIGURES

LIST OF MULTIMEDIA OBJECTS OR FILES

Movie A1: 18-hour movie of control β4 reporter comma-d1 cells in response to a scratch wound using a green differential interference contrast (DIC) background. Scale bar represents 25 micrometers.

Movie A2: Movie 1 without a DIC background. Scale bar represents 25 micrometers.

Movie A3: An 18-hour movie of YAP-transformed β4 reporter comma-d1 cells in response to a scratch wound using a green DIC background. Scale bar represents 25 micrometers.

Movie A4: Movie 3 without a DIC background. Scale bar represents 25 micrometers.

Movie A5: 72-hour movie of YAP-transformed β4 reporter comma-d1 cells in response to a scratch wound using a green DIC background. Scale bar represents 25 micrometers.

Movie A6: Movie 5 without a DIC background. Scale bar represents 25 micrometers.

LIST OF COPYRIGHTED MATERIAL PRODUCED BY AUTHOR

Chapter II: VEGF-neuropilin-2 signaling promotes stem-like traits in breast cancer cells by TAZ-mediated repression of the Rac GAP β2-chimaerin.

This work was originally published in *Science Signaling*. Ameer L. Elaimy, Santosh Guru, Cheng Chang, John J. Amante, Lihua Julie Zhu, Hira Lal Goel and Arthur M. Mercurio. VEGF-neuropilin-2 signaling promotes stem-like traits in breast cancer cells by TAZ-mediated repression of the Rac GAP β2-chimaerin. *Science Signaling*. 2018 May 1;11(528). pii: eaao6897. doi: 10.1126/scisignal.aao6897. From *Science Signaling*. Reprinted with permission from AAAS.

Chapter IV, section one: Convergence of VEGF and YAP/TAZ signaling: Implications for angiogenesis and cancer biology.

This work was originally published in *Science Signaling*. Ameer L. Elaimy and Arthur M. Mercurio. Convergence of VEGF and YAP/TAZ signaling: Implications for angiogenesis and cancer biology. *Science Signaling*. 2018 Oct 16;11(552). pii: eaau1165. doi: 10.1126/scisignal.aau1165. Review. From *Science Signaling*. Reprinted with permission from AAAS

CHAPTER I: INTRODUCTION

Overview

This thesis focuses on the mechanisms by which autocrine signaling by vascular endothelial growth factor (VEGF) mediated by neuropilin-2 (NRP2), a VEGF receptor, promotes stem-like traits, DNA repair and therapy resistance in breast cancer cells. These issues are timely because VEGF is an attractive therapeutic target for breast cancer patients, but the available agents have demonstrated little clinical efficacy (1) and do not block the association between VEGF and NRPs (2). Therefore, identifying mechanisms downstream of VEGF-NRP2 that contribute to the aggressive behavior of breast cancer cells has potentially substantial implications.

Breast cancer subtypes

Despite research and clinical advancements in the management of patients with breast cancer, it continues to be the most common non-skin malignancy in women and one of the leading causes of cancer-related mortality in women throughout the world (3). Breast cancer arises from the abnormal proliferation of epithelial cells in the breast resulting in carcinoma. Histological and molecular classifications of breast cancer exist that aid in predicting patient prognosis and response to various treatment modalities. Histologically, breast cancer can be divided into ductal (arising from abnormal proliferation of cell in ducts) or lobular (arising from abnormal proliferation cells in

lobules) subtypes (4). Ductal and lobular carcinoma progresses from a benign lesion termed flat epithelial atypia, to a pre-cancerous lesion termed atypical hyperplasia, to carcinoma *in situ* that does not invade the basement membrane, and, finally, to invasive carcinoma which is malignant (4).

Although histological classifications of breast cancer have provided some clinical usefulness, determining the expression of markers for targeted therapy is critical in tailoring treatment strategies to the individual patient (5). Expression of the estrogen receptor (ER^+) and progesterone receptor (PR^+) generally indicates a better outlook because these tumors can be treated with anti-hormonal therapy such as tamoxifen or aromatase inhibitors such as anastrozole or letrozole (6). Expression of human epidermal growth factor receptor 2 (HER2) generally indicates a worse prognosis because these tumors are more aggressive in nature due to enhanced proliferative and metastatic capacity (6). However, the development of HER2 blocking agents such as trastuzumab has improved the outcomes of patients with HER2 positive tumors (7). Triple negative breast cancer (TNBC) lacks expression of the ER, PR and HER2. These patients have the worst prognosis because TNBC is aggressive, poorly differentiated and effective targeted therapies are lacking (8).

In addition to assessing ER, PR and HER2 status of patients, gene expression profiling has revealed substantial insight into breast cancer by establishing several distinct subtypes that integrate hormonal profiles with neoplasm molecular cell biology (9). Luminal types compromise most breast cancer cases and generally have the best prognosis. They consist of luminal type A (40-55% of cases) (ER gene signature positive/HER2

negative) and luminal type B (15-20% of cases) (reduced ER gene signature with increased HER2). The HER2 subtype (7-12% of cases) is ER negative and characterized by HER2 amplification/overexpression leading to a high proliferation rate. Basal tumors are negative for ER and PR and, accordingly, have a basal/myoepithelial gene signature (e.g. basal cytokeratin expression). Claudin-low tumors are also ER and PR negative but exhibit an epithelial to mesenchymal-like gene signature. Basal and claudin-low tumors together compromise TNBC, which accounts for 13-25% of cases. Given the poor prognosis of TNBC patients and the lack of appropriate therapies, understanding the processes that contribute to its aggressive nature is of paramount importance. This leads to a discussion of cancer stem cells (CSCs).

Cancer stem cells

Breast cancer is a diverse disease composed of various cell types that differ between individual patients, but also within the same tumor (intratumor heterogeneity) (10). These cell types exhibit distinct properties such as morphology, proliferation, degree of differentiation, cell-cell environment, metastatic potential and sensitivity to chemo- and radiation therapy (11, 12). These observations have led to the CSC hypothesis. CSCs are defined by their ability to self-renew, differentiate into multi-lineage cancer cell hierarchies and form a new tumor when transplanted *in vivo* (13). Indeed, CSCs were identified by their cell surface marker expression ($CD44^{+/high}CD24^{-/low}$) following the transplantation of human breast cancer cells into immunocompromised mice (14).

It is thought that CSCs arise following the transformation of tissue stem cells, which, in part, may explain their ability to divide slowly, self-renew, give rise to more differentiated cell types and resist genotoxic stress (10). These properties ultimately facilitate their long-term survival. However, it is important to note that there are some distinctions between mammary stem cells and breast CSCs. For example, mammary stem cells express the cell surface marker CD24 (15), but, as mentioned above, CD24 is absent in breast CSCs (14). This suggests more complex mechanisms may contribute to the acquisition of CSCs, which are still being elucidated. One such mechanism may be the epithelial to mesenchymal transition (EMT) (16), which has been shown to promote CSC properties. The seminal study reporting an association between the EMT and CSCs induced an EMT in human mammary epithelial cells with either TGF-β or specific transcription factors and observed that this changed the cells from $CD44^{-/low}CD24^{+/high}$ to $CD44^{+/high}CD24^{-/low}$ (17). It also promoted tumor initiating properties *in vivo*.

These observations warrant a discussion regarding the relationship between CSCs and different breast cancer subtypes. TNBC, which is poorly differentiated, resists standard therapy, has the worst prognosis of all breast cancer subtypes exhibits the highest CSC burden (8, 18). These properties may explain, in part, why patients with TNBC respond poorly to first-line treatments and exhibit a high rate of tumor recurrence (19). The next advance in improving the outlook for TNBC patients will result from a greater understanding of its unique biological properties that can be leveraged for targeted therapy intervention. One viable option is disrupting DNA repair pathways, which next leads to a

discussion about the relationship between TNBC and homologous recombination (HR) repair.

Triple negative breast cancer and homologous recombination

Genomic integrity can be compromised by DNA damage from exogenous (e.g. radiation, chemicals) and endogenous (e.g. replications errors, reactive oxygen species) sources, which results in instability (20). DNA repair pathways provide a tightly controlled mechanism that maintains genomic integrity and resists the accumulation of deleterious mutations that may lead to cancer development. Of these DNA lesions, double-strand breaks (DSBs) have the potential to be the most harmful (21). The cell has evolved two predominant repair mechanisms that elicit highly specialized responses to DSBs: non-homologous end joining (NHEJ) and homologous recombination (HR). NHEJ can occur at any phase of the cell cycle but is predominant during G1 because it does not utilize a homologous template strand (22). NHEJ has the potential for error because it processes and ligates DNA at the break site, which can result in insertions and deletions (22). In contrast, HR occurs during the S and G2 phases of the cell cycle because a sister chromatid is present that is used as a template to guide repair (23). This results in high fidelity repair that resists the accumulation of mutations.

A fraction of breast cancers (~7) are hereditary and result from the inheritance of susceptibility genes (9). This is most often attributed to germline mutations in the *BRCA 1/2* genes, which are critical for HR-directed repair (24, 25). Specifically, *BRCA1* mutation frequency increases to up to 15% in patients with TNBC, whereas *BRCA2* mutations are

more commonly associated with ER^+ tumors (26, 27). Accordingly, these patients have a high HR deficiency (HRD) score, which is a clinical measure of genomic instability (28). It follows that TNBC patients with germline *BRCA1* mutations often develop cancer at a younger age (29). However, given the defects in DNA repair resulting from non-functional *BRCA1*, clinical studies have demonstrated that these patients benefit from distinct treatment modalities when compared to *BRCA*-wild type TNBC patients. Agents that induce HR, such as platinum analogues (cisplatin and carboplatin) and poly-(ADP ribose) polymerase (PARP) inhibitors, have proven uniquely effective for this subset of TNBC patients, which is a step closer to a "personalized medicine approach" (30-32). In contrast, the majority of TNBCs (~85%), which are *BRCA*-wild type and HR proficient, are typically treated with taxanes and/or anthracyclines (33). These observations have sparked intense interest into the underlying molecular mechanisms that govern HR and how they can be leveraged to sensitize DNA repair proficient tumors to agents such as platinum analogues. This leads to a discussion of the regulation and function of vascular endothelial growth factor (VEGF), which is the focus of this thesis.

VEGF

VEGF was originally isolated as an endothelial-cell specific factor that promotes angiogenesis and vascular permeability in several physiological and pathological contexts (34, 35). Although the original factor identified is now known as VEGF-A, it belongs to an extensive family of mitogens that also includes VEGF-B, VEGF-C, VEGF-D and placental growth factor (PlGF), which differ in their VEGF receptor binding capacity,

tissue expression and pathophysiological functions (36). VEGF-A, which is the focus of this thesis, is the classical and most heavily studied isoform and is more commonly referred to as VEGF. Additional complexity of VEGF biology is through alternative splicing, which produces several distinct VEGF variants (VEGF121, VEGF145, VEGF148, VEGF165, VEGF183, VEGF189, and VEGF206) that have distinct and overlapping functions (36).

Given its initial discovery in vascular and endothelial biology, VEGF regulation and function has dominated the angiogenesis and lymphangiogenesis fields (37). Specifically, studies have demonstrated that VEGF mediates the vascularization of tissues during development by stimulating several changes in endothelial cells including proliferation, sprouting, directed migration and reorganization of cell-cell junctions (38-40). These observations have extended beyond developmental biology because VEGF is now recognized as a key component of the tumor microenvironment that is essential for pathological angiogenesis and is also associated with poor patient prognosis (41-43). These observations have made VEGF and VEGF receptors attractive targets for therapeutic inhibition of tumor angiogenesis (44).

However, the functions of VEGF in cancer biology extends beyond its role in directing angiogenesis and vascular permeability. For example, VEGF can exert its effects on stromal cells such as tumor-associated fibroblasts (45) and immune cells dampening the anti-tumor response and contributing to tumorigenesis (46). In addition, studies have demonstrated that VEGF receptors are expressed on tumor cells and that autocrine and paracrine VEGF signaling can impact tumor initiation and progression independently of

angiogenesis (42). The focus of this thesis is the contribution of this autocrine VEGF signaling in sustaining the function of CSCs and contributing to DNA repair mechanisms.

VEGF receptors

There are two types of VEGF receptors: VEGF receptor tyrosine kinases (VEGFRs) and neuropilins (NRPs). The VEGFR family consists of VEGFR1 (Flt-1), VEGFR2 (Flk-1/KDR) and VEGFR3 (Flt-4) which have distinct functions and affinity for VEGF family members (47). For example, VEGFR2 exhibits a greater affinity for VEGF-A than VEGFR1, while VEGFR3 primarily functions as a VEGF-C and VEGF-D receptor (36, 48). Accordingly, VEGFR2 is recognized as the dominant receptor that mediates VEGF signaling in endothelial cells contributing to both developmental and pathological angiogenesis (47). As mentioned above, a central theme of this thesis is that tumor cells express VEGF receptors and autocrine and paracrine VEGF signaling can impact cancer cell function independently of angiogenesis. Several tumor types express VEGFR2, which can mediate VEGF signaling and is also associated with poor clinical outcomes (42, 49, 50).

The observations that some tumors lack VEGFR expression but still respond to VEGF stimulation launched studies analyzing the contribution of other types of VEGF receptors to tumor biology. Interestingly, tumor cells express NRPs in addition to VEGFRs (51, 52). NRPs were initially characterized in neurodevelopment as receptors for a class of axon guidance factors termed semaphorins (53, 54). Mammalian cells express two isoforms of NRPs (NRP1 and NRP2) that are about 40% homologous in amino acid

sequence but differ in their tissue expression patterns and pathophysiological functions (55). NRPs primarily function as co-receptors because they possess four extracellular domains that contribute to ligand (VEGF and semaphorin) binding and a cytoplasmic domain that does not have known enzymatic activity (56-58). NRPs do; however, contain a PDZ-binding domain that contributes to their association with other cell surface molecules. For example, NRP association with VEGFRs (59) and other receptors such as α6 integrins (60) occurs through its PDZ-binding domain. However, NRP splicing may differentially regulate their ability to interact with NRP interacting proteins through their PDZ domain (61). Although the classical role of NRPs in endothelial cell function and angiogenesis are to form complexes with VEGFRs to increase their affinity for VEGF (62), recent studies have demonstrated that autocrine and paracrine VEGF signaling mediated by NRPs can impact tumor cells independently of the VEGFRs (45, 60, 63, 64). These findings make NRPs attractive therapeutic targets for inhibition of VEGF signaling in tumor cells (65-67), and they are particularly important because bevacizumab, the most common anti-VEGF drug, does not block the VEGF-NRP association (2).

Regulation of neuropilins in tumor cells

The crucial observation that this thesis builds on is that NRPs are expressed on tumor cells and can function in VEGF-mediated support of oncogenic processes. The finding that mammary epithelial tissue exhibits very low NRP expression, but NRPs are highly expressed in TNBC (68) provides correlative support of their role in breast tumor biology. Several mechanisms have been proposed that promote NRP expression in tumors.

In TNBC, the hedgehog (Hh) effector Gli1 directly binds the NRP2 promoter and induces its expression (68). This promotes a positive feedback loop that sustains high NRP2 expression in TNBC because autocrine VEGF-NRP2 signaling also induces Gli1 (68). Studies in prostate cancer have also provided substantial insight into NRP2 regulation and function. Loss of phosphate of tensin homolog (PTEN) is a common pathologic driver of prostate cancer (69), which also induces NRP2 expression by a mechanism that involves c-jun N-terminal kinase (JNK) signaling and direct regulation of NRP2 by c-jun (66). Another possible mechanism that contributes to NRP2 expression in prostate cancer is through the analysis of COUP transcription factor II (COUP-TFII) which is associated with poor patient prognosis (70). This is because COUP-TFII has been shown to directly stimulate NRP2 transcription in lymphatic vessel development (71). Additionally, NRP1 expression is induced by Sox2 in squamous cell carcinoma which contributes to tumor initiation and progression (72).

VEGF, neuropilins and cancer stem cells

The above observations indicate a positive causal relationship between enhanced NRP expression and cancer, which suggests that NRP-mediated signaling is important for tumor progression. Indeed, VEGF-NRP signaling has been implicated in several aspects of tumor biology, especially the regulation and function of CSCs.

As mentioned above, TNBC harbors a higher frequency of CSCs compared to other breast cancer subtypes (18), and VEGF and NRP2 are preferentially expressed in TNBC (68). NRP2 associates with the α6β1 integrin in TNBC cells and autocrine VEGF-NRP2

signaling is critical for the α6β1 integrin to adhere to its extracellular matrix (ECM) ligand, laminin, and consequently activate focal adhesion kinase (FAK) (73). The mechanism by which this is presumed to occur is through the PDZ binding domain of NRP because it has been shown to be important for its association with and activation of α6 integrins in epidermal CSCs (60). Of note, NRP2, not NRP1, is preferentially expressed in breast CSCs (68). One mechanism proposed by which VEGF-NRP2 signaling confers CSCs properties and promotes breast tumor initiation is through its activation of the polycomb ring finger oncogene BMI-1 (68), which has previously been implicated in CSC function (74, 75). This occurs through a FAK-Ras-Gli1 signaling mechanism (68). The WNT-β-catenin pathway may also be regulated by VEGF-NRP signaling as a mechanism of CSC regulation (76), but more convincing evidence is needed regarding the mechanism by which these molecules intersect.

CSCs have been shown to be more efficient at protecting themselves from genomic insults when compared to non-CSCs (77), which includes DNA damage and oxidative stress. This point is worth mentioning because another interesting study demonstrated that the VEGF-C-NRP2 axis protects breast CSCs from oxidative stress by inducing the expression of superoxide dismutase 3 (Sod3) (78), which is a critical enzyme involved in buffering reactive oxygen species (ROS) (79). However, the signaling mechanism by which VEGF-C-NRP2 regulates Sod3 was not explored.

Together, these studies provided a causal role of VEGF-NRP signaling in the regulation of CSCs. However, a more in-depth analysis of the signaling mechanisms by which VEGF-NRP confers CSC properties is clearly needed. Specifically, exploration into

the convergence of VEGF-NRP signaling with transcriptional regulators that promote CSC function would provide a more integrated mechanism by which this signaling axis promotes the genetic signatures that sustain the function of CSCs. This approach is the foundation of this thesis and has the potential to yield substantial insight into VEGF-NRP biology, the regulation of CSCs and has important implications for therapy. The leads us next to an overview of the regulation and function of the hippo tumor suppressor pathway.

Hippo pathway: overview

The hippo tumor suppressor pathway was identified through mosaic screens designed to identify gene mutations involved in tissue overgrowth in Drosophila melanogaster (80-84). The hippo pathway is conserved in mammalian cells and consists of a core kinase cascade in which the MST1/2 kinases (orthologues of Drosophila hippo kinase) associate with their binding partner Salvador (SAV1) and phosphorylate and activate the large tumor suppressor kinases (LATS 1/2) (orthologues of Drosophila warts kinase). Other kinases including the mitogen activated protein kinase kinase kinase kinase 4 (MAP4K4) and thousand and one amino acid kinase (TAOK) can also act in parallel to MST1/2 activating LATS 1/2 (85-89).

Once activated, LATS kinases associate with another co-factor termed MOB-1 and directly phosphorylate and inhibit YAP and TAZ, which are the transcriptional effectors of the hippo pathway that are active when the pathway is "turned off." Yorkie is the YAP orthologue of Drosophila and was discovered through an analysis of warts-interacting proteins (90). YAP/TAZ phosphorylation results in the creation of binding sites for 14-3-

3 proteins, which inhibits their ability to regulate transcription because it results in their cytoplasmic retention and degradation (91, 92). YAP/TAZ do not directly bind DNA because they do not contain DNA binding domains. The primary transcription factor that they associate with to control gene expression are the mammalian TEA domain (TEAD) 1-4 family (orthologue of Drosophila Scaloped), which, together, regulates the expression numerous genes that control cell survival, proliferation and the acquisition of stem cell properties (93-95).

Since the discovery of the core hippo pathway, its characterization has provided substantial insight into developmental biology, organ growth control and tissue homeostasis (96). However, it is now known that the hippo pathway kinase cascade can be activated or inhibited by the intersection of numerous other molecular components. Merlin, the protein product of the neurofibromatosis type 2 (NF2) gene, is a potent activator of the hippo pathway. Merlin is an erzin, radixin, moesin (ERM)-related protein that functions as a scaffold at the membrane- cytoskeleton interface activating the MST-LATS kinase cascade (97). There is also evidence that Merlin can directly activate LATS kinases (98, 99). These observations highlight an important point relating cellular architecture and actin dynamics in hippo pathway regulation because mechanical tension is a strong activator of YAP/TAZ (100). Rho family GTPases have taken center stage in this regard because of their role in actin polymerization and stress fiber formation (101). What has been reported is that mechanical cues mediated by Rho GTPases inhibits LATS kinases and thereby facilitates YAP/TAZ nuclear localization and activation (89, 102, 103).

An area that is still emerging in hippo biology is the contribution of soluble factors and upstream receptor signaling in the regulation of hippo pathway components. One example of ligand-receptor signaling that has been explored rigorously is the role of ligand-G protein-coupled receptor (GPCR) signaling, which has been implicated in YAP/TAZ regulation by a mechanism involving Rho GTPases (103). Alternative WNT signaling is another example of a ligand-GPCR-Rho mechanism that regulates the transcriptional activity of YAP/TAZ (102). Mechanisms have been proposed that occur independently of GPCRs such as transforming growth factor beta (TGF-β) (104-106) and bone morphogenic protein (BMP) signaling mechanisms (107). Nonetheless, much remains to be learned regarding the broad landscape of ligand-receptor signaling and the intersection of different molecular pathways in hippo pathway regulation. This need is heightened because dysregulation of these and other pathways have been implicated in tumor initiation and progression.

YAP/TAZ are widely recognized as critical oncogenes involved in many of the hallmarks of cancer (108), which meshes with previous studies in Drosophila demonstrating that Yorkie promotes cell proliferation and resists apoptosis (90). A recent study reported dysregulation of hippo pathway components in a comprehensive analysis of over 9000 tumor samples, which includes squamous cell carcinoma, brain, gastrointestinal and other malignancies (109). Breast cancer is one of the most heavily studied tumor types that exhibits hyper-activation of YAP/TAZ, which is associated with CSC properties, high-grade, TNBCs and poor patient prognosis (110, 111). As mentioned above, CSCs exhibit properties of an EMT (16), which is significant because TAZ can induce an EMT in

mammary epithelial cells (112). Moreover, YAP/TAZ are critical for transcriptional addiction and therapy resistance in TNBC (113). Although they are attractive pharmacological targets, therapeutic inhibition of YAP/TAZ has been a challenge (114). Additionally, upstream signaling mechanisms that disrupt hippo signaling and contribute to enhanced YAP/TAZ activity in different tumor types are still being elucidated. Further investigation into these processes has the potential to uncover previously unknown regulators of the hippo pathway and may identify novel therapeutic targets that disrupt YAP/TAZ activity.

Rationale for thesis work

Although YAP/TAZ are crucial breast CSC oncogenes, the upstream signaling mechanisms that disrupt hippo signaling and contribute to their hyper-activation have remained elusive. Given the available evidence mentioned above, albeit limited, linking autocrine VEGF-NRP2 signaling and breast tumor initiation, I initiated the work in Chapter II of my thesis by pursuing the hypothesis that the mechanism by which the VEGF-NRP2 signaling axis confers CSC properties in breast cancer cells is through downstream YAP/TAZ activation. The results I obtained validated my hypothesis by uncovering a previously unknown positive feedback circuit that sustains enhanced YAP/TAZ activity involving the Rho family GTPase Rac1, and consequent repression of a Rac1 regulatory protein by YAP/TAZ-mediated transcriptional regulation.

In Chapter III of my thesis, I extended my conclusions from Chapter II that YAP/TAZ are downstream effectors of VEGF-NRP2 signaling by analyzing the

implications of this molecular association to DNA repair pathways and therapy resistance. This is because, although VEGF-NRP signaling and YAP/TAZ have been independently implicated in resistance to chemo- and radiotherapy in several tumor types, much remains to learned regarding the mechanisms by which they promote therapy resistance. Moreover, the contribution of both VEGF-NRP signaling and YAP/TAZ to DNA repair pathways has not been explored, which is ripe for investigation because many cancer therapies induce DNA damage. My hypothesis that VEGF-NRP2-YAP/TAZ signaling promotes resistance to DNA damaging agents is timely because recent clinical evidence has demonstrated the efficacy of specific treatment modalities for TNBC patients with deficiency in HR-directed repair. These findings have heightened the need for a better understanding of the mechanisms that contribute to efficient DNA repair in subgroups of TNBC patients to increase their response to HR-inducing therapies. In pursuit of this mechanism, I discovered that VEGF-NRP2-YAP/TAZ signaling promotes HR and therapy resistance in TNBC cells by directly regulating the expression of Rad51, which is a central enzyme in HR-directed repair.

CHAPTER II

VEGF-neuropilin-2 signaling promotes stem-like traits in breast cancer cells by TAZ-mediated repression of the Rac GAP β2-chimaerin

This work was originally published in *Science Signaling*. **Ameer L. Elaimy**, Santosh Guru, Cheng Chang, John J. Amante, Lihua Julie Zhu, Hira Lal Goel and Arthur M. Mercurio. VEGF-neuropilin-2 signaling promotes stem-like traits in breast cancer cells by TAZ-mediated repression of the Rac GAP β2-chimaerin. *Science Signaling*. 2018 May 1;11(528). pii: eaao6897. doi: 10.1126/scisignal.aao6897. From *Science Signaling*. Reprinted with permission from AAAS.

CONTRIBUTIONS:

Ameer L. Elaimy conceptualized the study, performed experiments, made the figures and wrote the manuscript. Santosh Guru performed immunofluorescence microscopy. Cheng Chang generated the EPTH and MES cells. John J. Amante provided technical support. Lihua Julia Zhu performed bioinformatics analyses. Hira Lal Goel provided feedback on data. Arthur M. Mercurio oversaw and conceptualized the study, provided feedback on experiments and wrote the manuscript.

Introduction

Vascular endothelial growth factor (VEGF) was originally characterized as a protein that promotes endothelial growth (34) and increases vascular permeability (35). For these and other reasons, it was presumed that the role of VEGF in cancer was limited to angiogenesis (34, 41, 44, 115). It is evident now, however, that there are angiogenesis-independent functions of VEGF in cancer that are mediated by specific receptors. Tumor cells express VEGF receptor tyrosine kinases (VEGFR1 and VEGFR2) and neuropilins (NRPs), another family of VEGF receptors. NRP1 and NRP2 were identified initially as neuronal receptors for semaphorins, which are axon guidance factors that function primarily in the developing nervous system (116). The finding that NRPs can also function as VEGF receptors and that they are expressed on endothelial and tumor cells launched studies aimed at understanding their contribution to angiogenesis and tumor biology (52). NRPs have the ability to interact with and modulate the function of VEGFR1 and VEGFR2, as well as other receptors (62, 117, 118). There is also evidence that NRPs are valid targets for therapeutic inhibition of angiogenesis and cancer (65-67, 119).

A surge of evidence has implicated autocrine VEGF signaling mediated by NRPs in the function of cancer stem cells (CSCs), a sub-population of cells that function in tumor initiation, the differentiation of multi-lineage cancer cell hierarchies, therapy resistance and metastasis (14, 42, 66, 120-124). These observations have led to intense investigation into the mechanisms by which VEGF sustains CSCs and how these processes can be exploited therapeutically. Previously, we reported that NRP2 is highly expressed in breast CSCs and that VEGF-NRP2 signaling contributes to breast tumor initiation (68). A key issue that

emerges from these findings is the mechanism by which VEGF-NRP2 signaling contributes to the function of CSCs. In pursuit of this issue, we were intrigued by reports that the Hippo pathway transducer TAZ confers stem cell properties and contributes to breast tumorigenesis, especially in high-grade tumors, which are distinguished by high NRP2 expression and VEGF-NRP2 signaling activity (68). Moreover, TAZ expression in breast cancer correlates with tumor grade (111) and high-grade tumors harbor a higher frequency of CSCs than do lower grade tumors (18). Mechanistic studies have shown that TAZ can induce an epithelial to mesenchymal transition (EMT) in mammary epithelial cells (112), a process that can increase stem cell properties (125). Moreover, TAZ is necessary for the self-renewal of CSCs (111). In contrast, the role of YAP in breast cancer is less clear and its expression does not correlate with clinical outcome (110).

The Hippo pathway consists of core kinases and regulatory molecules that facilitate TAZ phosphorylation, cytoplasmic retention and inactivation (91, 126, 127). For this reason, identifying upstream receptors that disrupt Hippo signaling and, consequently, enhance TAZ activity is critical for understanding how these effectors contribute to the function of CSCs. In this study, we discovered that VEGF-NRP2 signaling contributes to increased TAZ activity by a Rac1-dependent, feed-forward mechanism.

Results

VEGF-NRP2 Signaling Contributes to TAZ Activation: Initially, we assessed the contribution of VEGF-NRP2 signaling to TAZ activation. For this purpose, we used an

inducible system to transform MCF10A cells with Src, which generates a population of $CD44^{high}/CD24^{low}$ cells with CSC properties (128). This population is actually comprised of distinct epithelial (EPTH) and mesenchymal (MES) populations that differ in TAZ activity and tumor initiating potential. The MES population has enhanced TAZ activity, self-renewal potential and tumor initiating capability compared to the EPTH population (129). Importantly, MES cells express increased levels of VEGF and NRP2 compared to EPTH cells and are dependent on VEGF-NRP2 signaling for self-renewal (130). Expression of either NRP2 (**Figure 2.1A**) or VEGF (**Figure 2.1B**) was diminished in MES cells using shRNAs, which resulted in decreased TAZ abundance compared to control cells as assessed by immunoblotting (**Figures 2.1, A and B**). As reported previously, TAZ abundance is an indicator of its activation status (102, 131), as well as its nuclear localization. For this latter reason, we compared TAZ localization in control cells to VEGF- and NRP2-depleted cells by immunofluorescence (**Figure 2.1C; 2.9A**). TAZ is localized primarily in the nucleus in control MES cells (**Figure 2.1C; 2.9A**). In contrast, little, if any, TAZ was detected in VEGF- and NRP2-depleted cells, which is consistent with our immunoblotting data (**Figures 2.1, A and B**). The TAZ that was detected in VEGF-depleted cells is localized in the cytoplasm (**Figure 2.1C; 2.9A**).

Depletion of NRP2 in MES cells also reduced the mRNA expression of the TAZ target genes *CTGF* and *CYR61* (**Figure 2.1D**). To substantiate the data obtained with shRNAs, we treated MES cells with a function-blocking NRP2 antibody (65) and observed a concentration–dependent decrease in TAZ abundance (**Figure 2.1E**). Although similar results were obtained with YAP (**Figure 2.9B-C**), we focused subsequent experiments on

TAZ because convincing data correlating YAP expression and clinical parameters in breast cancer are lacking (110).

We extended this analysis to MDA-MB-231 cells because they exhibit mesenchymal properties and highly express VEGF and NRP2 (130). Similar to MES cells, NRP2 depletion reduced the abundance of TAZ, as well as TAZ target genes, (**Figures 2.1, F and G**) suggesting that NRP2 affects TAZ-mediated transcription. TAZ regulates gene expression by associating with the TEAD family of transcription factors (95), which infers that NRP2 should affect TEAD transcriptional activity. Indeed, the activity of a TEAD luciferase reporter was reduced significantly in MDA-MB-231 cells with diminished NRP2 expression compared to control cells (**Figure 2.1H**).

Rac1 Facilitates VEGF-NRP2–mediated Activation of TAZ: To investigate the mechanism by which VEGF-NRP2 signaling activates TAZ, we focused on Rac1 for several reasons. This GTPase is a major effector of NRP/plexin signaling in neurons (132, 133) and it has been implicated in VEGF signaling in endothelial cells (134, 135). Moreover, Rac1 has also been implicated in TAZ activation (102, 136-138). We observed that depleting VEGF expression or treating MES cells with the NRP2 function-blocking antibody resulted in a substantial decrease in Rac1 activity (**Figures 2.2, A and B**). Similar results were obtained with MDA-MB-231 cells (**Figure 2.2C**). Conversely, stimulating MDA-MB-231 cells with VEGF resulted in an increase in Rac1 activity (**Figure 2.2D**).

An important issue is whether VEGFRs contribute to Rac1 activation in breast cancer cells. Treatment of MDA-MB-231 cells with the VEGFR inhibitors pazopanib and

subitinib in the presence of VEGF did not decrease Rac1 activity compared to VEGF alone (**Figure 2.10**), suggesting that VEGF-NRP2 activation of Rac1 is VEGFR-independent. This result is not surprising because we reported previously that MDA-MB-231 and other breast cancer cell lines express very low levels of VEGFRs (139). In contrast, VEGF-NRP2–mediated Rac1 activation appears to be focal adhesion kinase (FAK)-dependent, because the FAK inhibitor FAK14 significantly decreased Rac1 activity in MES cells (**Figure 2.2E**). This result is consistent with previous findings that FAK is a downstream effector of VEGF-NRP2 signaling (68), and it has been implicated in Rac1 activation (140-142), as well as Hippo pathway regulation (143, 144).

The results described above prompted us to evaluate whether VEGF-NRP2 signals through Rac1 to promote TAZ activation. Based on our finding that depletion of NRP2 in MDA-MB-231 cells decreased the expression of TAZ target genes (**Figure 2.2G**), we found that expression of a constitutively active V12 Rac1 in these cells rescued their expression (**Figure 2.2F**). This result provides evidence that the VEGF-NRP2-Rac1 axis contributes to TAZ activation. Subsequently, we assessed the role of Rac1 inhibition on mammosphere formation in MES cells and observed decreased mammosphere formation upon treatment with the Rac inhibitors EHT1864 and NSC23766 (**Figure 2.2G**).

We next sought to investigate the mechanism by which VEGF-NRP2-mediated regulation of Rac1 contributes to TAZ activation. We focused on the LATS tumor suppressor kinases because they phosphorylate TAZ directly at the Ser^{89} position and promote its cytoplasmic retention and degradation when phosphorylated and activated on their hydrophobic motifs (Thr^{1079} in LATS1, Thr^{1041} in LATS2) (112, 145, 146).

Moreover, LATS can be regulated by Rac1 (102, 136, 137). Treatment of MES cells with the Rac inhibitor EHT1864 resulted in a concentration-dependent increase in the abundance of phosphorylated Ser^{89} ($pSer^{89}$) TAZ and a concomitant decrease in TAZ abundance (**Figure 2.3A**). It also increased the abundance of $pThr^{1079}$ LATS1 and decreased TAZ abundance as early as 15 minutes after treatment, and this pattern persisted for up to 6 hours **(Figure 2.3B**). Expression of dominant-negative N17 Rac1 also decreased TAZ abundance in MES cells (**Figure 2.3C**). Similar results were obtained with the NRP2 function-blocking antibody (**Figure 2.3D**). NRP2 knockdown in MDA-MB-231 cells also increased the abundance of $pSer^{89}$ TAZ and $pThr^{1079}$ LATS1 and decreased the abundance of TAZ (**Figures 2.3, E and F**). NRP2 depletion also increased LATS-mediated YAP phosphorylation ($pSer^{127}$) (**Figure 2.9B**). LATS knockdown rescued TAZ abundance in NRP2 depleted MDA-MB-231 cells, which shows that VEGF-NRP2-Rac1 regulation of TAZ is LATS-dependent (**Figure 2.11A**).

Given the importance of TAZ in promoting CSC properties (111), we hypothesized that VEGF-NRP2-Rac1-mediated LATS inhibition is a critical upstream regulator of TAZ-mediated mammosphere formation. Depletion of NRP2 in MDA-MB-231 cells significantly reduced mammosphere formation, which was partially rescued by expression of wild-type TAZ (**Figure 2.3G; 2.12**). Expression of S89A TAZ, which is resistant to LATS-mediated phosphorylation at that site, rescued mammosphere formation significantly more than did expression of wild-type TAZ (**Figure 2.3G; 2.12**). Similar results were obtained by VEGF depletion in MES cells (**Figure 2.3H**). These results indicate that the wild-type TAZ ectopically expressed is subject to regulation by upstream

VEGF-NRP2 signaling, but that the S89A TAZ mutant is not. Together, these data provide functional evidence that VEGF-NRP2-Rac1 promotes a TAZ-dependent stem-like phenotype through inhibition of LATS-mediated phosphorylation of TAZ at Ser^{89}.

To gain insight into the mechanism by which VEGF-NRP2-Rac1 signaling inhibits LATS activity, we postulated that this signaling regulates Merlin, the protein product of the Neurofibromatosis type 2 (NF2) gene, because phosphorylation of Merlin on Ser^{518} by p21-activated kinase (PAK) is inhibitory (147-149). Moreover, Merlin phosphorylation inhibits LATS phosphorylation (97). These findings are relevant because PAK is a Rac-activated kinase (150). Following these observations, we found that either Rac inhibition or NRP2 depletion in MES cells reduced the abundance of Ser^{518} -phosphorylated Merlin (**Figure 2.11B and C**).

VEGF-NRP2 Signaling Represses the Rac GAP β2-chimaerin: Rac1 cycles from GTP-bound active states to GDP-bound inactive states, which, in large part, is regulated by the expression of guanine nucleotide exchange factors (GEFs) and GAPs. Therefore, we profiled the expression of known Rac GEFs and GAPs in EPTH and MES cells (**Table 2.1**). Notably, we observed that the expression of the Rac GAP β2-chimaerin was markedly reduced in MES cells compared to EPTH cells (**Table 2.1**), which we verified by immunoblotting (**Figure 2.4A**). β2-chimaerin is a Rac-specific GAP that has been implicated as a tumor suppressor in breast cancer (151-155). Given that β2-chimaerin abundance is reduced in MES cells and these cells highly express VEGF and NRP2 (130), we assessed whether VEGF-NRP2 signaling repressed β2-chimaerin expression. Indeed, we observed that NRP2 depletion increased β2-chimaerin mRNA and protein expression

in MES cells (**Figures 2.4, B and C**). Treatment of MES cells with the NRP2 function-blocking antibody also increased β2-Chimaerin abundance (**Figure 2.4D**). These observations provide evidence that VEGF-NRP2 signaling represses β2-chimaerin expression.

TAZ Activates Rac1 by Repressing β2-chimaerin through a TEAD-Dependent Mechanism: Based on our observation that VEGF-NRP2 signaling activates TAZ and represses β2-chimaerin, we assessed the possibility that TAZ represses β2-chimaerin. This possibility is supported by studies demonstrating that TAZ can function in transcriptional repression (156, 157). Depletion of TAZ in MES cells caused an increase in β2-chimaerin mRNA and protein expression and a consequent decrease in Rac1 activity (**Figures 2.5, A to C**). TAZ knockdown in MDA-MB-435 cells (**Figure 2.5D**) and MDA-MB-231 cells (**Figure 2.5E**) also increased *β2-chimaerin* mRNA expression. Conversely, TAZ overexpression repressed *β2-chimaerin* mRNA expression in MDA-MB-231 cells (**Figure 2.5F**). Given our observations that Rac1 activates TAZ (**Figure 2.3**) and that TAZ represses β2-chimaerin expression, we inhibited Rac1 in MES cells using EHT1864 and observed an increase in the expression of *β2-chimaerin* mRNA (**Figure 2.5G**). These results provide evidence that VEGF-NRP2-Rac1-mediated TAZ activation maintains elevated Rac1 activity by repressing β2-chimaerin in a positive feedback loop.

TAZ-mediated transcriptional repression is dependent on the TEAD1-4 family of transcription factors (156, 157). TEAD4, in particular, is expressed at relatively high levels in breast cancer, especially triple negative breast cancer (158, 159). Given this information, we initially searched the encyclopedia of DNA elements (ENCODE) for TEAD4 ChIP-seq

datasets and found 4 cell types (h1-human embryonic stem cells, HCT116 colon cancer cells, Ishikawa endometrial adenocarcinoma cells and SK-N-SH neuroblastoma cells) where TEAD4 bound to the promoter region of the β2-chimaerin gene (**Figure 2.6A**). Specifically, a conserved peak was observed near position 29229000 (chr7) in all of the cell types. These findings are significant because they demonstrate direct binding of TEAD4 to the β2-chimaerin promoter. Also, h1-hESCs, HCT116, Ishikawa and SK-N-SH cells have enhanced TAZ/TEAD activity (160, 161). To validate the ENCODE data in our model system, we performed ChIP in MES cells using antibodies specific for TEAD4 and TAZ. The results verify that TEAD4 and TAZ are recruited to the genomic region in the β2-chimaerin promoter identified in ENCODE (**Figure 2.6B**). Based on these data, we depleted TEAD1/3/4 expression in MES cells and observed an increase in β2-chimaerin mRNA and protein expression (**Figures 2.6, C and D**) and a decrease in Rac1 activity (**Figure 2.6E**), consistent with our TAZ knockdown results (**Figures 2.5, A to C**). Similarly, expression of dominant-negative TEAD4 in MDA-MB-231 cells increased *β2-chimaerin* mRNA expression (**Figure 2.6F**).

β2-chimaerin Repression Contributes to Enhanced TAZ Activity: An important issue that arises from the data thus far is whether β2-chimaerin repression has a causal role in TAZ activation. Expression of β2-chimaerin in MDA-MB-231 cells decreased Rac1 activity, as well as the abundance of TAZ itself (**Figure 2.7A**) and TAZ target genes (**Figure 2.7B**). Conversely, β2-chimaerin knockdown in EPTH cells increased Rac1 activity, TAZ abundance (**Figure 2.7C**) and TAZ target genes (**Figure 2.7D**). Notably, β2-chimaerin-depleted EPTH cells exhibited increased mammosphere formation compared

to control EPTH cells (**Figure 2.7E**). Expression of β2-chimaerin also reduced TAZ-mediated, but not S89A TAZ-mediated, mammosphere formation in MDA-MB-231 cells (**Figure 2.7F**), providing further evidence that Rac1 inhibition of LATS contributes to TAZ activation and CSC properties.

These *in vitro* data indicating an inverse causal relationship between β2-chimaerin and TAZ and a positive causal relationship between VEGF-NRP2 and TAZ were substantiated by analysis of their expression in invasive breast carcinomas in The Cancer Genome Atlas (TCGA) database obtained from cBioPortal (162, 163) (**Figure 2.7G**). Indeed, the expression of TAZ and β2-chimaerin were inversely correlated. In contrast, the expression of TAZ correlated with that of VEGF and NRP2. An inverse correlation between TAZ and β2-chimaerin was also detected in glioblastoma and colorectal adenocarcinoma samples in the TCGA. These findings are significant because both glioblastoma and colon cancer exhibit enhanced TAZ activity (160, 164, 165). Lastly, TAZ and β2-chimaerin exhibited an inverse correlation in the cancer cell line encyclopedia obtained from cBioPortal (967 cell lines) (**Figure 2.7G**), which provides further evidence of a repressive role (162, 163).

Our data indicate that TAZ-mediated repression of β2-chimaerin is associated with a mesenchymal phenotype. To substantiate this conclusion, we analyzed a microarray (GSE48204) that utilized TGF-β-treated NMuMG mammary epithelial cells to induce an EMT (166). In support of our conclusion, we found that the EMT reduced β2-chimaerin expression and increased expression of VEGF and NRP2, as well as TAZ target genes (**Figure 2.13**). We also used cBioPortal to stratify breast cancer patients in

the TCGA database based on their expression of the estrogen receptor (ER), which is associated with an epithelial phenotype. Comparison of β2-chimaerin expression in the estrogen receptor-positive (ER^+) and ER^- subgroups revealed that ER^- patients have lower expression of β2-chimaerin compared to ER^+ patients (**Figure 2.7H**).

Discussion

The results of this study establish a causal role for VEGF-NRP2 signaling in sustaining the activation of TAZ, a critical effector molecule of the Hippo pathway that contributes to breast tumorigenesis and is associated with aggressive, high-grade tumors. An essential component of this mechanism is the repression of β2-chimaerin, a Rac GAP, by TAZ and the consequent activation of Rac1 resulting in a positive feedback loop driven by VEGF-NRP2 signaling that sustains TAZ activation (**Figure 8**). These findings increase our understanding of autocrine VEGF signaling in tumor cells and they substantiate the importance of Rac in the biology of CSCs and TAZ regulation.

Our conclusion that repression of β2-chimaerin contributes to TAZ activation and self-renewal indicates that this Rac GAP is an important gatekeeper that impedes the acquisition of stem cell properties. Based on the hypothesis that breast CSCs are de-differentiated and exhibit features of an EMT (125), this conclusion infers that repression of β2-chimaerin is a consequence of the EMT and that its expression is associated with an epithelial phenotype. Indeed, we uncovered that β2-chimaerin is repressed by the TGF-β-induced EMT of mammary epithelial cells. Importantly, we also demonstrated that ER^+

patients have higher β2-chimaerin expression compared to ER^- patients. These observations contrast with the report that β2-chimaerin reduces E-cadherin levels in an *in vitro* overexpression system (154). Interestingly, however, this report also demonstrated that low expression of β2-chimaerin is associated with reduced relapse-free survival of breast cancer patients, which supports our findings.

Our results need to be discussed in the context of the report that NRP2 binds β2-chimaerin directly, and that Semaphorin3F-NRP2 signaling reduces this association to activate β2-chimaerin and regulate axonal pruning in the hippocampus (133). Although β2-chimaerin and NRP2 exhibit an inverse expression pattern in breast cancer, we tested the hypothesis that residual β2-chimaerin may be sequestered and inactivated by NRP2 as a mechanism of Rac1 regulation. However, we were unable to co-immunopurify NRP2 with β2-chimaerin. This is not definitive, but it does suggest NRP2 regulation of β2-chimaerin differs in breast cancer cells and neurons. This difference may reflect the fact that different ligands (Semaphorin3F and VEGF) engage NRP2 in these cells types. It is also worth mentioning that we previously demonstrated that Semaphorin3A and VEGF compete for NRP binding in breast cancer cells, and that these two ligands have opposite effects on the behavior of these cells (167). Nonetheless, the existing data highlight an important causal effect of NRP2 on β2-chimaerin that is executed by distinct mechanisms.

A major conclusion of this study is that VEGF-NRP2 signaling contributes to TAZ activation by a Rac1-dependent mechanism. This role for Rac1 differs from its more established role in regulating cell invasion and migration in cancer, but it is consistent with other reports implicating Rac1 in the function of CSCs (168-170), as well as in YAP/TAZ

activation (102, 136-138). Our results on the ability of VEGF-NRP2 signaling to inhibit LATS by a Rac1-dependent mechanism support these observations and they identify a novel ligand-receptor interaction that can mediate this regulation. Furthermore, our data suggest that the ability of Rac1 to inhibit LATS is mediated by its regulation of Merlin, which is an important organizer of the membrane-cytoskeleton interface (89, 97-99, 147-149). Although we are not ruling out the possibility that VEGF-NRP2 signaling may activate RhoA, which has also been implicated in YAP/TAZ activation (89, 100, 102, 103, 136), we focused our attention on Rac1 because β2-chimaerin is Rac-specific and does not have GAP activity against Rho (151, 152).

Although many studies have implicated autocrine VEGF signaling in the function of CSCs (42), its ability to contribute to Hippo-TAZ regulation provides a new dimension to our understanding of VEGF biology. While this manuscript was in review, however, it was reported that VEGF-VEGFR2 signaling contributes to YAP/TAZ activation during developmental angiogenesis (171). Our data support the role of VEGF in promoting YAP/TAZ activation, but the mechanism used by breast cancer cells is distinct because it appears to be dependent on VEGF-NRP2 activation of FAK-Rac1 but independent of VEGFR. Moreover, our findings reveal a pivotal role for β2-chimaerin as a repressive intermediary between VEGF-NRP2 and TAZ activation. They also reinforce the hypothesis that targeting VEGF-NRP signaling is a viable therapeutic strategy for tumor cells that are dependent on TAZ activation.

Materials and Methods

Reagents and Antibodies

EHT1864 was purchased from Tocris, NSC23766 was purchased from Selleckchem, FAK14 was purchased from Sigma, Sunitinib and Pazopanib were purchased from LC Laboratories, human VEGFA165 was purchased from R&D Systems and the function-blocking Neuropilin-2 antibody was provided by Genentech (65). Immunoblotting antibodies were acquired as follows: Actin (A2066, Sigma), TAZ (560235, BD Biosciences), YAP/TAZ (8418S, Cell Signaling Technologies), pS89 TAZ (sc-17610, Santa Cruz Biotechnology), pS127 YAP (4911A, Cell Signaling Technologies), Neuropilin-2 (sc-7242, Santa Cruz Biotechnology), β2-chimaerin (CHN2) (HPA018989, Sigma), pT1079 LATS1 (8654S, Cell Signaling Technologies), LATS1 (9153S, Cell Signaling Technologies), VEGF (sc-152, Santa Cruz Biotechnology), Rac1 (610650, BD Biosciences), Pan-TEAD (13295S, Cell Signaling Technologies), pS518 Merlin (9163S, Cell Signaling Technologies), Merlin (6995S, Cell Signaling Technologies), HA-Tag (3724S, Cell Signaling Technologies), GST (sc-138, Santa Cruz Biotechnology) and Myc-Tag (2278S, Cell Signaling Technologies).

Constructs

The following lentiviral shRNA vectors were used: VEGF (TRCN0000003343, TRCN0000003344, TRCN0000003345), Neuropilin-2 (TRCN0000063309, TRCN0000063312, TRCN0000063310), β2-chimaerin (provided by Dr. Alex Kolodkin, Johns Hopkins Medical Institute (133)) and TEAD 1/3/4 (provided by Dr. Junhao Mao, University of Massachusetts Medical School (160)). Retroviral shTAZ vectors were used

as previously described (129). Stable shRNA expression was accomplished by selecting cells in 2 μg/mL puromycin for 2 to 4 days. Myc-tagged (6X) β2-chimaerin was provided by Dr. Alex Kolodkin, Johns Hopkins Medical Institute (133), Myc-tagged dominant negative TEAD4 was provided by Dr. Junhao Mao, University of Massachusetts Medical School, dominant negative Rac1 (N17Rac1) and constitutively active Rac1 (V12Rac1) were described previously (124). Human TAZ was cloned into pcDNA3.1 vector and site-directed mutagenesis was performed to generate TAZ S89A (**fig. S6**).

Cell Culture

ER-SRC transformed MCF10A cells were provided by Dr. Kevin Struhl (Harvard Medical School). To generate puromycin sensitive MCF10A ER-SRC cells, v-SRC was cloned from the cDNA pool of the original MCF10A ER-SRC cell line. Subsequently, pWZL Blast Twist ER plasmid (Addgene Plasmid #18799) was digested by BamHI to remove the Snai1 cDNA, and replaced with v-SRC cDNA, resulting in the expression of the fusion protein, v-SRC-ER, by the new recombinant plasmid. This plasmid was subsequently used to produce retrovirus for infecting MCF10A cells. Stable clones were selected by blasticidin. Isolation of the EPTH and MES populations of $CD44^{+}CD24^{-/low}$ MCF10A ER-SRC transformed cells using flow cytometry has been previously described (130). EPTH and MES cells were cultured as subclones for 2-3 passages and used for experiments. MDA-MB-231 and MDA-MB-435 cells were obtained from the American Type Culture Collection. All experiments were performed at a cell density of 25-35%.

Transfection and siRNA Knockdown

For overexpression, plasmids were transfected using Lipofectamine 2000 (Thermo Fisher Scientific). Cells were processed for immunoblotting, qPCR or mammosphere formation approximately 24 hours following transfection. For LATS 1/2 siRNA knockdown, MDA-MB-231 cells were transfected using DharmaFect 4 (Dharmacon). Cells were processed for immunoblotting 48 hours following transfection. LATS 1/2 siRNA has been previously described (129).

Mammosphere Assay

Cells were plated in UltraLow attachment 6 well plates in DMEM/F12 medium supplemented with B27, EGF and fibroblast growth factor as previously described (130). For serial passaging, mammospheres were pelleted and dissociated with 0.05% Trypsin for 15 minutes at 37 degrees Celsius to obtain single cells. These cells were washed in 1X PBS, counted and re-plated in UltraLow attachment 6 well plates.

Immunolotting

Cells were washed in 1X PBS and scraped on ice in RIPA buffer with EDTA and EGTA (BP-115DG, Boston Bioproducts) supplemented with protease and phosphatase inhibitors (Pierce, #88669). Laemmli 6X SDS sample buffer (BP-111R, Boston Bioproducts) was added to each sample and the protein lysate was boiled for 10 minutes and separated using SDS-PAGE. Rac activity was assessed using a GST fusion protein containing the Rac/cdc42 binding domain of PAK (PBD) as previously described (124, 172).

Luciferase Reporter Assay

TEAD transcriptional activity was assessed using a luciferase reporter construct (8XGTIIC-Addgene #34615) with the Dual-Luciferase Reporter Assay System (#E2940, Promega). Approximately 24 hours following transfection, luciferase activity was measured as the average ratio of firefly to Renilla luciferase.

Real time quantitative PCR

RNA extraction was accomplished using an RNA isolation kit (BS88133, Bio Basic Inc) and cDNAs were produced using qScrict cDNA synthesis kit (#95047, Quantabio). SYBR green (Applied Biosystems) was used as the qPCR master mix. Experiments were performed in triplicate and normalized to GAPDH. qPCR primer sequences were obtained from the Massachusetts General Hospital/Harvard Medical School PrimerBank (http://pga.mgh.harvard.edu/primerbank/).

Chromatin Immunoprecipitation (ChIP)

ChiP was performed using ChIP-IT Express Chromatin Immunoprecipitation kit (Active Motif). Antibodies used were TEAD4 (N-G2, Santa Cruz Biotechnology) and TAZ (70148S, Cell Signaling Technologies). The following qPCR primer sequence was used to amplify the region of the TEAD4 peak in the β2-chimaerin promoter identified in ENCODE: Forward primer 5'-GCTTACAGCTGGCTTCACTT-3' Reverse Primer 5'-GGCCGAGAGAGAGAGAGTTT-3'.

Immunoflourescence Confocal Microscopy

TAZ localization was performed by fixing cells with paraformaldehyde (4%) and permeabilizing them with Triton X-100 (0.1%) as described (111, 129). Cells were

blocked with 1% BSA and horse serum (2.5%) and incubated with TAZ antibody (1:100 dilution; sc-48805, Santa Cruz Biotechnology) overnight at 4°C. Subsequently, cells were washed with 1X PBS and incubated with fluorochrome-conjugated secondary antibodies. Images were captured at 20X magnification using a confocal microscope (Zeiss).

ENCODE Data Analysis

Encode TEAD4 binding signals were downloaded from www.encodeproject.org in bigwig format. The coverages of duplicate samples were pooled and then plotted along the promoter region of the β2-chimaerin (CHN2) gene.

cBioPortal Analysis

cBioPortal (www.cbioportal.org) was utilized to compare the mRNA expression (RNA Seq V2 RSEM) of TAZ, VEGFA, NRP2 and β2-chimaerin using the TCGA invasive breast carcinoma provisional dataset (162, 163). In addition, the mRNA expression (RNA Seq V2 RSEM) of TAZ and β2-chimaerin was compared in the TCGA glioblastoma provisional dataset and the TCGA colorectal adenocarcinoma Nature 2012 dataset. The cancer cell line encyclopedia (Novartis/Broad, Nature 2012) was used to compare the expression of TAZ and β2-chimaerin across various cell lines using the mRNA expression z-scores microarray. To determine whether the expression of two genes are inversely correlated, we performed the mutual exclusivity analysis with a z-score threshold of ± 1.5 as expressed, and calculated the log odds ratio between the two genes and *p* value using Fisher exact *t*-test. In addition, we stratified breast cancer patients in the TCGA Cell 2015 database based on their ER status, and compared β2-chimaerin expression in the ER^+ and ER^- subgroups using Welch *t*-test.

Microarray Data Analysis

The microarray dataset from GEO (GSE48204) (166) was download using the Bioconductor package *GEOquery* (version 2.41.0). Moderated *t*-test was used to identify differentially expressed genes between TGF-β induced EMT cells and NMuMG cells treated with vehicle. Genes with an adjusted *p*-value of ≤ 0.05 using B-H method were considered significant (173).

Figures

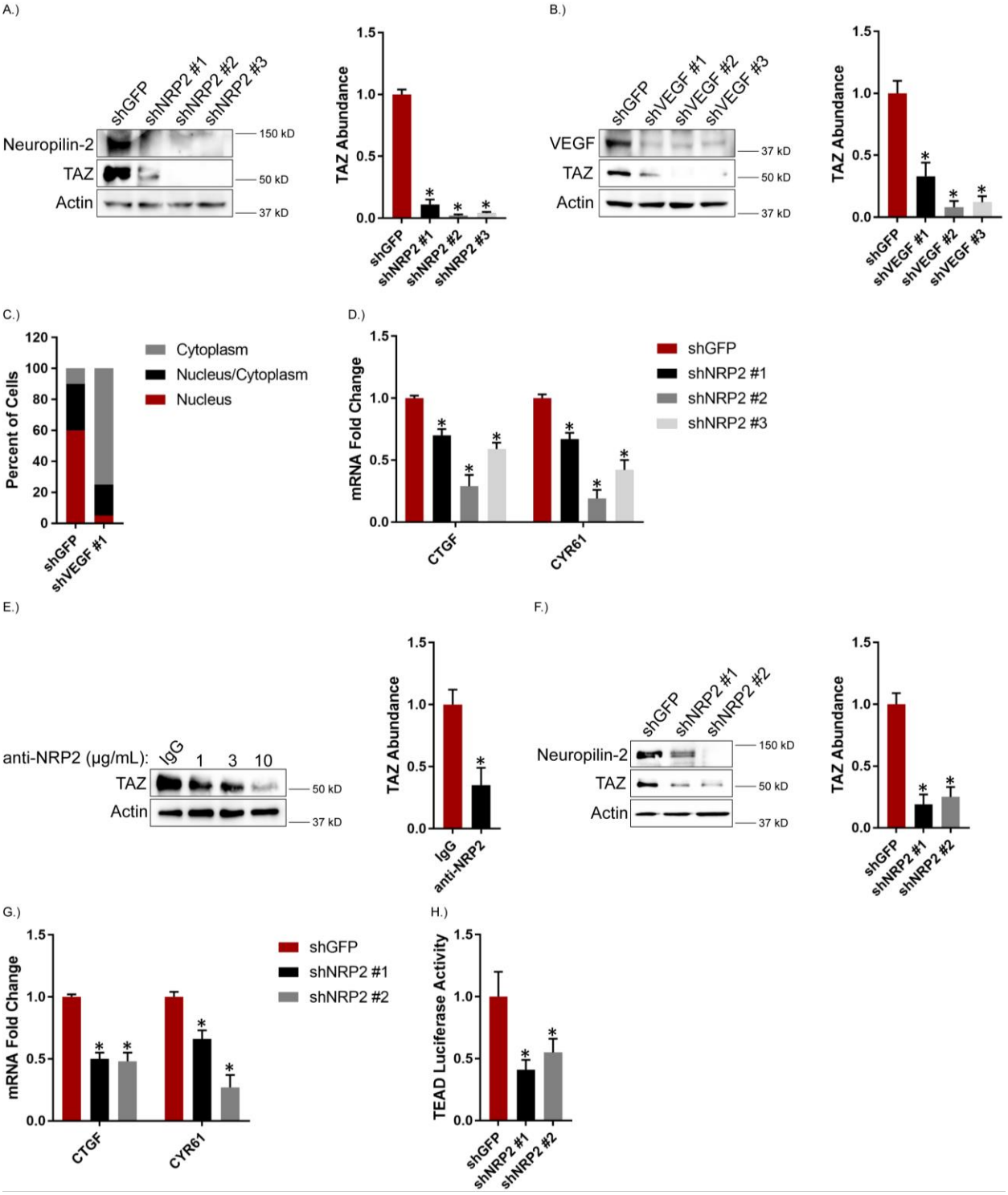
A.)
shGFP
shNRP2 #1
shNRP2 #2
shNRP2 #3
Neuropilin-2
TAZ
Actin
150 kD
50 kD
37 kD
TAZ Abundance
B.)
shVEGF #1
shVEGF #2
shVEGF #3
VEGF
C.)
Percent of Cells
Cytoplasm
Nucleus/Cytoplasm
Nucleus
shVEGF #1
D.)
mRNA Fold Change
CTGF
CYR61
E.)
anti-NRP2 (μg/mL):
IgG
1
3
10
F.)
G.)
H.)
TEAD Luciferase Activity

Figure 2.1: VEGF-NRP2 Signaling Contributes to TAZ Activation. Expression of NRP2 (*A*) and VEGF (*B*) was diminished in MES cells and the impact on TAZ abundance was quantified by immunoblotting. Representative blots are shown. Densitometric values were processed using ImageJ and are provided as bar graphs (mean ± SEM) of n = 3 biological replicates. *C*.) TAZ localization (cytoplasm, nucleus/cytoplasm and nucleus) in control and VEGF-depleted MES cells was determined by immunofluorescence confocal microscopy. Data are mean of n = 3 biological replicates. *D*.) mRNA expression of the indicated TAZ target genes was quantified by qPCR in NRP2-depleted MES cells. Data are mean ± SEM of n = 3 biological replicates. *E*.) MES cells were treated with the indicated concentrations of a function-blocking NRP2 antibody for 6 hours and the impact on TAZ abundance was quantified by immunoblotting. Representative blots are shown. Densitometric values are provided as bar graphs (mean ± SEM) of n = 3 biological replicates of MES cells treated with 3 μg/mL of the NRP2 function-blocking antibody. *F*.) NRP2 expression was diminished in MDA-MB-231 cells and the impact on TAZ abundance was quantified by immunoblotting. Representative blots are shown. Densitometric values are provided as bar graphs (mean ± SEM) of n = 3 biological replicates. *G*.) mRNA expression of the indicated TAZ target genes was quantified by qPCR in NRP2-depleted MDA-MB-231 cells. Data are mean ± SEM of n = 3 biological replicates. *H*.) NRP2-depleted MDA-MB-231 cells were transfected with an 8XGTIIC-luciferase reporter construct and assayed for TEAD transcriptional activity. Data are mean ± SEM of n = 3 biological replicates. * $p \leq 0.05$ by two-tailed *t* test.

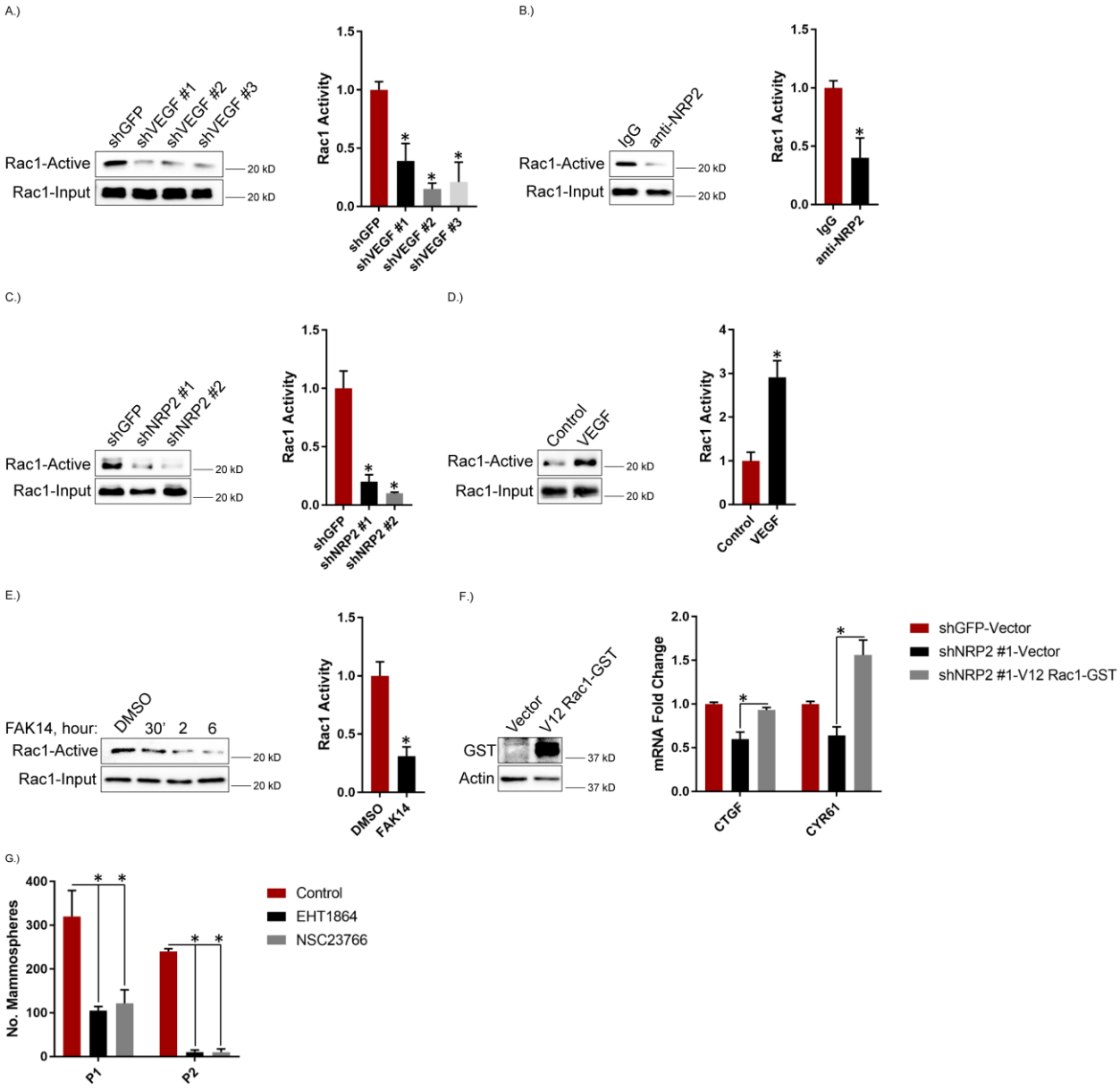

Figure 2.2: VEGF-NRP2 Signaling Activates Rac1. *A.*) Expression of VEGF was diminished in MES cells and the impact on Rac1 activity was assessed using a GST fusion protein containing the Rac/cdc42 binding domain of PAK (PBD). Representative blots are shown. Densitometric values are provided as bar graphs (mean ± SEM) of n = 3 biological replicates. *B.*) MES cells were treated with 3 µg/mL of a function blocking NRP2 antibody

for 6 hours and assayed for Rac1 activity. Representative blots are shown. Densitometric values are provided as bar graphs (mean ± SEM) of n = 3 biological replicates. *C*.) NRP2 expression was diminished in MDA-MB-231 cells and the impact on Rac1 activity was assessed. Representative blots are shown. Densitometric values are provided as bar graphs (mean ± SEM) of n = 3 biological replicates. *D*.) MDA-MB-231 cells were serum-starved for 24 hours, treated with 50 ng/mL of VEGF for 30 minutes and assayed for Rac1 activity. Representative blots are shown. Densitometric values are provided as bar graphs (mean ± SEM) of n = 3 biological replicates. *E*.) MES cells were treated with 2 μM of FAK14 for the indicated time points and assayed for Rac1 activity. Representative blots are shown. Densitometric values are provided as bar graphs (mean ± SEM) of n = 3 biological replicates of MES cells treated with FAK14 for 6 hours. *F*.) NRP2 expression was diminished in MDA-MB-231 cells that were then transfected with constitutively active V12 Rac1-GST. GST expression was quantified by immunoblotting. mRNA expression of the indicated TAZ target genes was quantified by qPCR. Data are mean ± SEM of n = 3 biological replicates. *G*.) MES cells were treated with 50 μM of the Rac inhibitors EHT1864 or NSC23766 and assayed for self-renewal by serial passage mammosphere formation (P1: passage 1; P2: passage 2). Data are mean ± SEM of n = 3 biological replicates. * $p \leq 0.05$ by two-tailed *t* test.

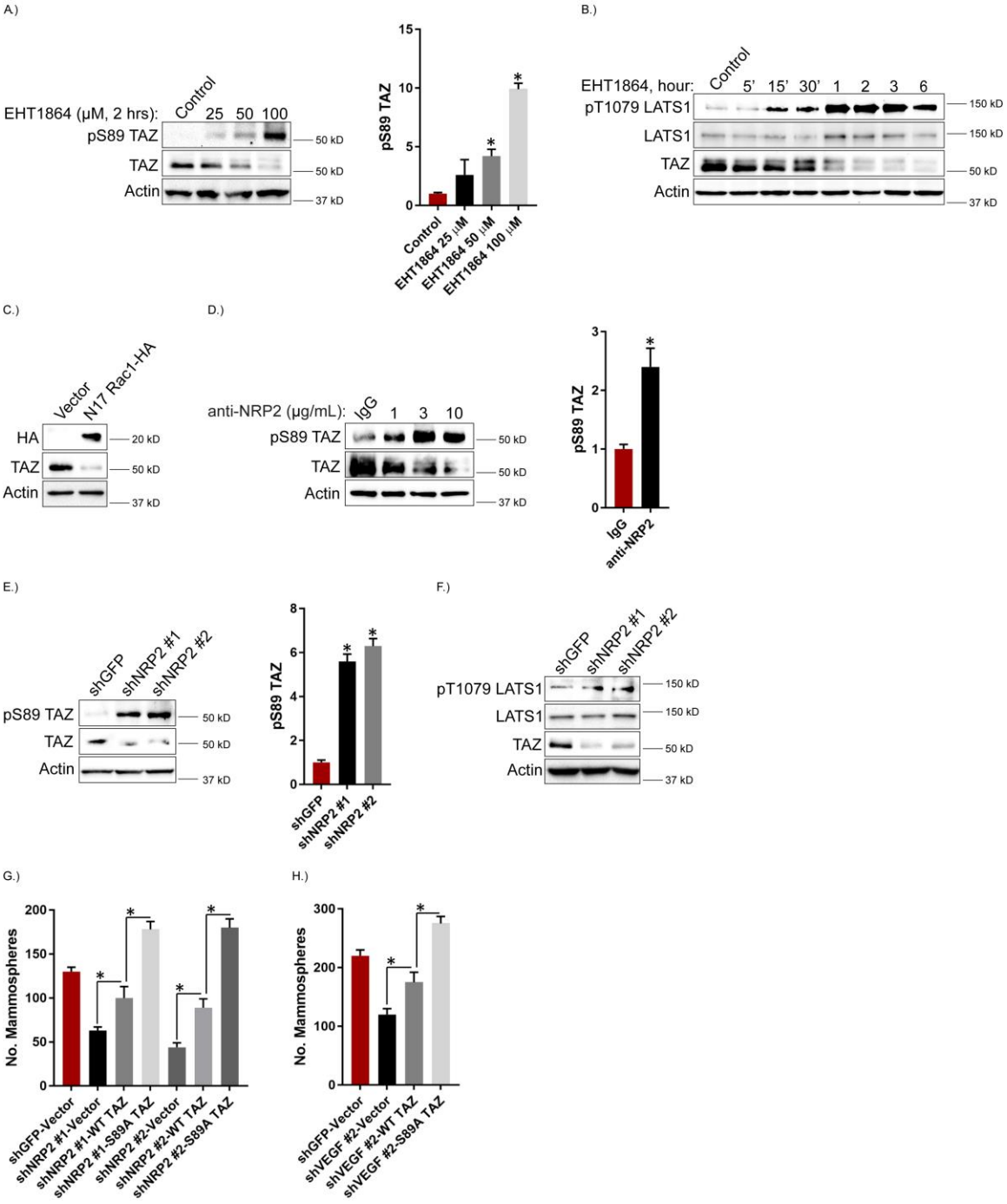
A.)
EHT1864 (μM, 2 hrs):
Control
25
50
100
pS89 TAZ
TAZ
Actin
50 kD
50 kD
37 kD
pS89 TAZ
Control
EHT1864 25 μM
EHT1864 50 μM
EHT1864 100 μM
B.)
EHT1864, hour:
Control
5'
15'
30'
1
2
3
6
pT1079 LATS1
LATS1
TAZ
Actin
150 kD
150 kD
50 kD
37 kD
C.)
Vector
N17 Rac1-HA
HA
TAZ
Actin
20 kD
50 kD
37 kD
D.)
anti-NRP2 (μg/mL):
IgG
1
3
10
pS89 TAZ
TAZ
Actin
50 kD
50 kD
37 kD
pS89 TAZ
IgG
anti-NRP2
E.)
shGFP
shNRP2 #1
shNRP2 #2
pS89 TAZ
TAZ
Actin
50 kD
50 kD
37 kD
pS89 TAZ
shGFP
shNRP2 #1
shNRP2 #2
F.)
shGFP
shNRP2 #1
shNRP2 #2
pT1079 LATS1
LATS1
TAZ
Actin
150 kD
150 kD
50 kD
37 kD
G.)
No. Mammospheres
shGFP-Vector
shNRP2 #1-Vector
shNRP2 #1-WT TAZ
shNRP2 #1-S89A TAZ
shNRP2 #2-Vector
shNRP2 #2-WT TAZ
shNRP2 #2-S89A TAZ
H.)
No. Mammospheres
shGFP-Vector
shVEGF #2-Vector
shVEGF #2-WT TAZ
shVEGF #2-S89A TAZ

Figure 2.3: Rac1 Facilitates VEGF-NRP2 Activation of TAZ through Inhibition of LATS. *A.*) MES cells were treated with the indicated concentrations of the Rac inhibitor EHT1864 for 2 hours and the impact on $pSer^{89}$ TAZ and TAZ abundance was quantified by immunoblotting. Representative blots are shown. Densitometric values are provided as bar graphs (mean ± SEM) of n = 3 biological replicates. *B.*) MES cells were treated with the Rac inhibitor EHT1864 (100 µM), lysed at the indicated time points and the impact on $pThr^{1079}$ LATS1, LATS1 and TAZ abundance was quantified by immunoblotting. Data are representative of n = 2 biological replicates. *C.*) MES cells were transfected with dominant negative N17 Rac1-HA and the impact on TAZ abundance was quantified by immunoblotting. Data are representative of n = 2 biological replicates. *D.*) MES cells were treated with the indicated concentrations of a function-blocking NRP2 antibody for 6 hours and the impact on $pSer^{89}$ TAZ and TAZ abundance was quantified by immunoblotting. Representative blots are shown. Densitometric values are provided as bar graphs (mean ± SEM) of n = 3 biological replicates of MES cells treated with 3 µg/mL of the NRP2 function-blocking antibody. *E.*) NRP2 expression was diminished in MDA-MB-231 cells and the impact on $pSer^{89}$ TAZ and TAZ abundance was quantified by immunoblotting. Representative blots are shown. Densitometric values are provided as bar graphs (mean ± SEM) of n = 3 biological replicates. *F.*) NRP2 expression was diminished in MDA-MB-231 cells and the impact on $pThr^{1079}$ LATS1 and LATS1 was quantified by immunoblotting. Data are representative of n = 2 biological replicates. *G.*) NRP2-depleted MDA-MB-231 cells were transfected with empty vector, wild-type TAZ or S89A TAZ and assayed for self-renewal by serial passage mammosphere formation.

Data are mean ± SEM of n = 3 biological replicates. *H*.) VEGF-depleted MES cells were transfected with empty vector, wild-type TAZ or S89A TAZ and assayed for self-renewal by serial passage mammosphere formation. Error bars indicate standard deviation from 3 technical replicates. Data are representative of n = 2 biological replicates. * $p \leq 0.05$ by two-tailed *t* test.

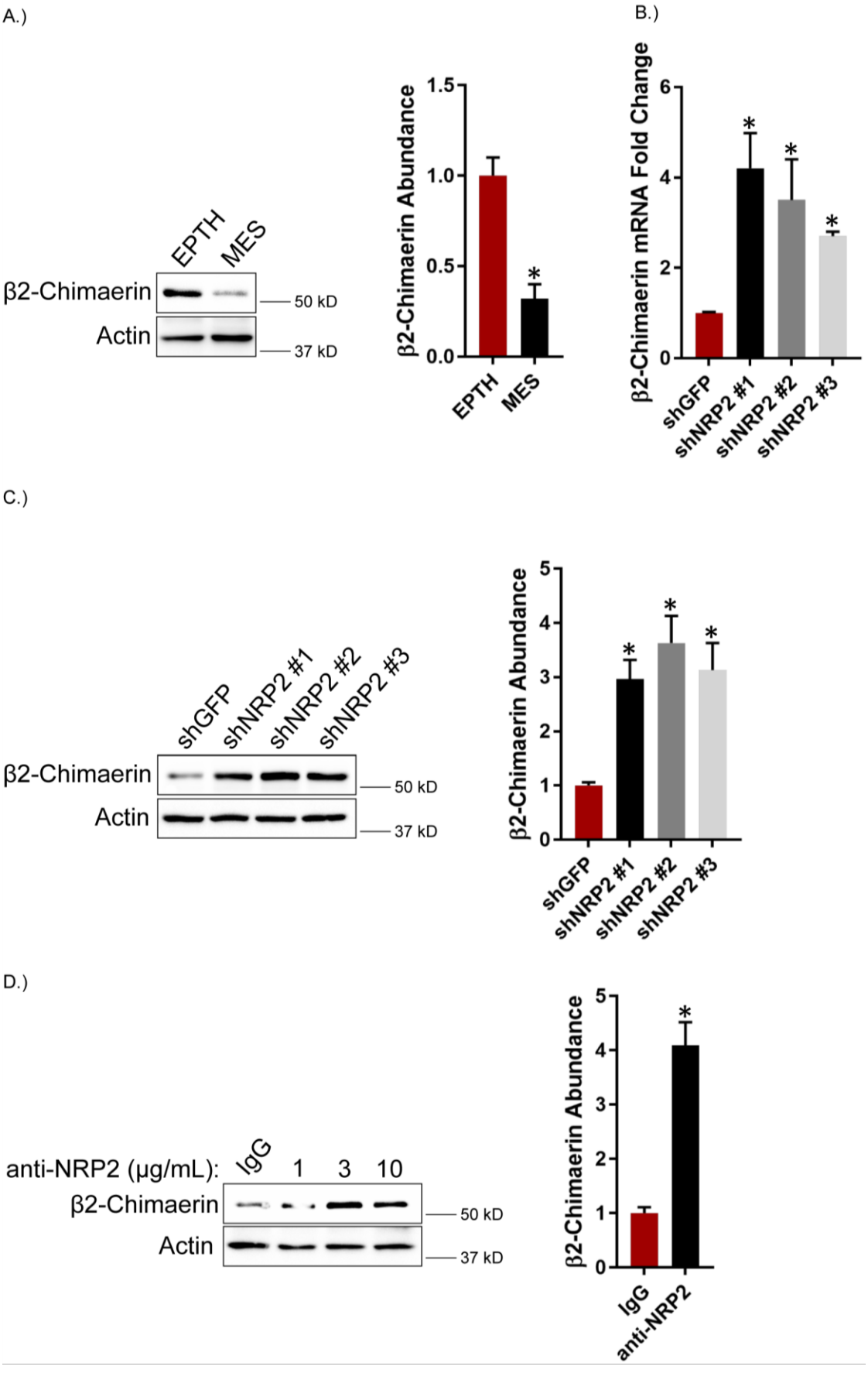
A.)
EPTH
MES
β2-Chimaerin
Actin
50 kD
37 kD
β2-Chimaerin Abundance
1.5
1.0
0.5
0.0
EPTH
MES
B.)
β2-Chimaerin mRNA Fold Change
6
4
2
0
shGFP
shNRP2 #1
shNRP2 #2
shNRP2 #3
C.)
shGFP
shNRP2 #1
shNRP2 #2
shNRP2 #3
β2-Chimaerin
Actin
50 kD
37 kD
β2-Chimaerin Abundance
5
4
3
2
1
0
D.)
anti-NRP2 (μg/mL):
IgG
1
3
10
β2-Chimaerin
Actin
50 kD
37 kD
β2-Chimaerin Abundance
5
4
3
2
1
0
IgG
anti-NRP2

Figure 2.4: VEGF-NRP2 Signaling Represses the Rac GAP β2-chimaerin. *A.*) Abundance of β2-chimaerin was quantified by immunoblotting in EPTH and MES cells. Representative blots are shown. Densitometric values are provided as bar graphs (mean ± SEM) of n = 3 biological replicates. *B.*) Expression of NRP2 was diminished in MES cells and *β2-chimaerin* mRNA expression was quantified by qPCR. Data are mean ± SEM of n = 3 biological replicates. *C.*) β2-chimaerin abundance was quantified by immunoblotting in NRP2-depleted MES cells. Representative blots are shown. Densitometric values are provided as bar graphs (mean ± SEM) of n = 3 biological replicates. *D.*) MES cells were treated with the indicated concentrations of a function blocking NRP2 antibody for 6 hours and abundance of β2-chimaerin was quantified by immunoblotting. Representative blots are shown. Densitometric values are provided as bar graphs (mean ± SEM) of n = 3 biological replicates of MES cells treated with 3 μg/mL of the NRP2 function-blocking antibody. * $p \leq 0.05$ by two-tailed *t* test.

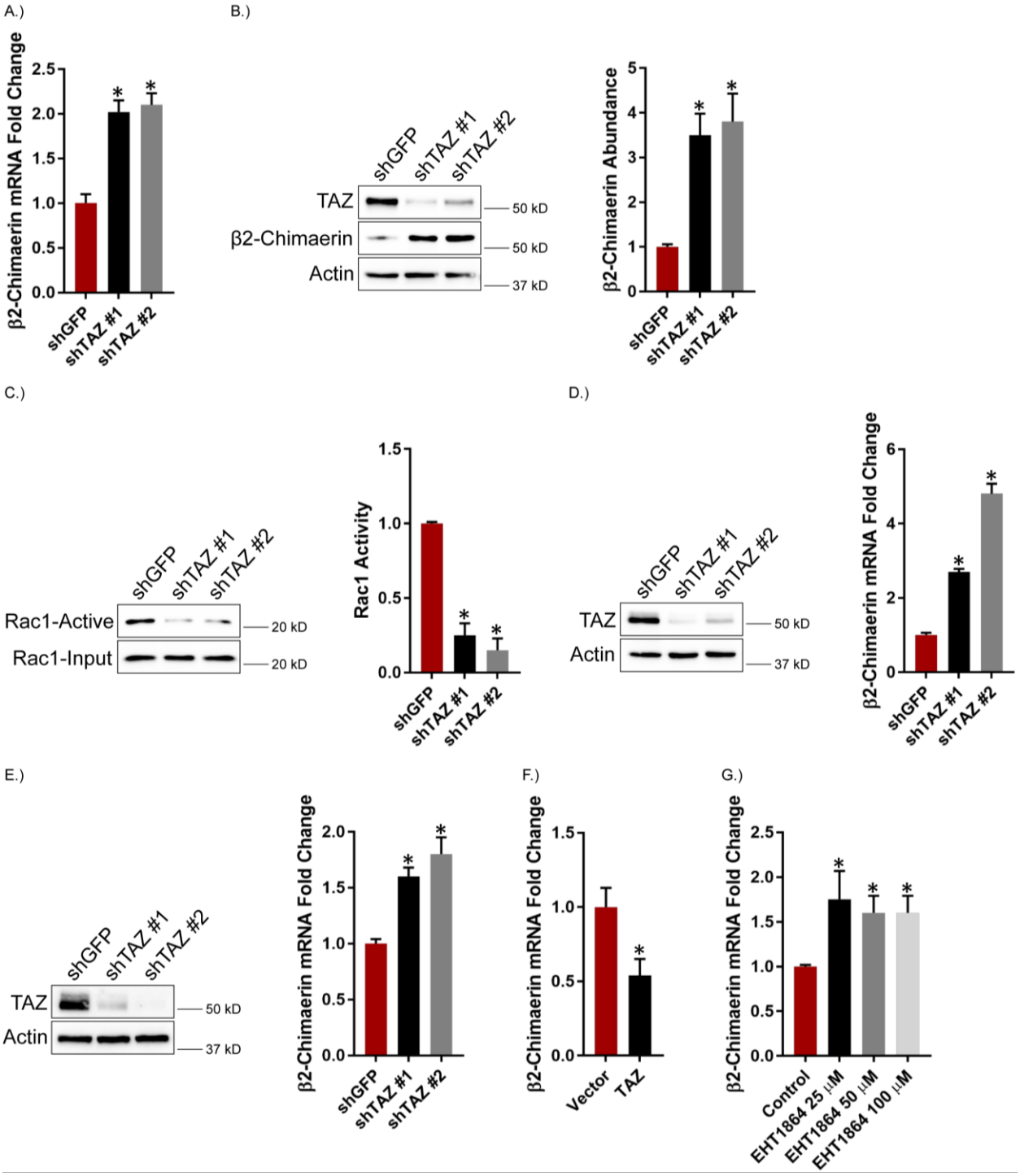

Figure 2.5: TAZ Activates Rac1 by Repressing β2-chimaerin. *A.*) TAZ expression was diminished in MES cells and the impact on *β2-chimaerin* mRNA expression was quantified

by qPCR. Data are mean ± SEM of n = 3 biological replicates. (*B* and *C*) β2-chimaerin abundance (*B*) and Rac1 activity (*C*) were assessed in TAZ knockdown MES cells. Representative blots are shown. Densitometric values are provided as bar graphs (mean ± SEM) of n = 3 biological replicates. *D.*) TAZ expression was diminished in MDA-MB-435 cells and the impact on *β2-chimaerin* mRNA expression was quantified by qPCR. Data are mean ± SEM of n = 3 biological replicates. *E*.) TAZ expression was diminished in MDA-MB-231 cells and the impact on *β2-chimaerin* mRNA expression was quantified by qPCR. Data are mean ± SEM of n = 3 biological replicates. *F*.) MDA-MB-231 cells were transfected with TAZ and the impact on *β2-chimaerin* mRNA expression was quantified by qPCR. Data are mean ± SEM of n = 3 biological replicates. *G*.) MES cells were treated with the indicated concentrations of the Rac inhibitor EHT1864 for 2 hours and *β2-chimaerin* mRNA expression was quantified by qPCR. Data are mean ± SEM of n = 3 biological replicates. * $p \leq 0.05$ by two-tailed *t* test.

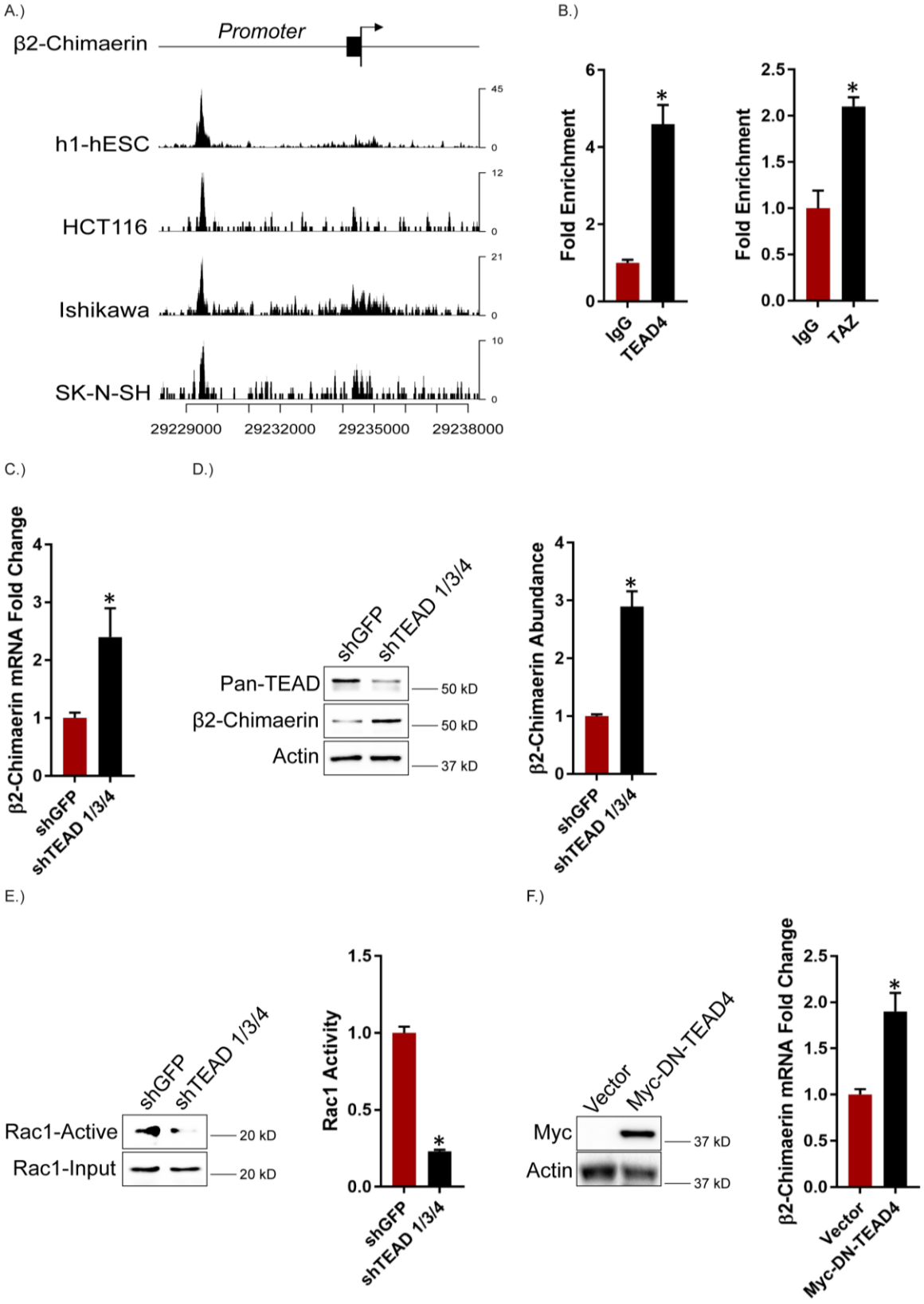
A.)
β2-Chimaerin
Promoter
h1-hESC
HCT116
Ishikawa
SK-N-SH
45
0
12
0
21
0
10
0
29229000
29232000
29235000
29238000
B.)
Fold Enrichment
IgG
TEAD4
IgG
TAZ
C.)
β2-Chimaerin mRNA Fold Change
shGFP
shTEAD 1/3/4
D.)
shGFP
shTEAD 1/3/4
Pan-TEAD
β2-Chimaerin
Actin
50 kD
50 kD
37 kD
β2-Chimaerin Abundance
shGFP
shTEAD 1/3/4
E.)
shGFP
shTEAD 1/3/4
Rac1-Active
Rac1-Input
20 kD
20 kD
Rac1 Activity
shGFP
shTEAD 1/3/4
F.)
Vector
Myc-DN-TEAD4
Myc
Actin
37 kD
37 kD
β2-Chimaerin mRNA Fold Change
Vector
Myc-DN-TEAD4

Figure 2.6: TEAD Mediates Repression of β2-chimaerin by TAZ. *A.*) Using ENCODE, TEAD4 binding signals were analyzed from ChIP-seq datasets from h1-hESCs (human embryonic stem cells), HCT116 (colon cancer), Ishikawa (endometrial adenocarcinoma) and SK-N-SH (neuroblastoma) cells in the promoter region of the β2-chimaerin gene. *B.*) Binding of TEAD4 and TAZ on the β2-chimaerin promoter was analyzed using ChIP in MES cells. Error bars indicate standard deviation from 3 technical replicates. Data are representative of n = 2 biological replicates. *C.*) TEAD 1/3/4 expression was diminished in MES cells and the impact on *β2-chimaerin* mRNA expression was quantified by qPCR. Data are mean ± SEM of n = 3 biological replicates. (*D* and *E*) β2-chimaerin abundance (*D*) and Rac1 activity (*E*) were assessed in TEAD 1/3/4 knockdown MES cells. Representative blots are shown. Densitometric values are provided as bar graphs (mean ± SEM) of n = 3 biological replicates. *F.*) *β2-chimaerin* mRNA expression was quantified by qPCR in MDA-MB-231 cells expressing either a control vector or dominant-negative TEAD4. Data are mean ± SEM of n = 3 biological replicates. * $p \leq 0.05$ by two-tailed *t* test.

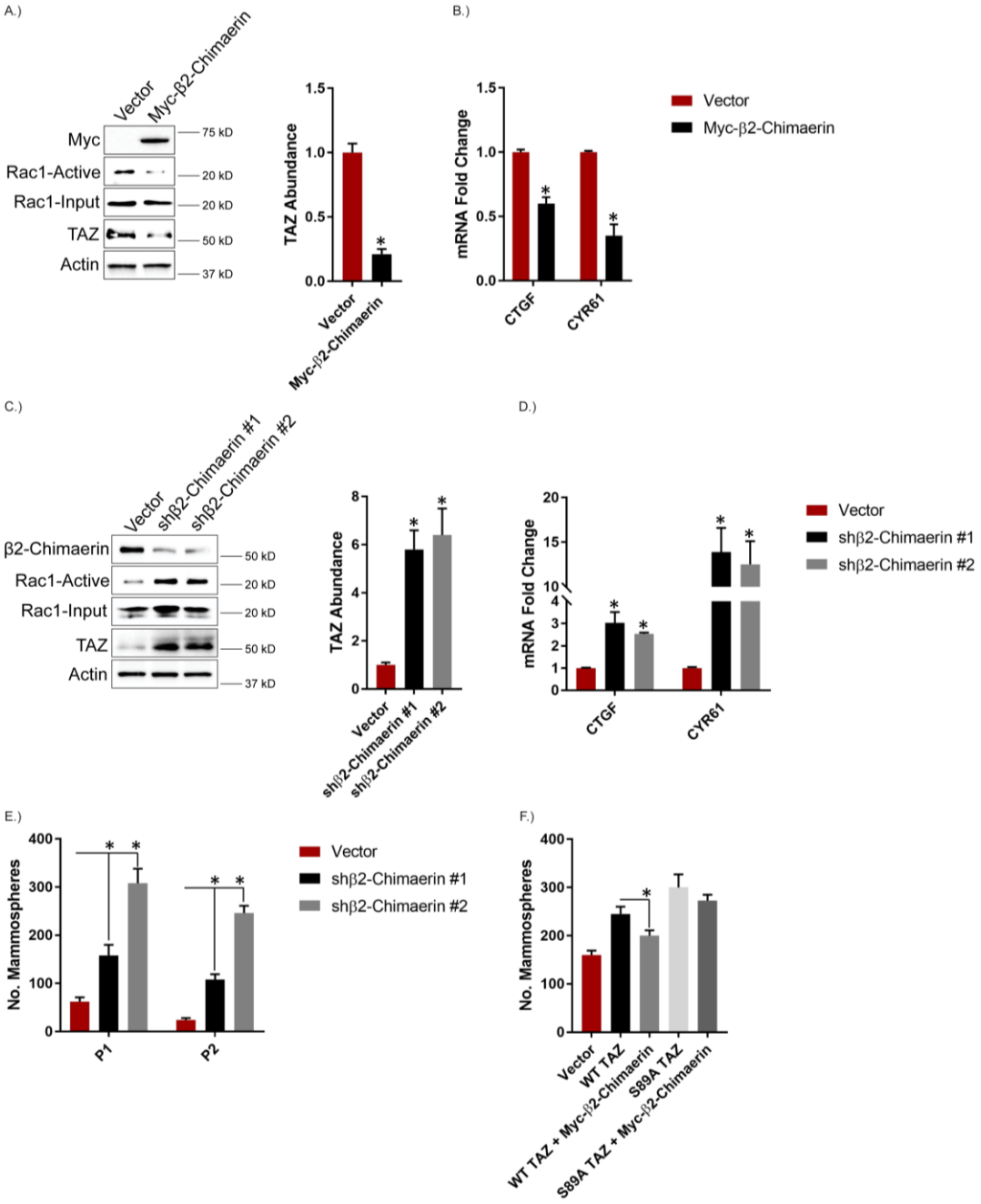

G.)

Invasive Breast Carcinoma

Gene Analysis	Log Odds Ratio	*p* Value	No. Patients
TAZ vs. β2-Chimaerin	-2.2	0.002	1093
TAZ vs. NRP2	+1.7	<0.001	1093
TAZ vs. VEGFA	+1.4	<0.001	1093

TAZ vs. β2-Chimaerin

Cancer Type	Log Odds Ratio	*p* Value	No. Patients
Glioblastoma	-3	0.055	160
Colorectal Adenocarcinoma	-3	0.086	244
Cancer Cell Line Encyclopedia	-1.4	0.021	-

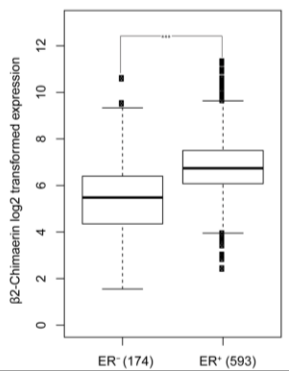

Figure 2.7: β2-chimaerin Repression Contributes to Enhanced TAZ activity. *A.*) MDA-MB-231 cells were transfected with Myc-tagged β2-chimaerin and Rac1 activity and TAZ abundance were assessed. Representative blots are shown. Densitometric values are provided as bar graphs (mean ± SEM) of n = 3 biological replicates. *B.*) mRNA expression of the indicated TAZ target genes was quantified by qPCR in MDA-MB-231 cells transfected with Myc-tagged β2-chimaerin. Data are mean ± SEM of n = 3 biological replicates. *C.*) Expression of β2-chimaerin was diminished in EPTH cells and the impact on Rac1 activity and TAZ abundance were assessed. Representative blots are shown. Densitometric values are provided as bar graphs (mean ± SEM) of n = 3 biological replicates. *D.*) mRNA expression of the indicated TAZ target genes was quantified by qPCR in β2-chimaerin-depleted EPTH cells. Data are mean ± SEM of n = 3 biological replicates. *E.*) β2-chimaerin-depleted EPTH cells were assayed for self-renewal by serial passage mammosphere formation (P1: passage 1; P2: passage 2). Data are mean ± SEM of n = 3 biological replicates. *F.*) MDA-MB-231 cells were transfected with empty vector, wild-type TAZ or S89A TAZ with and without Myc-tagged β2-chimaerin and assayed for self-renewal by serial passage mammosphere formation. Error bars indicate standard deviation from 3 technical replicates. Data are representative of n = 2 biological replicates. *G.*) cBioPortal for cancer genomics was used to compare TAZ expression with β2-chimaerin, NRP2 and VEGFA expression in the invasive breast carcinoma dataset from the Cancer Genome Atlas (TCGA). The expression of TAZ vs. β2-chimaerin was also compared in the TCGA glioblastoma and colorectal adenocarcinoma databases as well as the cancer cell line encyclopedia (967 cell lines). Log odds ratios and *p* values were

calculated using fisher exact *t* test with the mutual exclusivity tool on cBioPortal. *H.*) cBioPortal for cancer genomics was used to analyze the expression of β2-chimaerin in ER^+ vs. ER^- breast cancer patients from the TCGA invasive breast carcinoma database. * $p \leq 0.05$ by two-tailed *t* test; *** $p < 0.0001$ by Welch *t* test.

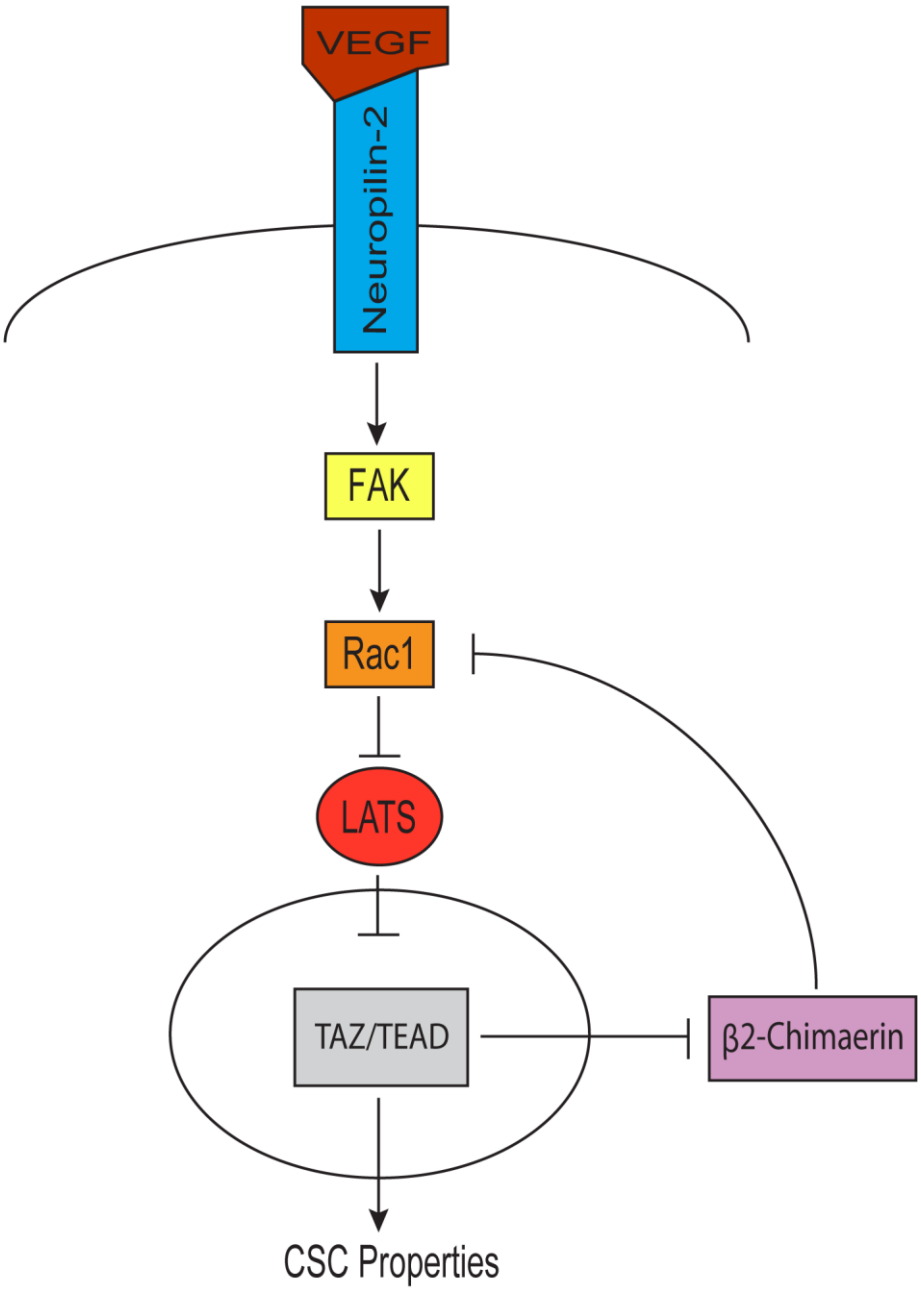

Figure 2.8: Model depicting the major findings of this study. VEGF-NRP2 signaling promotes FAK-mediated Rac1 activation, which inhibits LATS. Consequently, TAZ is

located in the nucleus where it associates with TEAD and represses the Rac GAP β2-chimaerin to maintain elevated Rac1 activity in a positive feedback loop.

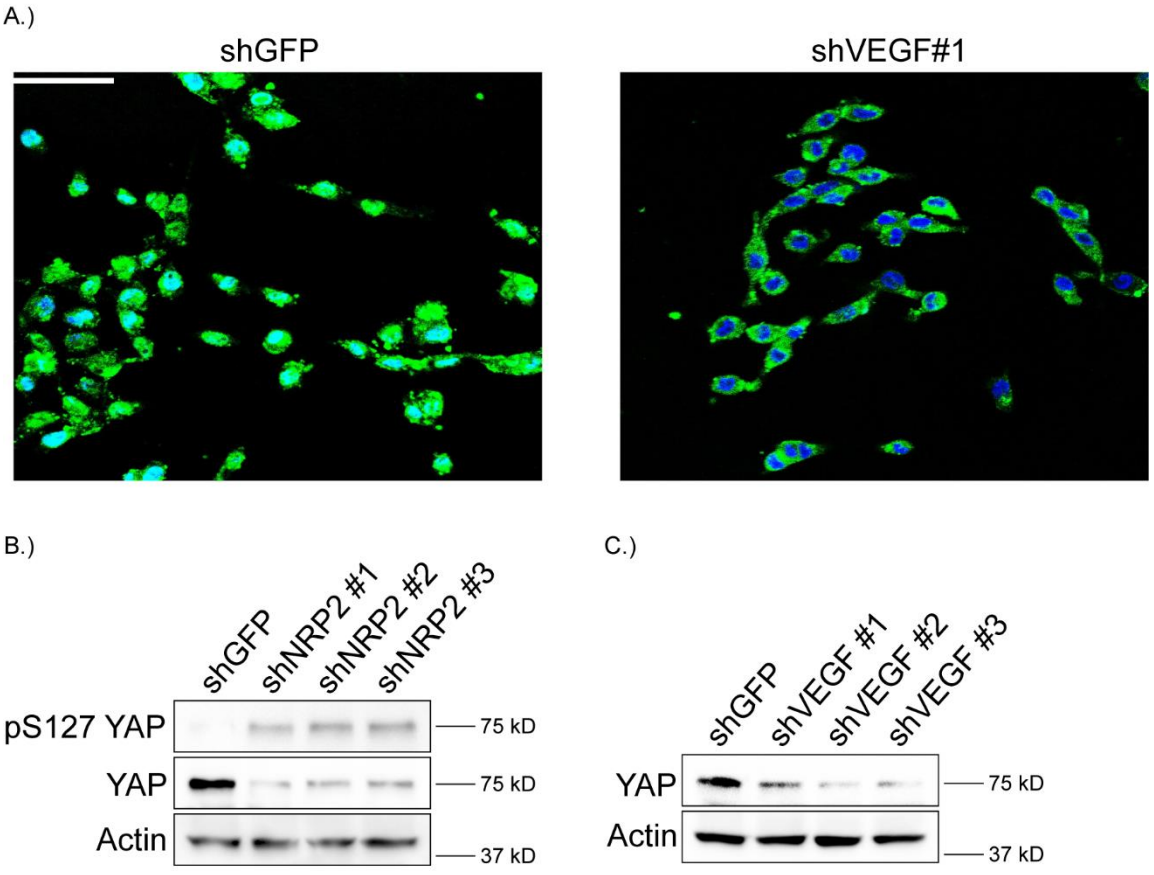

Figure 2.9. VEGF-NRP2 Signaling Contributes to YAP Activation. **(A)** TAZ localization (green) in control and VEGF-depleted MES cells was determined by immunofluorescence confocal microscopy. The nucleus is stained with DAPI (blue). Scale bar, 20 μm. Data are representative of n = 3 biological replicates. **(B)** Expression of NRP2 was diminished in MES cells and the impact on pSer^{127} YAP and YAP abundance was assessed by immunoblotting. Data are representative of n = 2 biological replicates. **(C)** Expression of VEGF was diminished in MES cells and the impact on YAP abundance was assessed by immunoblotting. Data are representative of n = 2 biological replicates.

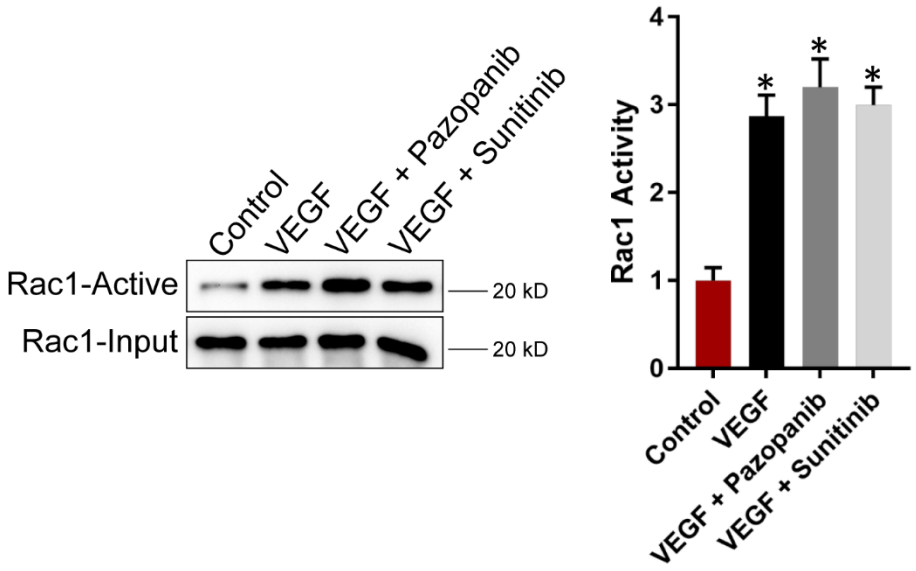

Figure 2.10. VEGF-NRP2 Activation of Rac1 is independent of VEGFR. MDA-MB-231 cells were serum-starved for 24 hours, treated with VEGF (50 ng/mL) with or without Pazopanib or Sunitinib (as indicated; each 2 μM) for 30 min and assayed for Rac1 activity. Representative blots are shown. Densitometry are mean ± SEM of n = 3 biological replicates.

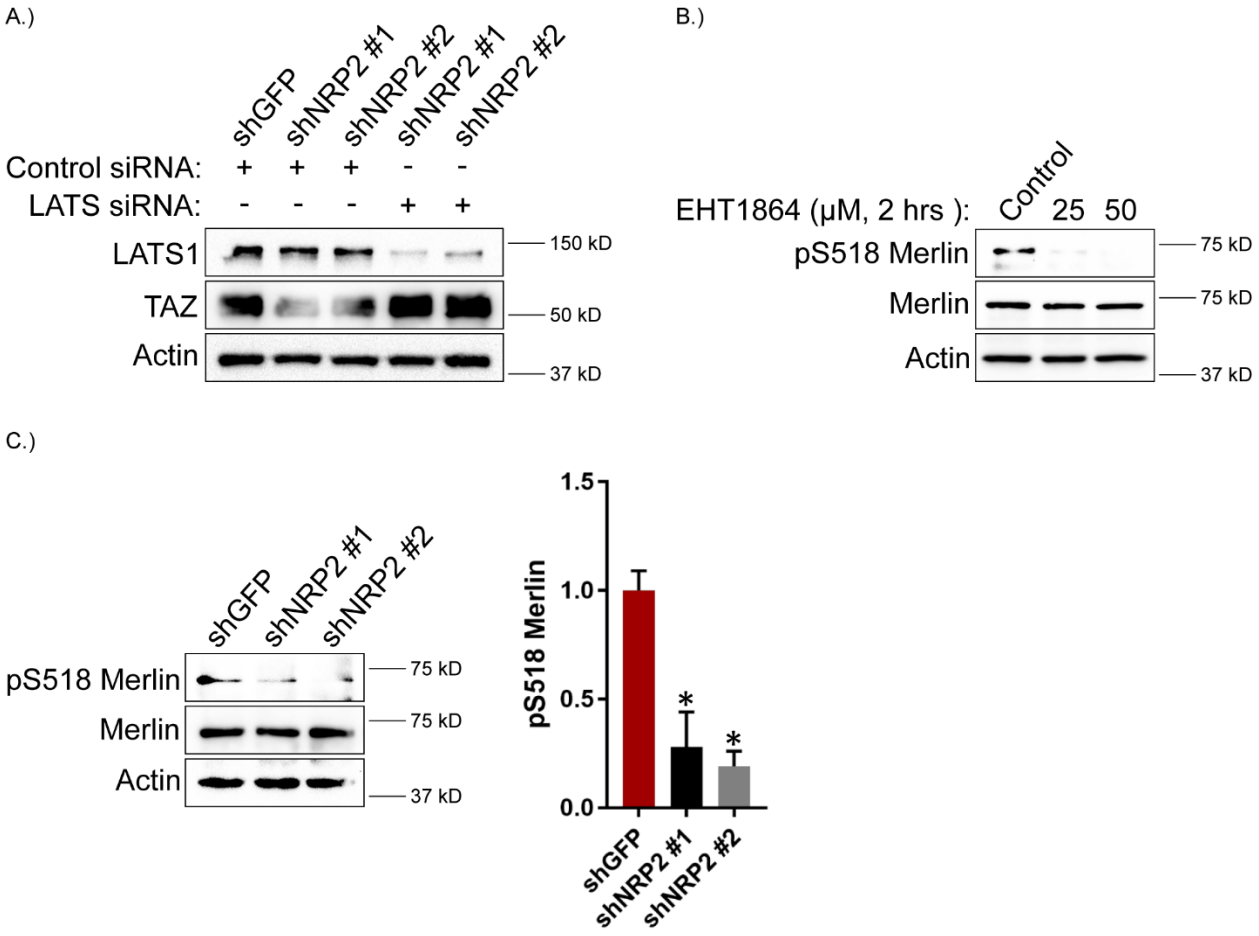

Figure 2.11. VEGF-Neuropilin-2-Rac1 Regulation of Merlin Phosphorylation (pSer^{518}) is LATS Dependent. (A) NRP2 expression was diminished in MDA-MB-231 cells which were then transfected with control siRNA or LATS 1/2 siRNA (20 nM). Approximately 48 hours after transfection, the impact on TAZ abundance was assessed by immunoblotting. Data are representative of n = 2 biological replicates. **(B)** MES cells were treated with the indicated concentrations of the Rac inhibitor EHT1864 for 2 hours and the impact on pSer^{518} Merlin and Merlin was assessed by immunoblotting. Data are

representative of n = 2 biological replicates. **(C)** NRP2 expression was diminished in MES cells and the impact on pSer^{518} Merlin and Merlin was quantified by immunoblotting. Representative blots are shown. Densitometric values are provided as bar graphs (mean ± SEM) of n = 3 biological replicates.

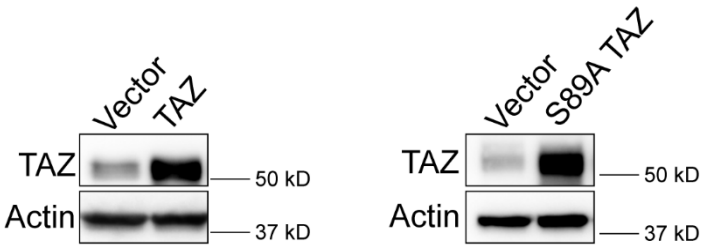

Figure 2.12. Expression of Wild-Type and S89A TAZ Constructs. MDA-MB-231 cells were transfected with empty vector, wild-type TAZ or S89A TAZ and processed for immunoblotting.

Gene	TGF-β trx (EMT) log fc	Adjusted *p* Value
E-Cadherin	-3.6	2.7×10^{-6}
Vimentin	+0.4	4.0×10^{-3}
β2-Chimaerin	-0.9	8.0×10^{-4}
VEGF	+1.7	1.3×10^{-5}
NRP2	+0.9	2.0×10^{-4}
CTGF	+1.7	6.8×10^{-5}
CYR61	+1.7	2.2×10^{-5}

Figure 2.13. β2-chimaerin is Repressed by the EMT. The indicated genes from a microarray (accession number GSE48204) using TGF-β to induce an EMT in NMuMG mammary epithelial cells were analyzed. Log fold change (fc) in expression and adjusted *p* values are shown.

	EPTH	MES
GEFs		
PRex1	NE	NE
PRex2	NE	NE
Tiam1	1 (0.13)	0.52 (0.04)
Tiam2	NE	NE
SOS1	1 (0.01)	0.62 (0.04)
ARHGEF7	1 (0.08)	1.1 (0.01)
Dock1	1 (0.08)	0.56 (0.13)
VAV1	NE	NE
VAV2	1 (0.07)	0.63 (0.02)
VAV3	1 (0.1)	0.69 (0.17)
Trio	1 (0.05)	0.76 (0.02)
GAPs		
β2-chimaerin	1 (0.08)	0.16 (0.07)
ARHGAP10	1 (0.05)	0.7 (0.05)

Table 2.1: mRNA screen of Rac GEFs and GAPs in EPTH and MES cells. The expression of the indicated Rac GEFs and GAPs was compared in EPTH and MES cells using qPCR. Table 1 shows fold change in mRNA expression upon normalization with EPTH cells, which was set as 1. NE indicates not expressed. Numbers in parentheses indicate standard deviation.

CHAPTER III

The VEGF receptor neuropilin-2 promotes homologous recombination by stimulating YAP/TAZ-mediated Rad51 expression

Ameer L. Elaimy, John J. Amante, Lihua Julie Zhua, Mengdie Wang, Charlotte Walmsley, Hira Lal Goel and Arthur M. Mercurio

CONTRIBUTIONS:

Ameer L. Elaimy conceptualized the study, performed experiments, made the figures and wrote the manuscript. John J. Amante contributed to flow cytometry experiments. Lihua Julia Zhu performed bioinformatics analyses. Mengdie Wang aided in genetic depletion studies. Charlotte Walmsley contributed to the olaparib experiment. Hira Lal Goel cultured organoids and provided feedback on data. Arthur M. Mercurio oversaw and conceptualized the study, provided feedback on experiments and wrote the manuscript.

Introduction

The role of vascular endothelial growth factor (VEGF) in cancer is not limited to angiogenesis and vascular biology (34, 35, 41, 115). Tumor cells express VEGF receptors and VEGF signaling in these cells has been implicated in the aggressive nature and chemoresistance of many cancers, independently of its function in angiogenesis (42). In addition to tyrosine kinase VEGF receptors (VEGFR1 and VEGFR2), tumor cells express neuropilins (NRPs), another family of VEGF receptors. Although NRPs have the ability to interact with and regulate VEGFR1 and VEGFR2 (62, 117), they can also mediate VEGF signaling in tumor cells independently of these tyrosine kinase receptors (45, 60, 63, 64, 174). The fact that VEGF-NRP signaling is characteristic of more aggressive tumors that often respond poorly to therapy has profound clinical implications and it heightens the importance of understanding how VEGF-NRP signaling promotes resistance. This problem is exemplified in aggressive breast cancers, such as the triple-negative subtype (TNBC), that manifest VEGF-NRP2 signaling (68) and are resistant to standard therapy (8).

One potentially promising area that has not been explored rigorously with respect to VEGF-NRP signaling in breast and other cancers is its contribution to DNA repair pathways. The integrity of such pathways is a major reason for resistance to therapy. Specifically, the ability to execute efficient homologous recombination (HR) DNA repair is considered to be critical for the ability of tumors to resist platinum-based chemotherapies, poly (ADP-ribose) polymerase (PARP) inhibitors and radiation therapy (175). Conversely, HR deficiency, which is most often attributed to germline *BRCA 1/2*

mutations or loss of *BRCA 1* expression through promoter hypermethylation in breast cancer, provides an 'Achilles heel' that renders sensitivity to these agents. For example, clinical studies have demonstrated favorable outcomes of TNBC patients with HR deficiency treated with neoadjuvant platinum chemotherapy (28, 30-33). However, only 11-15% of TNBC patients harbor germline *BRCA* mutations (25, 27), a fact that indicates that many TNBCs are HR proficient and, consequently, resistant to therapies that induce DNA damage. In this study, we investigated the potential contribution of VEGF-NRP2 signaling to HR in breast cancer cells, and we pursued the mechanism involved. The results obtained validate our hypothesis and they reveal that VEGF-NRP2 signaling regulates Rad51, a central HR enzyme that catalyzes homology strand exchange and facilitates the repair of damaged DNA (176). Importantly, we also made the novel observation that the ability of VEGF-NRP2 signaling to regulate Rad51 is mediated by YAP/TAZ and that Rad51 is a novel YAP/TAZ target gene.

Results

VEGF-NRP2 promotes protection from DNA damaging agents. Initially, we assessed the potential contribution of NRP2 and VEGF in the response of TNBC cells to DNA damage. We focused our attention on cisplatin because platinum chemotherapy is particularly effective for tumors with HR deficiency (28, 30-33). For this purpose, we depleted NRP2 and VEGF with short hairpin RNAs (shRNAs) in MDA-MB-231 cells, a *BRCA 1* wild type TNBC cell line (177) that exhibits VEGF-NRP2 signaling (63, 130),

and assessed DNA damage by measuring γH2AX levels. We observed that NRP2 and VEGF depletion resulted in increased DNA damage in comparison to cisplatin-treated control cells (**Fig. 3.1A**). Similar results were obtained with NRP2 depletion in response to cisplatin in Hs578t cells, which are another *BRCA 1* wild type TNBC cell line (177) that expresses VEGF and NRP2 (**Fig. 3.1B**). Negligible γH2AX was detected under baseline conditions in control and NRP2 and VEGF depleted MDA-MB-231 cells (**Fig. 3.8A**).

VEGF-NRP signaling can function in TNBC and other cancer cells independently of the VEGFRs (45, 60, 63, 64, 174). This observation is significant because bevacizumab, the most common anti-VEGF therapy, blocks VEGF binding to VEGFRs, but it does not disrupt the VEGF-NRP association or signaling (2). To assess the relative contribution of NRP2 and VEGFRs to the protection of TNBC cells from cisplatin-induced DNA damage, we treated Hs578t cells with cisplatin in the presence of a NRP2-function blocking antibody (65) or bevacizumab and observed that NRP2 inhibition resulted in increased γH2AX abundance relative to cisplatin-treated control cells, but that bevacizumab did not (**Fig. 3.1C**). We substantiated these results by treating *BRCA* proficient mouse mammary tumor organoids, which were established to exhibit resistance to HR-inducing agents (178), with either cisplatin, the NRP2 function blocking antibody, bevacizumab, or combinations of these reagents, and observed that NRP2 inhibition sensitizes these tumor organoids to cisplatin but that bevacizumab does not (**Fig. 3.1D**). These findings indicate that VEGF-NRP2 signaling mediates protection from cisplatin-induced DNA damage independently of the VEGFRs.

Following the results obtained with cisplatin, we next sought to determine if VEGF-NRP2 mediates resistance to a broader variety of agents used in TNBC. We focused our attention on PARP inhibition and ionizing radiation (IR). Indeed, we observed that NRP2 depletion sensitizes Hs578t cells to olaparib (**Fig. 3.8B**) and IR (Fig. 8C). Similar to our results with cisplatin, treatment of Hs578t cells with IR and the NRP2 function blocking antibody resulted in increased γH2AX abundance compared to radiation-treated control cells (**Fig. 3.8D**).

YAP/TAZ are necessary for VEGF-NRP2 protection from cisplatin-induced DNA damage. The hippo pathway transducers YAP and TAZ are critical downstream effectors of VEGF signaling in several distinct cell types (179). Moreover, VEGF-NRP2 activation of YAP/TAZ in TNBC cells occurs through a VEGFR-independent mechanism (63). For these reasons, we hypothesized that VEGF-NRP2 promotes genomic integrity and cisplatin resistance through downstream YAP/TAZ activation. To test this hypothesis, we assessed DNA damage in response to cisplatin in NRP2-depleted Hs578t cells expressing the S89A TAZ mutant, which is resistant to inhibitory phosphorylation at that site (127), or empty vector and found that S89A TAZ rescued the increase in γH2AX observed upon NRP2 depletion (**Fig. 3.2A**). Importantly, S89A TAZ also rescued cell viability in NRP2-depleted Hs578t cells treated with cisplatin (**Fig. 3.2B**). Similar results were obtained in Hs578t cells expressing S127A YAP, which is resistant to inhibitory phosphorylation at a homologous phosphorylation site (**Fig. 3.2C and D**) (127). Together, these data provide evidence that VEGF-NRP2 signaling protects the genome from DNA damage caused by cisplatin by a mechanism that involves downstream YAP/TAZ activation.

YAP/TAZ facilitate homologous recombination and contribute to Rad51 expression. Given that YAP/TAZ rescued the defects in DNA repair and cell viability in NRP2-depleted cells in response to cisplatin (**Fig. 3.2**), we assessed the potential contribution of YAP and TAZ to HR. For this purpose, we utilized the well-established HR reporter assay (DR-GFP) (180). This assay is based on the expression of functional GFP as a result of HR in response to a double-strand break induced by the I-SceI endonuclease, which can be quantified by flow cytometry. For this assay, we used MCF7 cells, a *BRCA 1* wild type ER^+ breast cancer cell line (177), engineered to stably express DR-GFP because they exhibit low YAP/TAZ activity. Consequently, expression of YAP/TAZ in these cells provides a robust system to study their role in HR. To ensure that the expressed YAP/TAZ were active, we used the S89A TAZ and S127A YAP mutants, which are resistant to inhibitory phosphorylation at those sites (127). Expression of either of these mutants in DR-GFP MCF-7 cells resulted in a significant increase in the number of GFP-positive cells following a double-strand break by I-SceI compared to control cells, providing evidence that YAP/TAZ contribute to HR (**Fig. 3.3A and Fig. 3.9A, B**).

To identify the mechanism by which YAP/TAZ promote HR, we analyzed published microarray data (GSE59230) (181) derived from YAP/TAZ depletion in MDA-MB-231 cells for significant alterations in the expression of genes that could contribute to HR. Most notably, the mRNA expression of Rad51, a central HR enzyme that catalyzes homology strand exchange and facilitates the repair of damaged DNA (176), was reduced in this microarray dataset upon YAP/TAZ depletion to a similar degree as the established YAP/TAZ target genes CTGF and Cyr61 (**Fig. 3.3B**). Rad51 mediates resistance of TNBC

cells to therapy (182), and its expression is up-regulated in breast and other cancer cells (182, 183), which may result from increased activity at its promoter (184, 185). However, mechanisms that control Rad51 transcription and function in specific tumors are poorly understood. Given this information, we developed the hypothesis that VEGF-NRP2 facilitates YAP/TAZ-mediated Rad51 expression and HR in TNBC.

Initially, we assessed whether a correlation exists between enhanced YAP/TAZ activity and Rad51 expression in patient samples. A YAP/TAZ gene signature, as well as elevated TAZ mRNA expression, is associated with hormone receptor negative, high-grade breast tumors (110, 111). Therefore, we analyzed the expression of Rad51 and compared it to markers of enhanced YAP/TAZ activity in patient tumors in the Metabric breast cancer database obtained from cBioPortal (162, 163). Specifically, we observed that Rad51 expression is higher in ER^- tumors compared to ER^+ tumors (**Fig. 3.3C**) and that Rad51 expression correlates positively with breast tumor grade (**Fig. 3.3D**), as well as with TAZ and the YAP/TAZ target genes CTGF and Cyr61 (**Fig. 3.3E**). We validated a causal role for YAP/TAZ in regulating Rad51 in MDA-MB-231 cells (**Fig. 3.4A**). Similarly, we observed that siRNA knockdown of YAP/TAZ in Hs578t cells reduced Rad51 abundance (**Fig. 3.4B**). Consistent with our results using YAP/TAZ siRNA, MDA-MB-231 cells with stable depletion of TAZ and treated with verteporfin to inhibit YAP exhibited a decrease in Rad51 mRNA expression (**Fig. 3.4C**). Similar results were obtained when assessing Rad51 protein abundance in response to shTAZ alone, verteporfin alone or the combination in MDA-MB-231 cells (**Fig. 3.4D**). A reduction in nuclear and total Rad51 abundance was also observed by immunofluorescence microscopy in YAP/TAZ-depleted MDA-MB-231

cells treated with cisplatin to induce HR (**Fig. 3.4E**). Conversely, expression of S89A TAZ in MCF7 DR-GFP cells increased Rad51 abundance (**Fig. 3.4F**). Together, these data indicate that a YAP/TAZ-Rad51 axis contributes to efficient HR in TNBC cells.

Rad51 is a YAP/TAZ-TEAD target gene. YAP/TAZ-mediated transcriptional regulation occurs through the TEAD 1-4 family of transcription factors (127, 146). TEAD4, in particular, has been shown to play a dominant role in TNBC (158, 159). In light of this information, we analyzed the encyclopedia of DNA elements (ENCODE) database for TEAD4 chromatin immunoprecipitation sequencing (ChIP-seq) experiments to determine if YAP/TAZ-dependent control of Rad51 expression occurs through a direct mechanism mediated by TEAD. We found four cell types in ENCODE (h1-human embryonic stem cells (hESCs), HCT116 colon cancer cells, Ishikawa endometrial adenocarcinoma cells and SK-N-SH neuroblastoma cells), which have been previously shown to have enhanced YAP/TAZ activity (161, 186), where TEAD4 bound directly to the promoter region of Rad51 (**Fig. 3.5A**). Subsequently, we performed ChIP in MDA-MB-231 and Hs578t cells to validate direct binding of TEAD4 to the Rad51 promoter in TNBC cells (**Fig. 3.5B**). To obtain additional evidence to implicate TEAD4 in Rad51 transcription, we used a Rad51 promoter luciferase assay (185). We expressed this reporter construct in MDA-MB-231 cells stably expressing dominant negative TEAD4 and observed a reduction in luciferase activity at the Rad51 promoter (**Fig. 3.5C**). Dominant negative TEAD4 also caused a decrease in Rad51 abundance (**Fig. 3.5D**). These results provide evidence that a YAP/TAZ-TEAD transcriptional program governs Rad51 expression and activity in TNBC.

Rad51 mediates VEGF-NRP2-YAP/TAZ-dependent DNA repair. A key issue that emerges from these findings is the role of YAP/TAZ-mediated Rad51 expression in DNA repair in the cellular response to cisplatin. As shown in **Fig. 6A and B**, YAP/TAZ depletion in Hs578t cells treated with cisplatin resulted in increased DNA damage as measured by γH2AX in comparison to cisplatin-treated control cells. Importantly, re-expression of Rad51 rescued the increase in γH2AX observed upon YAP/TAZ depletion (**Fig. 3.6A, B and 3.10A**). These results substantiate the data shown in **Fig. 3.3A and 3.9A**, **B** that YAP/TAZ contribute to HR and they provide evidence that YAP/TAZ-mediated HR occurs through downstream Rad51 expression. Similar to VEGF and NRP2 downregulation, negligible γH2AX was observed under baseline conditions in YAP/TAZ depleted Hs578t cells (**Fig. 3.10B**). We also assessed the effects of cisplatin and TAZ depletion on cell viability in MDA-MB-231 cells and observed that TAZ downregulation promotes cisplatin sensitization, which is rescued by Rad51 re-expression (**Fig. 6C and 3.10C**). Along these lines, we tested the effects of either cisplatin, verteporfin or the combination on *BRCA* proficient mouse mammary tumor organoids and observed that YAP inhibition with verteporfin sensitizes these tumor organoids to cisplatin (**Fig. 3.6D**), similar to the results obtained with NRP2 inhibition (**Fig. 3.1D**).

Given that *BRCA1* is required for Rad51-mediated HR (187), we hypothesized that YAP/TAZ should not affect DNA damage in *BRCA1* mutant cells. To test this hypothesis, we assessed DNA damage in response to cisplatin in SUM-1315 cells, which are a *BRCA1* mutant TNBC cell line (177). Notably, although we detected a reduction in Rad51

abundance, we did not observe an increase in γH2AX in response to cisplatin in cells depleted of TAZ and treated with verteporfin to inhibit YAP (**Fig. 3.11A and B**).

We postulated that the mechanism by which VEGF-NRP2 protects from DNA damage is through YAP/TAZ-mediated Rad51 expression. This postulate is based on the finding that VEGF-NRP2 signaling is an important upstream regulator of YAP/TAZ (63) and our observations that YAP and TAZ rescued the defects in DNA repair in NRP2-depleted cells (**Fig. 3.2**) and that Rad51 rescued the defects in DNA repair in YAP/TAZ-depleted cells (**Fig. 3.6A-C**). Indeed, we observed that both NRP2 and VEGF depletion in MDA-MB-231 cells reduced Rad51 abundance (Fig. **3.7A and B**). Stimulation of VEGF-depleted MDA-MB-231 cells with exogenous VEGF rescued the increase in γH2AX and reduction in Rad51 abundance in response to cisplatin (**Fig. 3.7C**). We also observed that treating Hs578t cells with the function-blocking NRP2 antibody reduces HR as measured by DR-GFP analysis (**Fig. 3.7D and 3.12A**). Importantly, we observed that inhibiting NRP2 in cells ectopically expressing Rad51 does not influence HR (**Fig. 7D and 3.12A**). This result provides evidence that downstream Rad51 expression is critical for VEGF-NRP2-mediated HR. Similar to our results inhibiting YAP/TAZ (**Fig. 3.6C and D**), Rad51 rescued cell viability in response to cisplatin in NRP2-depleted Hs578t cells (**Fig. 7E and 3.12B**). Lastly, in support of our *in vitro* data, we found that Rad51 expression correlates positively with VEGF and NRP2 in breast cancer patients in the Metabric dataset obtained from cBioPortal (**Fig. 7F**) (162, 163).

Discussion

The results of this study establish a significant and novel role for VEGF-NRP signaling in HR by promoting the expression and function of Rad51. Importantly, we also demonstrate that this novel mechanism is mediated by YAP/TAZ and that Rad51 is a YAP/TAZ target gene. These findings integrate salient characteristics of aggressive breast tumors: dependence on VEGF-NRP2 signaling (63, 68), hyper-activation of YAP/TAZ (110, 111) and high Rad51 expression (182, 188) into a unified mechanism that accounts for their therapy resistance. They also provide one mechanism for how Rad51 transcription is regulated in cancer, an area that is poorly understood.

Although many studies have revealed the importance of VEGF-NRP signaling in tumor cells, independently of its role in angiogenesis (42), its contribution to DNA repair mechanisms is novel and significant. Of note, VEGF-NRP signaling has been implicated in drug resistance in multiple tumors but satisfying mechanisms have been elusive (64, 189-191). Given that efficient HR is a key determinant of such resistance, our results implicating this signaling in HR-directed repair provides one such mechanism as exemplified by the data we obtained with cisplatin, olaparib and IR in breast cancer cells and organoids. Our results are timely because, for example, platinum chemotherapy has garnered interest in recent years as a therapeutic option for TNBC patients, especially those with loss of *BRCA* function and/or features of genomic instability (28, 30-33). However, the majority of TNBC patients do not have germline *BRCA* mutations and, accordingly, platinum analogues do not provide these patients with significant clinical benefits over mechanistically distinct drugs (33). We provide evidence for the causality of NRP

signaling in this resistance by demonstrating that HR-inducing agents are more efficacious in killing breast tumor cells and organoids when simultaneously inhibiting NRP2 function.

The second major advance provided by our data is that the Hippo pathway transcriptional effectors YAP and TAZ contribute to HR by regulating Rad51 transcription. Although considerable evidence indicates that these transcriptional co-activators contribute to the aggressive behavior and therapy resistance of TNBC and other cancers (110, 113), much remains to be learned about their transcriptional targets and how they function. From this perspective, our implication of their involvement in HR by regulating Rad51 is significant. Our previous work established that VEGF-NRP2 signaling activates YAP/TAZ (63), but the contribution of these critical Hippo effectors to DNA repair mechanisms was not known. Our findings mesh with the emerging view that YAP/TAZ mediate the transcriptional addiction of cancer cells, a process implicated in drug resistance (113). The implications of our data for therapy are potentially substantial because targeted inhibition of YAP/TAZ increases the sensitivity of breast cancer cells and organoids to cisplatin, which is similar to blocking NRP2. Moreover, the selectivity that either NRP2 or YAP/TAZ inhibition is likely to display towards transcriptional-addicted tumors is a viable experimental approach and it has the potential to limit toxicities that may be associated with Rad51 chemical inhibition (192).

Materials and Methods

Reagents, antibodies and cell culture. Verteporfin and cisplatin were purchased from Tocris, olaparib was purchased from Selleckchem and human VEGFA was purchased from R & D Systems. The NRP2 function blocking antibody was provided by Genentech (65). Bevacizumab was provided by the UMASS Medical School oncology pharmacy. Cisplatin was used at a concentration of 10 μM for 24 hours, verteporfin was used at a concentration of 2 μM for 24 hours, olaparib was used at a concentration of 20 μM for 24 hours and the NRP2 function blocking antibody and bevacizumab were used at a concentration of 10 μg/mL for 24 hours. Immunoblotting antibodies were acquired as follows: Actin (MA5-15739, Thermo Fisher Scientific), TAZ (560235, BD Biosciences), YAP/TAZ (8418S, Cell Signaling Technologies), Rad51 (8875S, Cell Signaling Technologies), NRP2 (AF2215, R & D Systems), γH2AX (05-636, Millipore), HA-tag (3724S, Cell Signaling Technologies), FLAG-tag (F3165, Sigma-Aldrich) and Myc-tag (2278S, Cell Signaling Technologies). MDA-MB-231 and Hs578t were obtained from the American Type Culture Collection and SUM-1315 cells were provided by Dr. Stephen Ethier.

Constructs, transfection and siRNA knockdown. shNRP2, shVEGF, shTAZ, S89A TAZ pcDNA 3.1 and Myc-tagged dominant negative TEAD4 were used as previously described (63). Retroviral S127A YAP (plasmid #33092) and lentiviral S89A TAZ (plasmid #52084) were purchased from Addgene. Rad51 was provided by Dr. Maria Jasin (Memorial Sloan Kettering Cancer Cancer) (180). Lipofectamine 3000 (Thermo Fisher Scientific) was used for plasmid expression and DharmaFect 4 (Dharmacon) was used for siRNA knockdown. YAP/TAZ siRNA has been previously described (100).

Cell viability assay and organoid culture. To assess viability, cells were seeded and subsequently treated with cisplatin, olaparib, IR, the NRP2 function blocking antibody, bevacizumab, verteporfin, or combinations the following day as described in the figure legends. After 24 hours, cells were washed with 1X phosphate-buffered saline (PBS) and complete medium was added. Cells were counted 3 days following treatment using trypan blue exclusion. Cell number was normalized to 1 based on the control sample. *BRCA* proficient mammary tumor organoids were provided by Dr. Jos Jonkers (Netherlands Cancer Institute) and cell viability was assessed as previously described (178).

Immunoblotting. Cells were scraped on ice in RIPA buffer with EDTA and EGTA (BP-115DG, Boston Bioproducts) supplemented with protease inhibitor cocktail (Roche, 04693132001). Subsequently, laemmli buffer (BP-111R, Boston Bioproducts) was added to each sample and the lysate was boiled and separated using sodium dodecyl sulfate polyacrylamide gel electrophoresis.

Luciferase reporter assay. The Rad51 promoter luciferase construct was provided by Dr. Vera Gorbunova (University of Rochester) and Dual-Luciferase Reporter Assay System (#E2940, Promega) was used to asses Rad51 luciferase activity, which was measured as the average ratio of firefly to Renilla luciferase.

Real-time qPCR. An RNA isolation kit (BS88133, Bio Basic Inc) was used to extract RNA and cDNAs were synthesized using qScript cDNA kit (#95047, Quantabio). The qPCR master mix used was SYBR green (Applied Biosystems). Experiments were performed

with three technical replicates and normalized to GAPDH. Rad51 qPCR primer sequence has been previously described (185).

Chromatin immunoprecipitation. ChIP-IT Express Chromatin Immunoprecipitation kit (Active Motif) was used for TEAD4 antibody (N-G2, Santa Cruz Biotechnology) ChiP experiments. The following qPCR primer sequence was used to amplify the region of the TEAD4 signal in the Rad51 promoter identified in ENCODE: Forward primer 5'-TTGCTCCAGGAATGCGAGTA-3' Reverse primer 5'-AGCGCTCTTGTGGTTTGTTT-3'.

DR-GFP assay. Puromycin resistant DR-GFP MCF7 cells were provided by Dr. Sharon Cantor (University of Massachusetts Medical School). Stable expression of S89A TAZ (Addgene plasmid #52084) was accomplished by selecting cells in blasticidin and stable expression of S127A YAP (Addgene plasmid #33092) was accomplished by selecting cells in hygromycin. DR-GFP reporter plasmid was purchased from Addgene and was electroporated into Hs578t cells (Addgene plasmid #26475). Subsequently, cells were transfected with I-SceI (Addgene plasmid #26477) and processed for flow cytometry 72 hours later using two-color fluorescence analysis (180) with DsRed. FL1 indicates green fluorescence and FL2 indicates red fluorescence.

Immunofluorescence microscopy. Rad51 and γH2AX immunofluorescence microscopy was performed by fixing cells with paraformaldehyde (4%) and permeabilizing them with triton X-100 (0.1%). Cells were blocked with 0.5% BSA and incubated with Rad51 antibody (ab63801, Abcam) or γH2AX antibody (05-636, Millipore) overnight at 4°C. The

following morning, cells were washed with 1X PBS and incubated with fluorochrome-conjugated secondary antibodies at room temperature for 45 minutes. A confocal microscope (Zeiss) was used to capture images at 20X magnification. FociCounter http://focicounter.sourceforge.net/ was used to quantify γH2AX positive cells.

ENCODE data analysis. TEAD4 binding signals were downloaded from www.encodeproject.org in bigwig format. The signals of duplicate samples were pooled and then plotted along the promoter region of the Rad51 gene using trackViewer package (193).

Metabric analysis. cBioPortal (www.cbioportal.org) was used to compare the mRNA expression of Rad51, TAZ, CTGF, Cyr61, VEGFA and NRP2 using the Metabric breast cancer dataset (162, 163). To determine if the expression of two genes exhibit an inverse correlation, we performed the mutual exclusivity analysis with a z-score threshold of ± 2 as expressed, and calculated the log odds ratio between two genes and *p* value using Fisher exact *t*-test. We also stratified breast cancer patients in the Metabric dataset based on their ER status and tumor grade, and Welch *t*-test was used to compare Rad51 expression in ER^+ and ER^- and tumor grade 1-3 patient groups.

Microarray analysis. The Bioconductor package *GEOquery* (version 2.41.0) (194) was used to download the microarray dataset from GEO (GSE59230) (181). Differentially expressed genes between MDA-MB-231 cells transfected with siRNA control and two different siRNAs targeting YAP/TAZ were identified using moderated *t*-test with limma

package (195). Genes with an adjusted *p*-value of ≤ 0.05 using Benjamini-Hochberg method were considered significant (196).

Figures

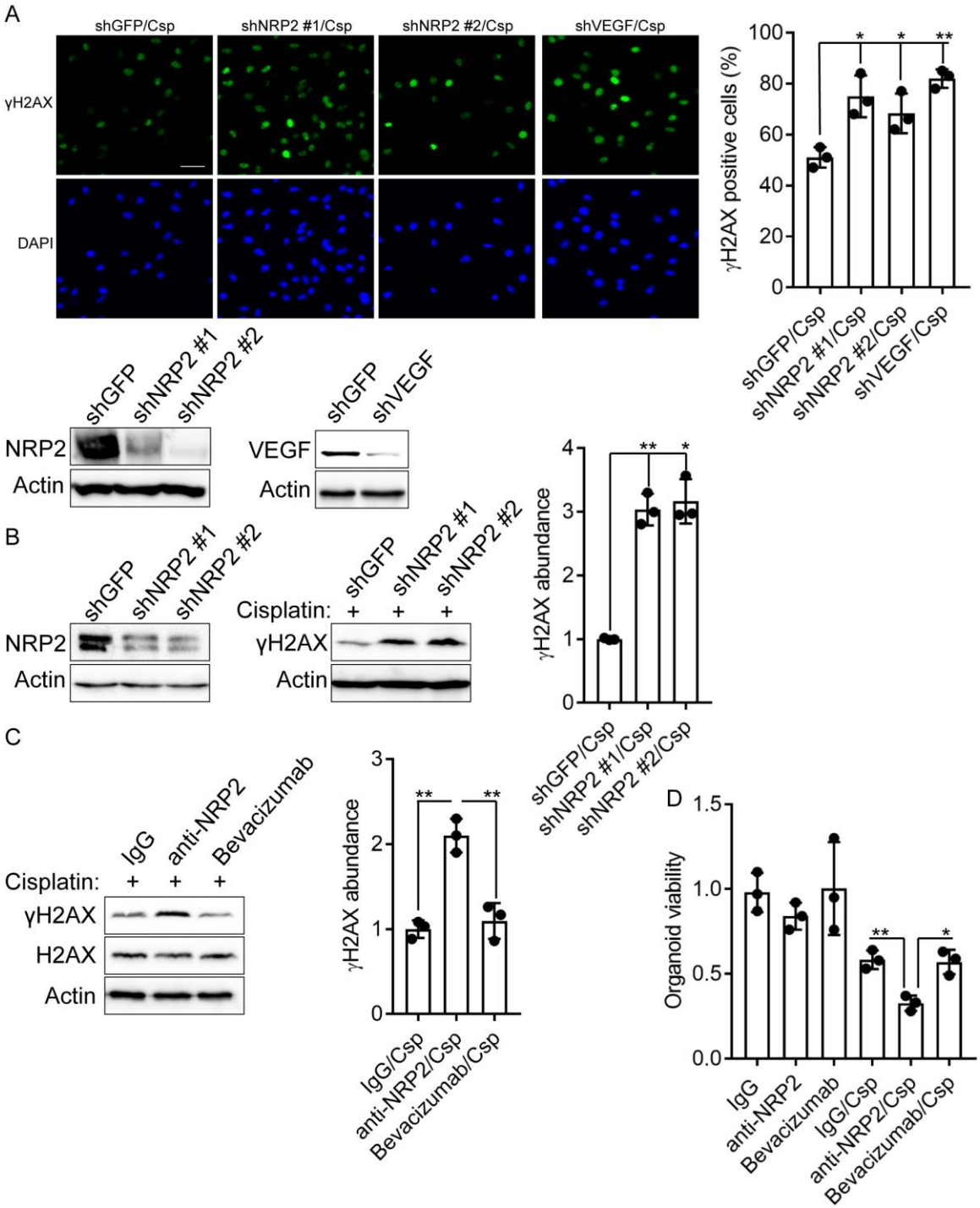
A
shGFP/Csp
shNRP2 #1/Csp
shNRP2 #2/Csp
shVEGF/Csp
γH2AX
DAPI
γH2AX positive cells (%)
shGFP
shNRP2 #1
shNRP2 #2
NRP2
Actin
shGFP
shVEGF
VEGF
Actin
B
shGFP
shNRP2 #1
shNRP2 #2
Cisplatin: + + +
NRP2
Actin
γH2AX
Actin
γH2AX abundance
C
IgG
anti-NRP2
Bevacizumab
Cisplatin: + + +
γH2AX
H2AX
Actin
γH2AX abundance
IgG/Csp
anti-NRP2/Csp
Bevacizumab/Csp
D
Organoid viability
IgG
anti-NRP2
Bevacizumab
IgG/Csp
anti-NRP2/Csp
Bevacizumab/Csp

Fig. 3.1. VEGF-NRP2 promotes protection from cisplatin-induced DNA damage. (A) Expression of NRP2 and VEGF was diminished with shRNAs in MDA-MB-231 cells. Subsequently, cells were treated with cisplatin and processed for γH2AX immunofluorescence microscopy. Scale bar represents 50 μm. (B) Expression of NRP2 was diminished in Hs578t cells. Subsequently, cells were treated with cisplatin and the impact on γH2AX abundance was quantified by immunoblotting. Densitometry was assessed using ImageJ (right bar graph). (C) Hs578t cells were treated with a control IgG, a NRP2 function antibody or bevacizumab in the presence of cisplatin and the impact on γH2AX abundance was quantified by immunoblotting. Densitometry was assessed using ImageJ (right bar graph). (D) Cell viability in BRCA proficient mouse mammary tumor organoids treated with a control IgG, a NRP2 function blocking antibody or bevacizumab with and without cisplatin was assessed. Dot plots (mean ± standard deviation) represent three independent experiments. * $p \leq 0.05$, ** $p \leq 0.005$, *** $p \leq 0.0005$ by two-tailed t test.

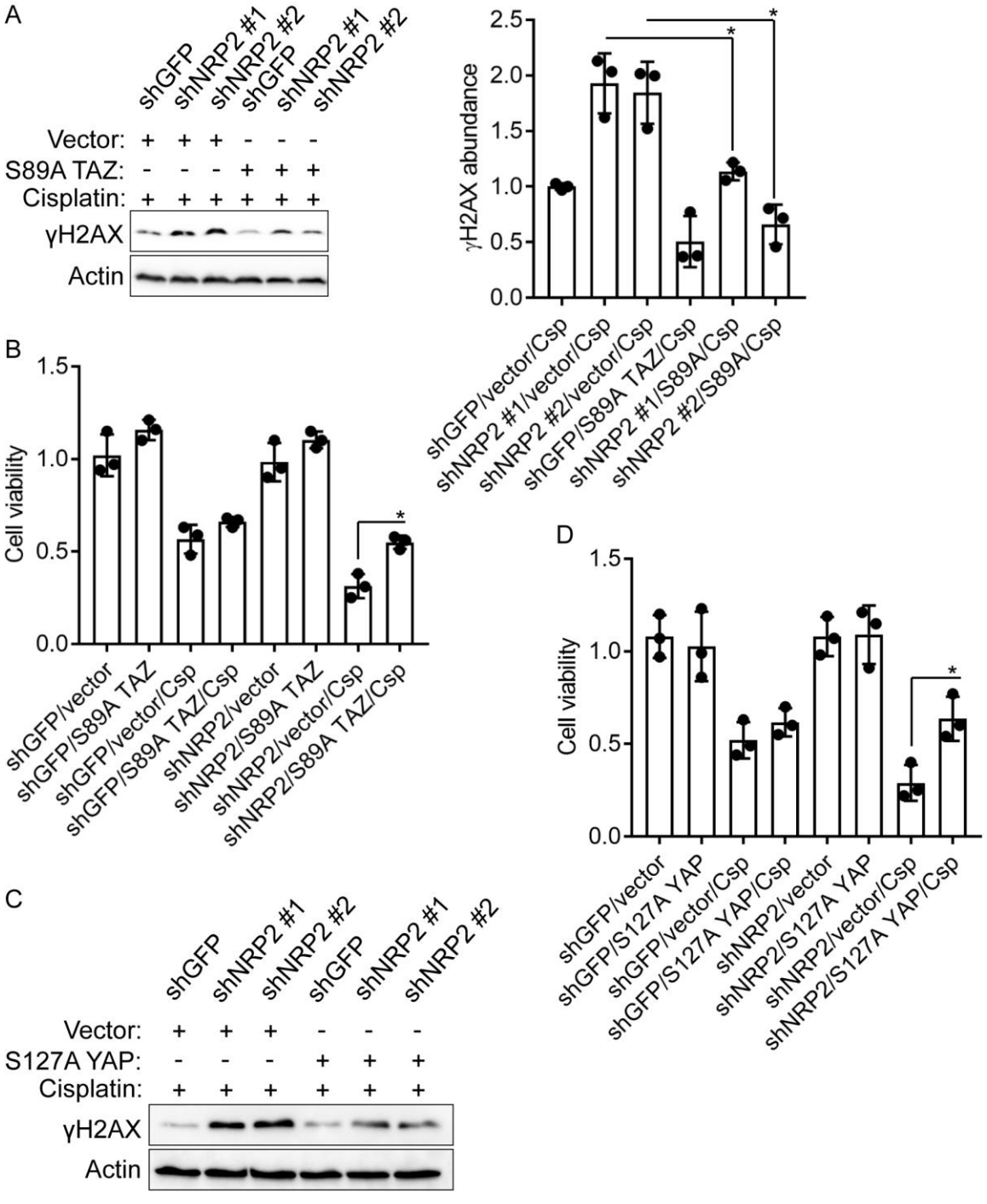
A
shGFP
shNRP2 #1
shNRP2 #2
shGFP
shNRP2 #1
shNRP2 #2
Vector: + + + - - -
S89A TAZ: - - - + + +
Cisplatin: + + + + + +
γH2AX
Actin
γH2AX abundance
2.5
2.0
1.5
1.0
0.5
0.0
*
*
shGFP/vector/Csp
shNRP2 #1/vector/Csp
shNRP2 #2/vector/Csp
shGFP/S89A TAZ/Csp
shNRP2 #1/S89A/Csp
shNRP2 #2/S89A/Csp
B
Cell viability
1.5
1.0
0.5
0.0
*
shGFP/vector
shGFP/S89A TAZ
shGFP/vector/Csp
shGFP/S89A TAZ/Csp
shNRP2/vector
shNRP2/S89A TAZ
shNRP2/vector/Csp
shNRP2/S89A TAZ/Csp
C
shGFP
shNRP2 #1
shNRP2 #2
shGFP
shNRP2 #1
shNRP2 #2
Vector: + + + - - -
S127A YAP: - - - + + +
Cisplatin: + + + + + +
γH2AX
Actin
D
Cell viability
1.5
1.0
0.5
0.0
*
shGFP/vector
shGFP/S127A YAP
shGFP/vector/Csp
shGFP/S127A YAP/Csp
shNRP2/vector
shNRP2/S127A YAP
shNRP2/vector/Csp
shNRP2/S127A YAP/Csp

Fig. 3.2. YAP/TAZ are necessary for VEGF-NRP2 protection from cisplatin-induced DNA damage. NRP2-depleted Hs578t cells expressing S89A TAZ or a control vector were treated with cisplatin and the impact on γH2AX abundance *(A)* and cell viability *(B)* was assessed. Densitometry was assessed using ImageJ (right bar graph of *B*). NRP2-depleted Hs578t cells expressing S127A YAP or a control vector were treated with cisplatin and the impact on γH2AX abundance *(C)* and cell viability *(D)* was assessed. Dot plots (mean ± standard deviation) represent three independent experiments. * $p \leq 0.05$, ** $p \leq 0.005$, *** $p \leq 0.0005$ by two-tailed *t* test.

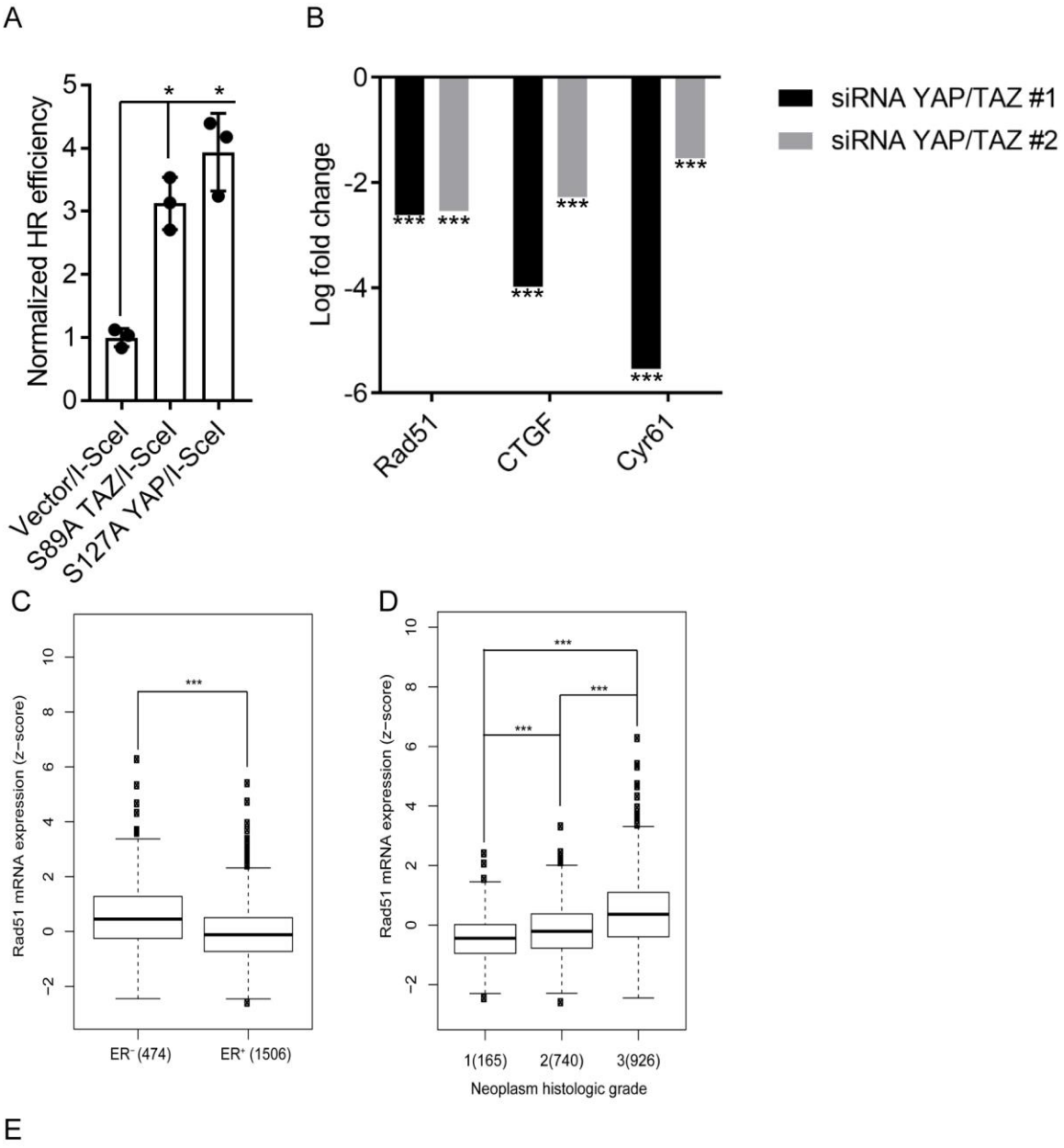

E

Gene analysis	Log odds ratio	*p* value	No. samples
Rad51 vs. TAZ	+1.3	< 0.001	2509
Rad51 vs. CTGF	+1.4	< 0.001	2509
Rad51 vs. Cyr61	+1.4	0.002	2509

Fig. 3.3. YAP/TAZ promote homologous recombination and correlate with Rad51 in patient tumors. *(A)* DR-GFP MCF7 cells engineered to express S89A TAZ, S127A YAP

or empty vector were transfected with I-SceI and processed for flow cytometry to quantify GFP positive cells, which were normalized to 1 and are depicted as HR efficiency. Dot plot (mean ± standard deviation) represents three independent experiments. * $p \leq 0.05$ by two-tailed *t* test. *(B)* The indicated genes from a microarray (accession number GSE59230 (181)) using siRNA to deplete YAP/TAZ in MDA-MB-231 cells were analyzed. Log fold change in expression from four biological replicates is shown relative to siRNA control, and adjusted *p* value of ≤ 0.0005 is indicated by ***. cBioPortal for cancer genomics was used to analyze the expression of Rad51 based on expression of the ER *(C)* and tumor grade *(D)* in breast cancer patients from the Metabric database. *** $p < 0.0005$ by Welch *t* test. *(E)* The expression of Rad51 was compared with TAZ and the YAP/TAZ target genes CTGF and Cyr61 in the Metabric database. Log odds ratios were generated and *p* values were calculated using fisher exact *t* test.

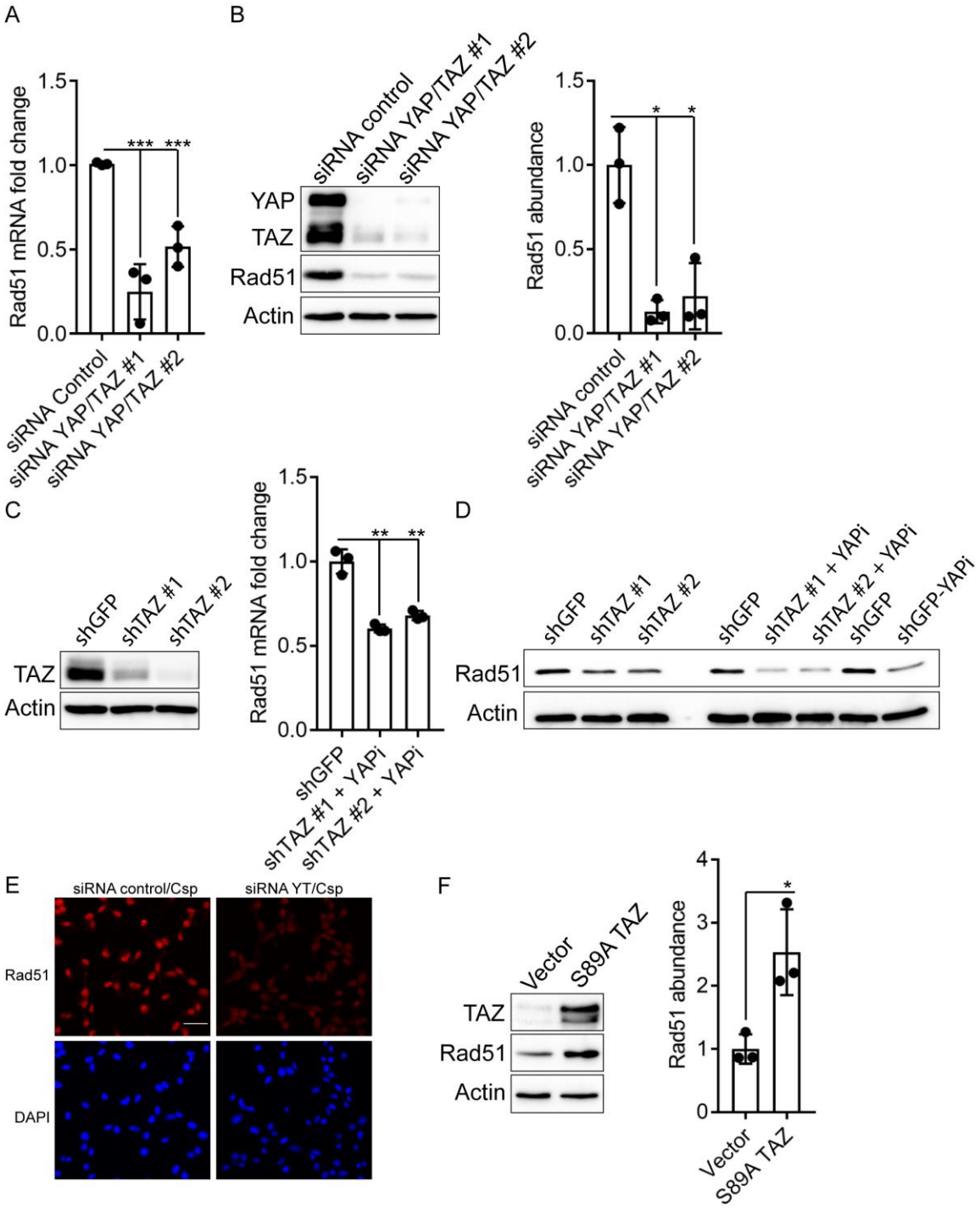

Fig. 3.4. YAP/TAZ contribute to Rad51 expression. *(A)* Expression of YAP/TAZ was diminished with siRNAs in MDA-MB-231 cells and the impact on Rad51 mRNA

expression was quantified by qPCR. *(B)* Rad51 abundance was quantified by immunoblotting in YAP/TAZ-depleted Hs578t cells. Densitometry was assessed using ImageJ (right bar graph). *(C)* Knockdown of TAZ was quantified by immunoblotting in MDA-MB-231 cells (left). These cells were subsequently treated with verteporfin to also inhibit YAP and Rad51 mRNA expression was quantified by qPCR (right). *(D)* Rad51 abundance was quantified by immunoblotting in TAZ-depleted MDA-MB-231 cells, verteporfin-treated MDA-MB-231 cells and the combination. *(E)* YAP/TAZ-depleted MDA-MB-231 cells were treated with cisplatin and the impact on Rad51 was assessed by immunofluorescence microscopy. Scale bar represents 50 μm. *(F)* DR-GFP MCF7 cells were transfected with either S89A TAZ or empty vector and Rad51 abundance was quantified by immunoblotting. Densitometry was assessed using ImageJ (right bar graph). Dot plots (mean ± standard deviation) represent three independent experiments. * $p \leq 0.05$, ** $p \leq 0.005$, *** $p \leq 0.0005$ by two-tailed *t* test.

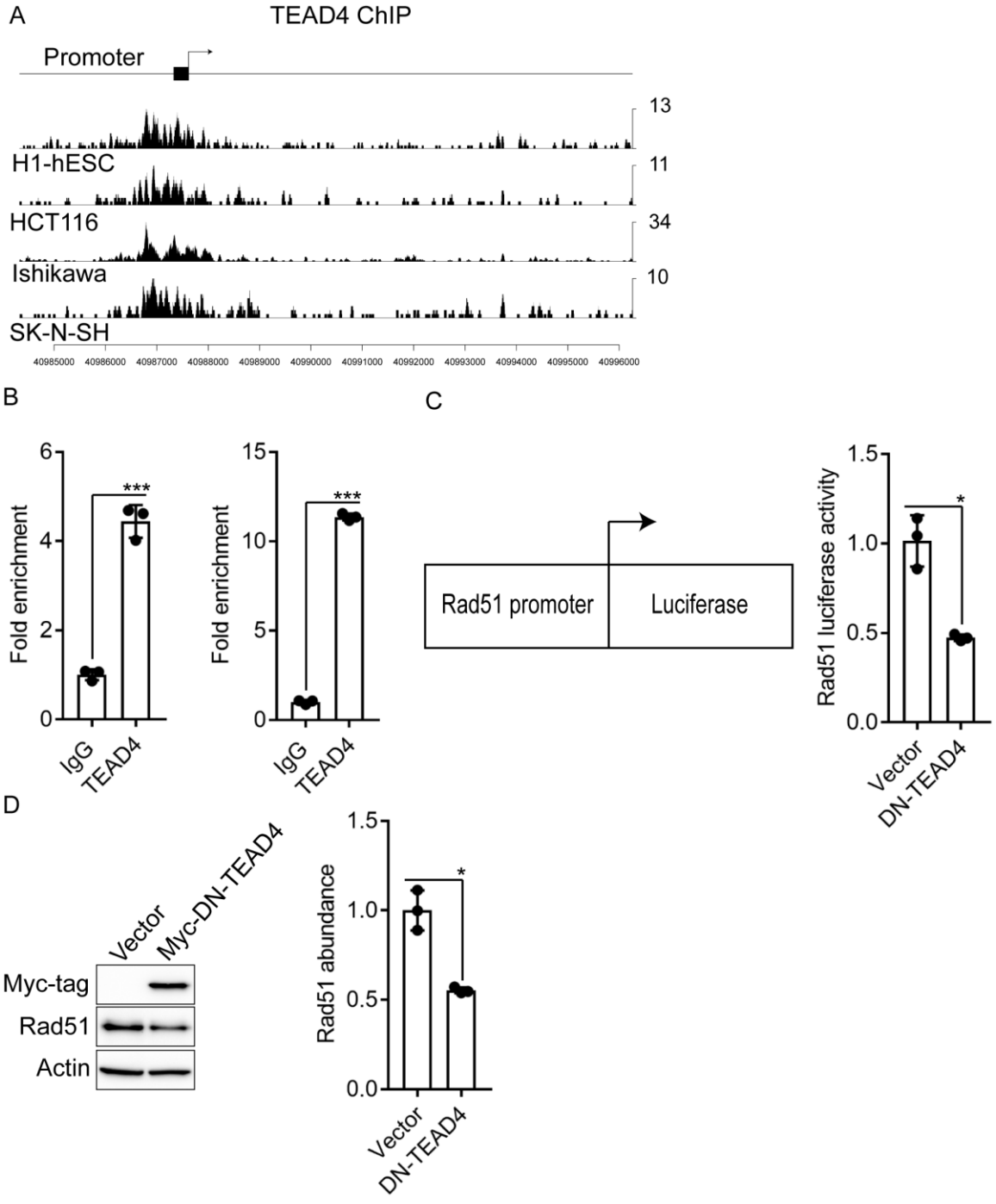

Fig. 3.5. Rad51 is a direct YAP/TAZ-TEAD target gene. *(A)* TEAD4 binding signals from ENCODE were analyzed in ChIP-seq datasets from h1-hESCs (human embryonic stem cells), HCT116 (colon cancer), Ishikawa (endometrial adenocarcinoma) and SK-N-

SH (neuroblastoma) cells in the promoter region of the Rad51 gene. *(B)* Binding of TEAD4 on the Rad51 promoter was analyzed using ChIP in MDA-MB-231 (left) and Hs578t (right) cells. *(C)* MDA-MB-231 cells expressing dominant-negative TEAD4 were transfected with pRad51-Luc that utilizes the Rad51 promoter to control expression of firefly luciferase and assayed for Rad51 transcriptional activity. *(D)* Rad51 abundance was quantified by immunoblotting in MDA-MB-231 cells expressing dominant-negative TEAD4. Densitometry was assessed using ImageJ (right bar graph). Dot plots (mean ± standard deviation) represent three independent experiments. * $p \leq 0.05$, ** $p \leq 0.005$, *** $p \leq 0.0005$ by two-tailed *t* test.

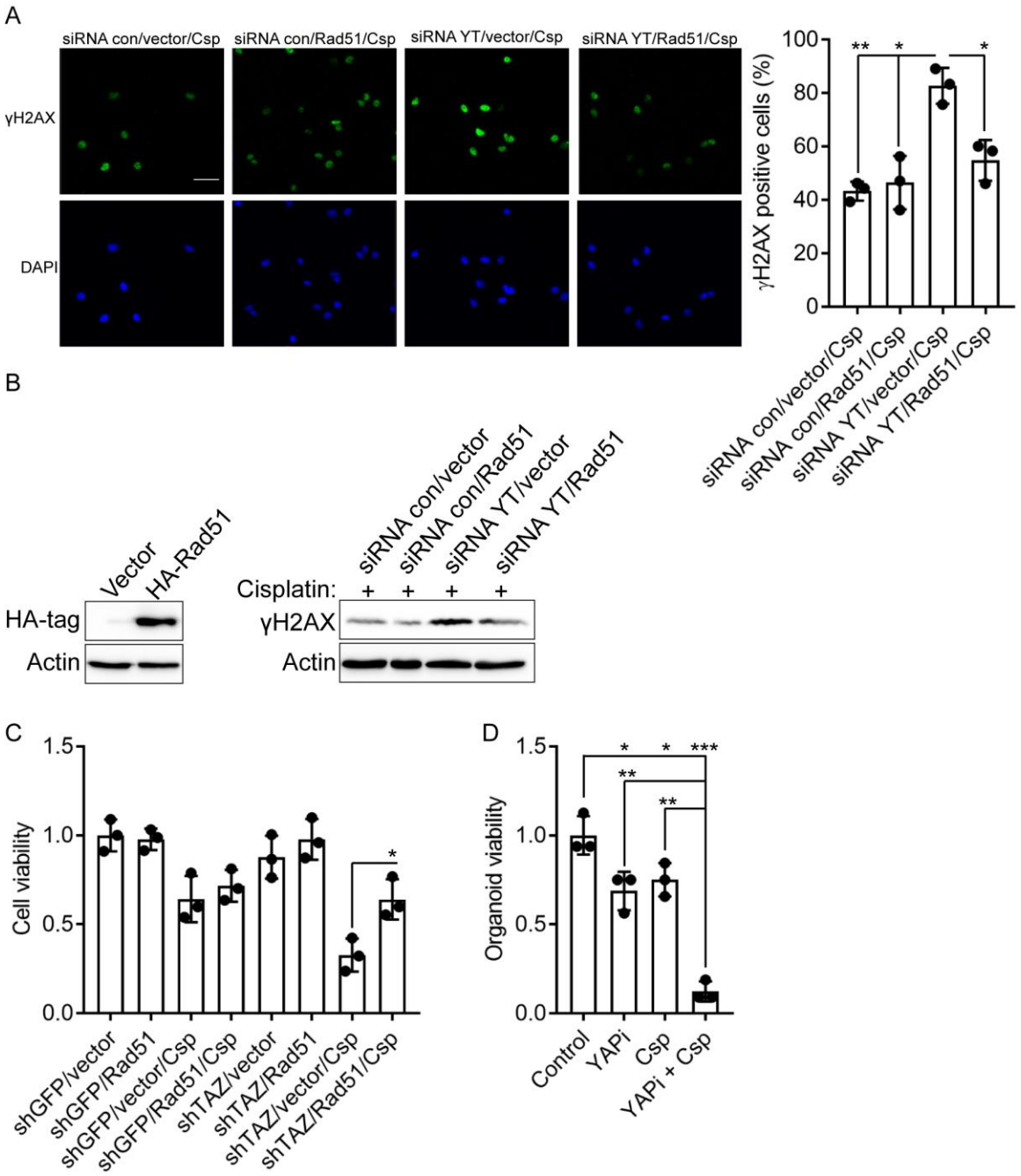

Fig. 3.6. Rad51 mediates YAP/TAZ-dependent DNA repair. Expression of YAP/TAZ was diminished in Hs578t cells (siRNA YT). Cells were then transfected with HA-tagged Rad51 or empty vector. Subsequently, cells were treated with cisplatin and processed for

(A) immunofluorescence microscopy or *(B)* immunoblotting to quantify γH2AX. Scale bar represents 50 μm. *(C)* TAZ-depleted MDA-MB-231 cells expressing Rad51 or a control vector were treated with cisplatin and the impact on cell viability was assessed. *(D)* Cell viability in *BRCA* proficient mouse mammary tumor organoids treated with either verteporfin, cisplatin or the combination was assessed. Dot plots (mean ± standard deviation) represent three independent experiments. * $p \leq 0.05$, ** $p \leq 0.005$, *** $p \leq 0.0005$ by two-tailed *t* test.

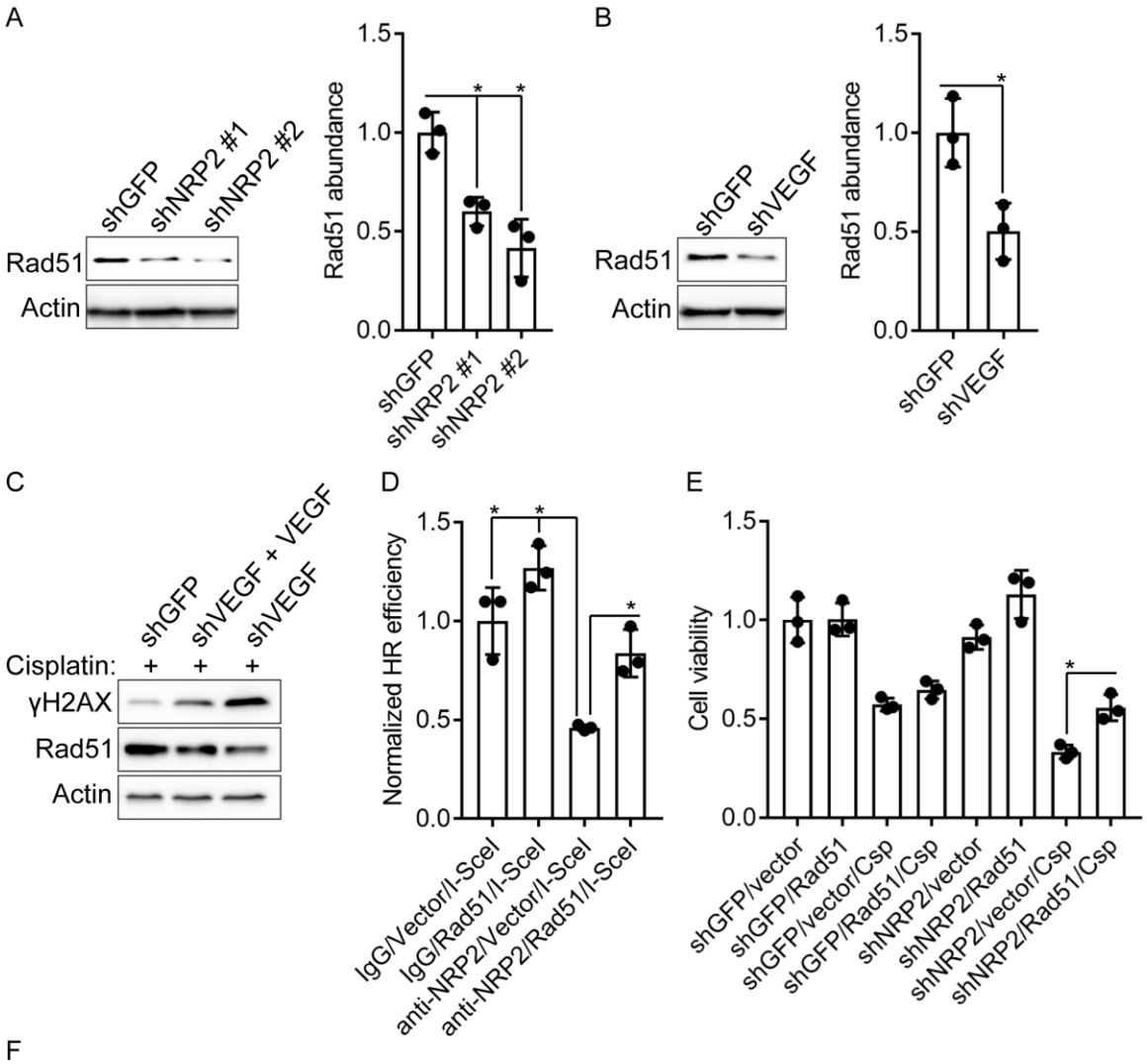

F

Gene analysis	Log odds ratio	*p* value	No. samples
Rad51 vs. VEGFA	+1.6	< 0.001	2509
Rad51 vs. NRP2	+0.9	0.02	2509

Fig. 3.7. VEGF-NRP2 controls YAP/TAZ-mediated Rad51 expression and HR. Expression of *(A)* NRP2 and *(B)* VEGF was diminished in MDA-MB-231 cells and the impact on Rad51 abundance was quantified by immunoblotting. Densitometry was assessed using ImageJ (right bar graphs). *(C)* VEGF-depleted MDA-MB-231 cells were treated with 50 ng/mL of VEGF for 24 hours. Medium was then replaced, and cells were

treated with cisplatin and also 50 ng/mL of VEGF in VEGF-depleted cells. γH2AX and Rad51 abundance was quantified by immunoblotting. *(D)* Hs578t DR-GFP cells were transfected with Rad51 or empty vector. Subsequently, they were treated with a control IgG or a NRP2 function blocking antibody and processed for flow cytometry to quantify GFP positive cells. GFP positive cells were normalized to 1 and are depicted as HR efficiency. *(E)* NRP2-depleted Hs578t cells expressing Rad51 or a control vector were treated with cisplatin and the impact on cell viability was assessed. *(F)* The expression of Rad51 was compared with VEGFA and NRP2 in the Metabric database. Log odds ratios were generated and *p* values were calculated using fisher exact *t* test. Dot plots (mean ± standard deviation) represent three independent experiments. * $p \leq 0.05$, ** $p \leq 0.005$, *** $p \leq 0.0005$ by two-tailed *t* test.

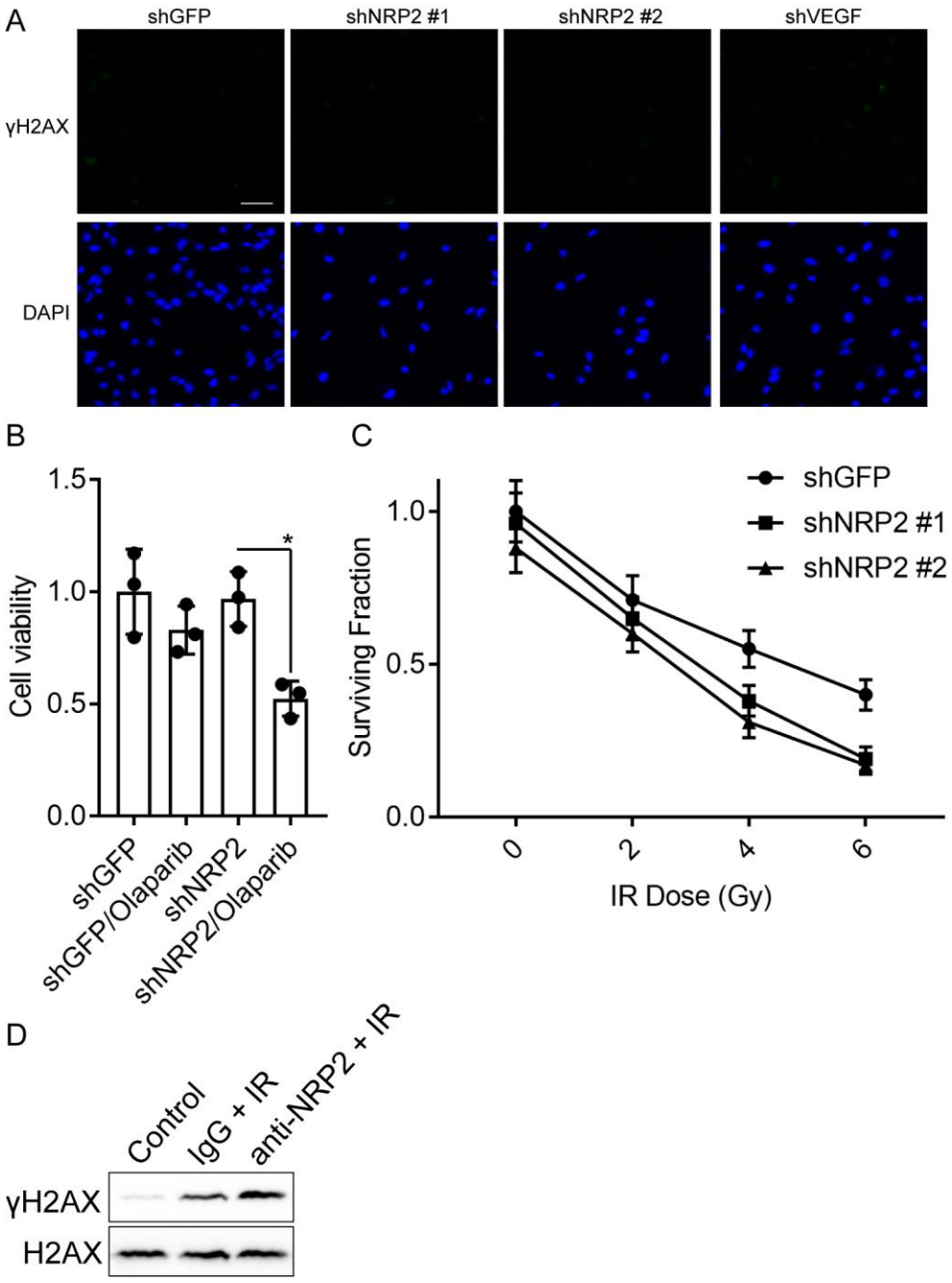

Fig. 3.8. VEGF-NRP2 promotes resistance to PARP inhibition and ionizing radiation. *(A)* Expression of NRP2 and VEGF was diminished with shRNAs in MDA-MB-231 cells, which were subsequently processed for immunofluorescence microscopy to assess baseline

γH2AX. Scale bar represents 50 μm. *(B)* Cell viability in control and NRP2-depleted Hs578t cells treated with and without olaparib was assessed. *(C)* Cell viability in control and NRP2-depleted Hs578t cells treated with the indicated doses of IR was assessed. *(D)* Hs578t cells were pre-treated with a control IgG or a NRP2 function blocking antibody. Subsequently, they were treated with 6 Gy of IR and the impact on γH2AX abundance was quantified by immunoblotting 30 minutes following IR. Dot plot (mean ± standard deviation) represents three independent experiments. * $p \leq 0.05$ by two-tailed *t* test.

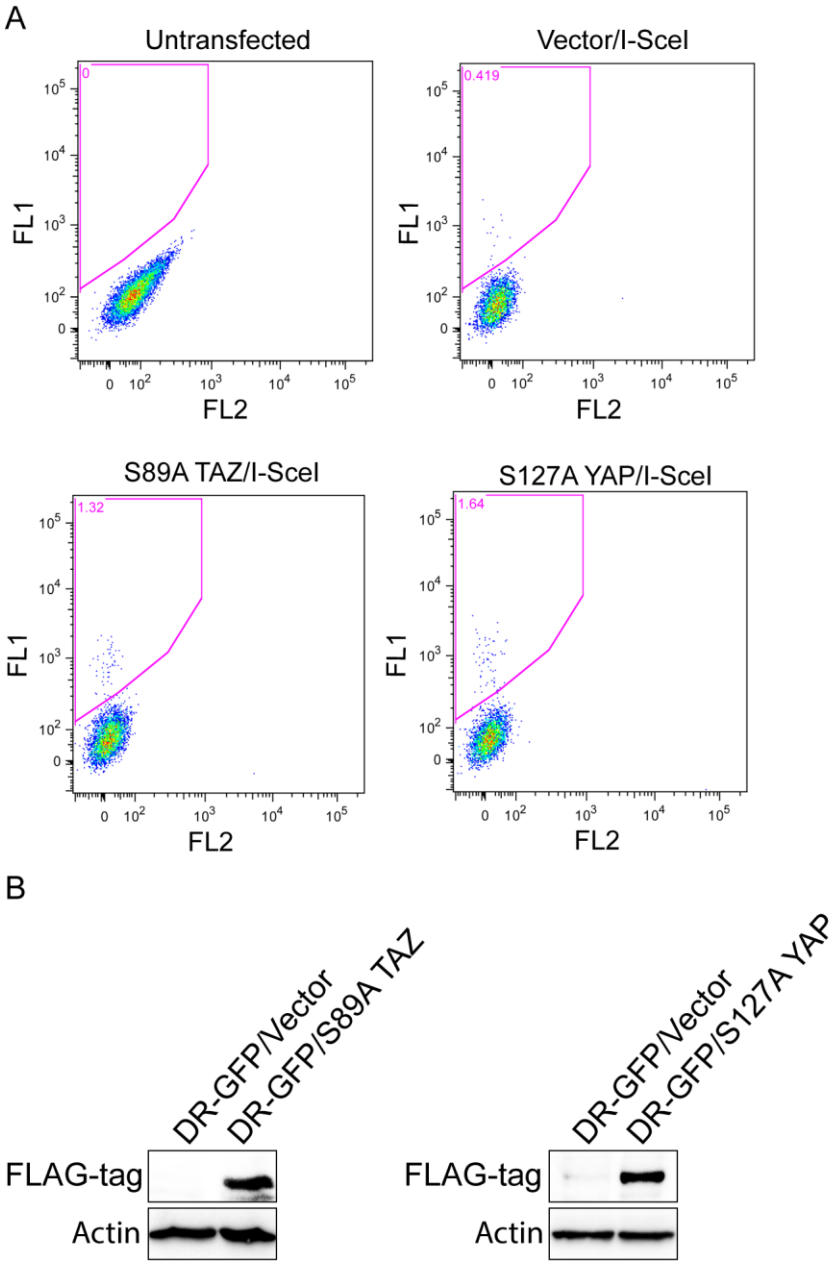

Fig. 3.9. YAP/TAZ promote homologous recombination by DR-GFP analysis. *(A)* Representative flow cytometry of MCF7 DR-GFP cells expressing a control vector, S89A TAZ or S127A YAP. *(B)* Expression of FLAG-tagged S89A TAZ and S127A YAP in MCF7 DR-GFP cells was assessed by immunoblotting.

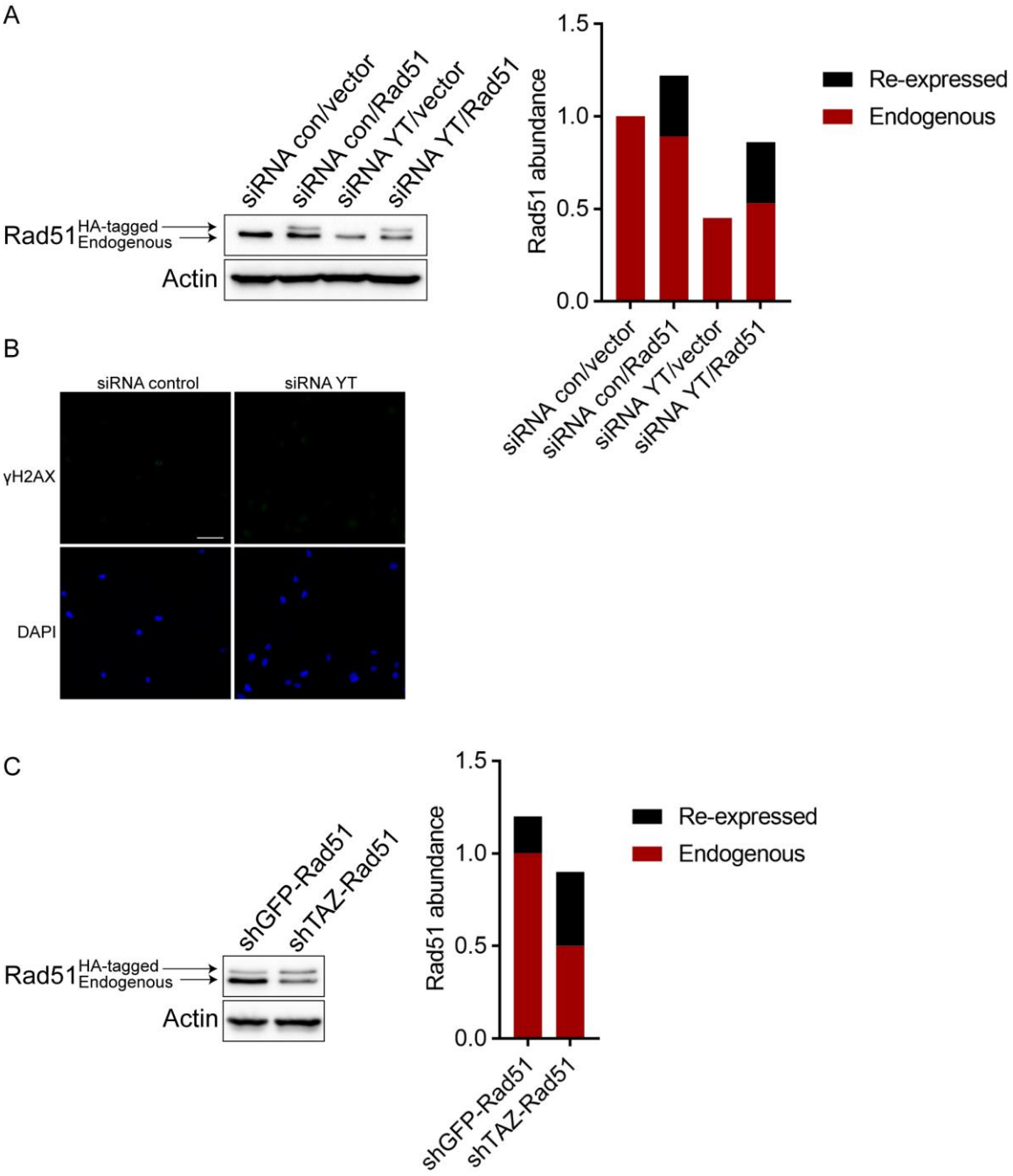

Fig. 3.10. Rad51 rescue levels in YAP/TAZ-depleted cells and baseline γH2AX upon YAP/TAZ depletion. *(A)* Expression of YAP/TAZ was diminished with siRNA in Hs578t cells (siRNA YT). Cells were then transfected with HA-tagged Rad51 or empty

vector and processed for immunoblotting to quantify the degree of Rad51 rescue. Densitometry was assessed using ImageJ (right bar graph). *(B)* Expression of YAP/TAZ was diminished with siRNA in Hs578t cells, which were subsequently processed for immunofluorescence microscopy to assess baseline γH2AX. Scale bar represents 50 μm. *(C)* Expression of Rad51 was quantified in control and TAZ-depleted MDA-MB-231 cells by immunoblotting to determine the degree of Rad51 rescue. Densitometry was assessed using ImageJ (right bar graph).

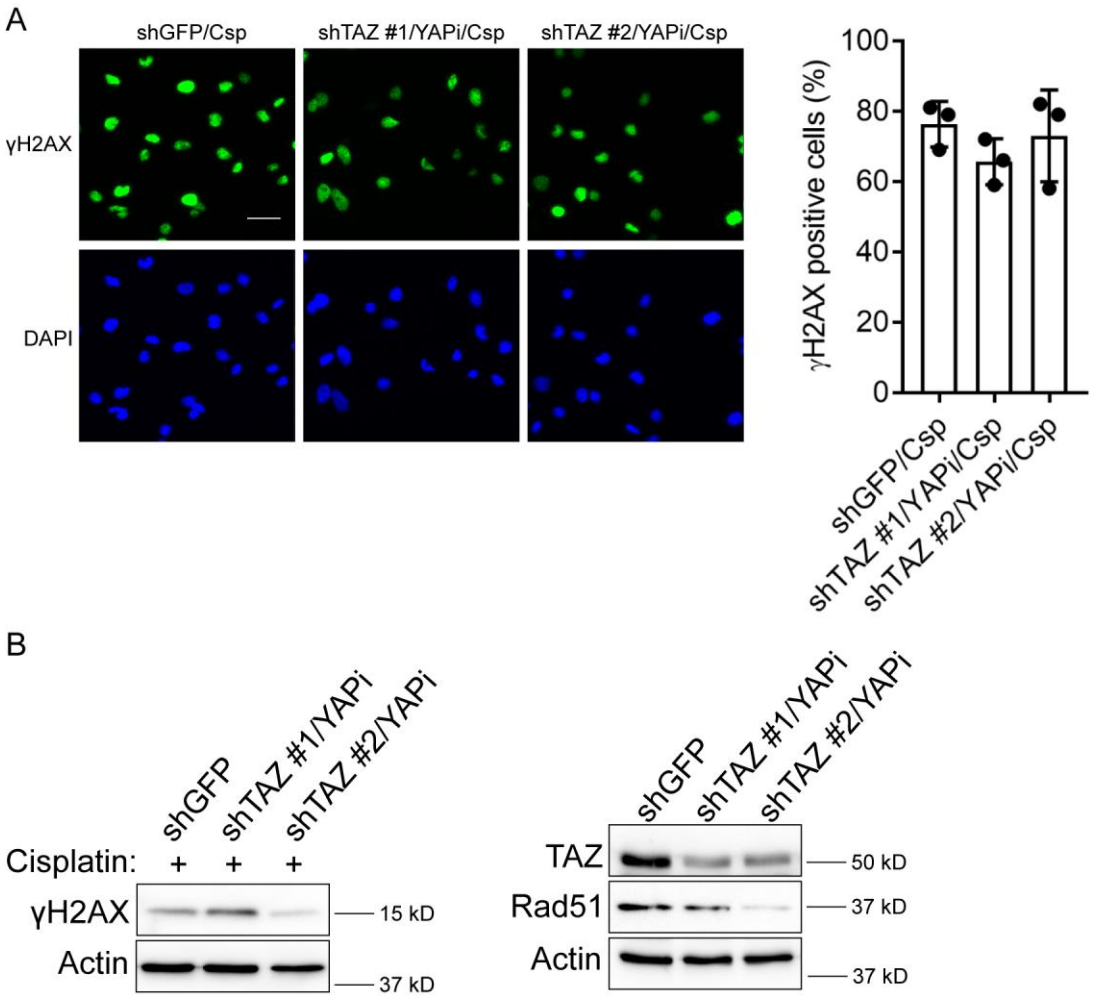

Fig. 3.11. YAP/TAZ do not regulate DNA damage dynamics in *BRCA1* mutant cells. Expression of TAZ was depleted in SUM-1315 cells, which were treated with verteporfin and cisplatin and processed for *(A)* immunofluorescence microscopy to assess γH2AX and *(B)* immunoblotting to assess γH2AX and Rad51. Scale bar represents 50 µm. Dot plot (mean ± standard deviation) represents three independent experiments.

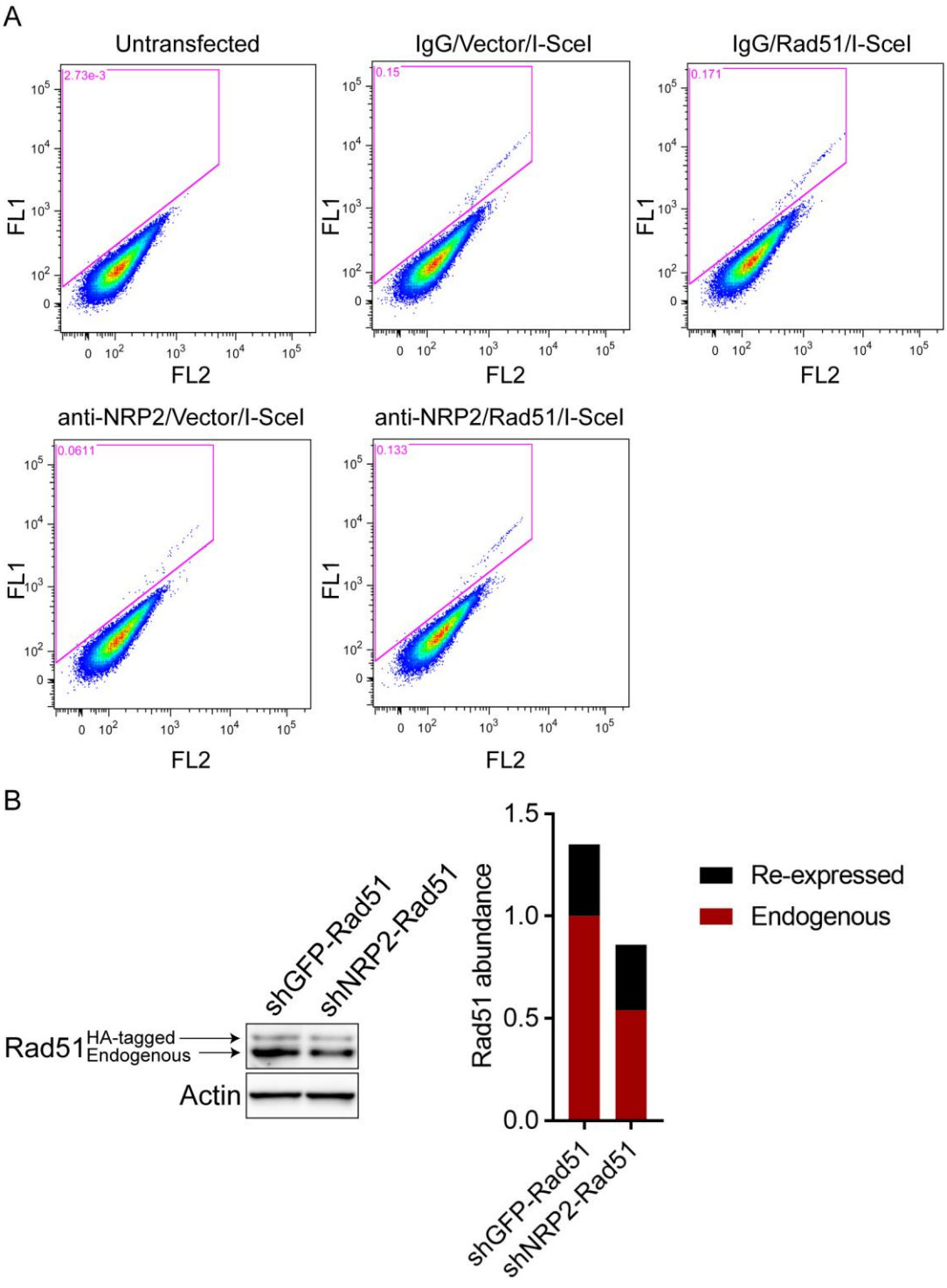

Fig. 3.12. Rad51 rescues homologous recombination upon NRP2 inhibition by DR-GFP analysis. *(A)* Representative flow cytometry of Hs578t cells transfected with empty

vector or Rad51 and subsequently treated with a control IgG or a function blocking NRP2 antibody. *(B)* Expression of Rad51 was quantified in control and NRP2-depleted cells by immunoblotting to determine the degree of Rad51 rescue. Densitometry was assessed using ImageJ (right bar graph).

CHAPTER IV: DISCUSSION

Overview

This thesis has focused on the mechanisms by which autocrine VEGF signaling mediated by NRP2 confers CSC properties, DNA repair and resistance to therapy in TNBC cells. The first chapter revealed that VEGF-NRP2 signaling converges on the hippo pathway transducers TAZ and YAP by a Rac1-dependent, feed-forward mechanism. It also characterized the Rac GAP β2-chimaerin as a novel target gene repressed by YAP/TAZ-TEAD-dependent gene regulation. Importantly, I discovered that β2-chimaerin repression is critical for the acquisition of CSC properties mediated by upstream VEGF-NRP2-YAP/TAZ signaling. These observations provide one mechanism that sustains enhanced YAP/TAZ activity and CSC properties in breast cancer. They are also significant because they link VEGF, a key component of the tumor microenvironment, with YAP/TAZ regulation, which is independent of its function in angiogenesis.

In the second chapter of this thesis, I extended my analysis of the VEGF-NRP2-YAP/TAZ signaling axis to therapy resistance in TNBC cells. Specifically, I observed that VEGF-NRP2-YAP/TAZ promotes resistance to agents that induce DNA damage by promoting HR-directed DNA repair. This mechanism occurs through direct transcriptional regulation of the HR recombinase Rad51 by YAP/TAZ-TEAD dependent gene regulation. My findings link important characteristics of TNBC: dependence on VEGF-NRP2 signaling, hyper-activation of YAP/TAZ and high Rad51 mechanism into a mechanism

that accounts for its resistance to therapy. These results are significant because efficient HR is an important predictor of TNBC patient response to treatment, and they demonstrate that targeting VEGF-NRP2 or YAP/TAZ may lead to more favorable response to platinum chemotherapy.

Convergence of VEGF and YAP/TAZ signaling: Implications for angiogenesis and cancer biology

The first section of Chapter IV titled "Convergence of VEGF and YAP/TAZ signaling: Implications for angiogenesis and cancer biology" represents a review article previously published.

This work was originally published in *Science Signaling*. **Ameer L. Elaimy** and Arthur M. Mercurio. Convergence of VEGF and YAP/TAZ signaling: Implications for angiogenesis and cancer biology. *Science Signaling*. 2018 Oct 16;11(552). pii: eaau1165. doi: 10.1126/scisignal.aau1165. From *Science Signaling*. Reprinted with permission from AAAS.

CONTRIBUTIONS:

Ameer L. Elaimy and Arthur M. Mercurio conceptualized and wrote the review article.

Introduction

Vascular endothelial growth factor (VEGF) was identified and isolated as an endothelial cell-specific mitogen that has the capacity to induce developmental and pathological angiogenesis (34, 35). More recent work has revealed the ability of VEGF to target tumor cells, especially cells with stem-like traits, referred to as cancer stem cells (CSCs) and, consequently, contribute to tumor initiation, progression, and recurrence directly (42). These vital functions of VEGF are mediated by specific receptors expressed on endothelial and tumor cells including receptor tyrosine kinases (VEGFR1 and VEGFR2) and the neuropilins (NRPs), which function as VEGF co-receptors (52, 62, 117, 118, 197). The mechanisms by which these VEGF receptors execute these diverse functions are of paramount importance because of their potential as therapeutic targets. Not surprisingly, VEGF-mediated signaling events have been studied intensely but much remains to be learned. In particular, a better understanding of how VEGF signaling impacts the cell biology that underlies vascular growth and remodeling (angiogenesis) and self-renewal (CSCs) is needed. In this direction, recent work has uncovered a convergence of VEGF and Hippo signaling that has the potential to provide considerably new insight into angiogenesis and CSC function.

The Hippo pathway is critical for development because it restricts proliferation and controls organ size (198). Inhibition of this pathway results in the activation of YAP and TAZ, transcriptional co-activators that have profound effects on cell behavior. Active YAP and TAZ reside in the nucleus where they associate with the TEA domain (TEAD) family of transcription factors and regulate the expression of numerous target collectively known

as a YAP/TAZ "signature". Several cues, such as high cell density and polarity, can activate the core Hippo tumor suppressor pathway and thereby inhibit YAP/TAZ. This pathway consists of a kinase cascade mediated by the MST 1/2 kinases, which phosphorylate and activate the LATS 1/2 kinases (146). Activated LATS 1/2 directly phosphorylates YAP/TAZ at several conserved residues, with serine 127 of YAP and serine 89 of TAZ being the classical and most heavily studied LATS 1/2 phosphorylation sites. YAP/TAZ phosphorylation creates 14-3-3 binding sites, which results in their cytoplasmic retention, separation from the TEAD family of transcription factors, and functional inactivation (91, 146). In addition to core MST/LATS kinase Hippo signaling, YAP/TAZ activity can be controlled by several other molecular factors termed the "extended" Hippo pathway. Although the core Hippo pathway and its extended components are well-characterized (89), a rigorous understanding of signaling at the cell surface that leads to inactivation of the Hippo pathway and contributes to enhanced YAP/TAZ activity is still emerging. What has been shown recently is that VEGF receptor signaling can repress the Hippo pathway resulting in YAP/TAZ activation. The essence of these findings is that VEGF signaling impacts Rho family GTPase activity and cytoskeletal dynamics, which contribute to YAP/TAZ activation, and that YAP/TAZ-mediated transcriptional changes sustain GTPase activity and cytoskeletal dynamics to affect vascular growth and remodeling in endothelial cells and the acquisition of stem-like traits in tumor cells (**Figure 4.1**). These findings are significant because of their pathophysiological importance and their connection to other receptor-mediated pathways. This review discusses these findings and highlights areas for future study.

YAP/TAZ as Effectors of VEGF Signaling in Developmental Angiogenesis

The vascularization of tissues during development is a precisely orchestrated angiogenic process mediated primarily by VEGF that involves endothelial cell proliferation and survival, loss of cell-cell contacts, basement membrane degradation and directed migration (199). These diverse functions of endothelial cells are mediated, in part, by transcriptional and cytoskeletal alterations, but the mechanisms responsible for these alterations are still being elucidated. For this reason, the initial report describing VEGF-mediated YAP/TAZ activation in promoting developmental angiogenesis was a significant advance (171). More specifically, this study observed VEGF-mediated YAP/TAZ activation in a variety of endothelial cells *in vitro*. They also performed endothelial-cell specific deletions of YAP/TAZ and demonstrated their importance in embryonic and postnatal vascular development. YAP/TAZ deletion resulted in an impaired vascular response to VEGF indicating that YAP/TAZ are important regulators of angiogenesis downstream of VEGF. The mechanism by which VEGF activates YAP/TAZ in endothelial cells involves VEGFR2 activation of Src family kinases and subsequent cytoskeletal rearrangements mediated by Src activation of Rho family GTPases. Inhibiting VEGF-VEGFR2-Src-Rho GTPase signaling promoted LATS-mediated YAP/TAZ phosphorylation, which is consistent with reports that the generation of mechanical tension by Rho GTPases inhibits LATS kinases and activates YAP/TAZ (89, 102, 103, 136). This study also uncovered a positive feedback loop enabled by YAP/TAZ-dependent transcriptional alterations that sustains cytoskeletal alterations and Rho GTPase activity. More specifically, chromatin immunoprecipitation sequencing (ChIP-Seq) analysis

revealed that VEGF-VEGFR2-Src-Rho GTPase signaling promotes YAP/TAZ dependent expression of several cytoskeletal remodeling genes, including Myosin 1C (171). This finding is significant because Myosin 1C has been implicated in VEGFR2 trafficking from the Golgi apparatus to the plasma membrane (200). Consequently, enhanced YAP/TAZ activity was shown to be critical in retaining VEGFR2 on the cell surface and promoting a feedforward loop sustaining VEGF-VEGFR2-Src-Rho family GTPase activation of YAP/TAZ that contributes to developmental angiogenesis. In this direction, YAP/TAZ have been reported to activate the Rho GTPase Cdc42 as a mechanism of endothelial cell migration in angiogenesis. There is conflicting evidence, however, whether YAP/TAZ regulate Cdc42 expression and activity directly (201) or by an indirect mechanism (202). Nonetheless, these studies highlight a critical function of YAP/TAZ in the regulation of Rho family GTPases and cytoskeletal dynamics in the context of endothelial cell function. The more novel finding that is emerging from this work is that VEGF may be a key regulator of these processes.

Other studies have independently established that LATS kinases are regulated by upstream VEGF-Rho GTPase signaling in endothelial cells (203). Inhibitors of VEGFRs were identified as enhancers of LATS kinase activity using a novel bioluminescence-based biosensor to monitor LATS kinase activity in response to treatment with a small molecule kinase inhibitor library (204). This screen prompted the analysis and validation of VEGF-VEGFR2-mediated LATS inhibition and YAP/TAZ activation in *in vitro* and *in vivo* angiogenesis assays. Together, the studies described reveal a casual role of VEGF-mediated YAP/TAZ activation in developmental angiogenesis by mechanisms that

modulate LATS kinase activity, and they highlight the critical involvement of Rho family GTPases and the cytoskeleton. It is important to note that other studies had implicated Hippo signaling in angiogenesis (205), but they did not assess the potential role of VEGF signaling in regulating this pathway. This issue is timely because a recent study implicated BMP signaling and discounted the involvement of VEGF in YAP/TAZ regulation of sprouting angiogenesis in the mouse retina (107). Clearly, more work is needed to define the contribution of VEGF signaling to YAP/TAZ activation in developmental angiogenesis and to assess its relationship to other signaling pathways.

Role of VEGF-mediated YAP/TAZ Activation in Cancer Stem Cells

The seminal finding that VEGF-mediated angiogenesis is a hallmark of cancer sparked intense interest in the identification of signaling pathways in tumor-associated endothelial cells that are driven by VEGF and how they can be exploited for therapeutic purposes (44). To date, YAP and TAZ have not been implicated in tumor angiogenesis, although such a role seems likely given the data described above on developmental angiogenesis. Another significant contribution of VEGF-mediated YAP/TAZ activation involves tumor cells themselves. More specifically, autocrine VEGF signaling has emerged as an essential pathway for many CSCs and the NRPs appear to play a major role in mediating this signaling (42). CSCs are defined as a subpopulation of cells that exhibit properties of stem cells including self-renewal and function in tumor initiation, differentiation into heterogeneous cancer cell lineages, and therapy resistance. The role of

VEGF signaling mediated by the NRPs in sustaining self-renewal and CSC functions has been demonstrated for several types of cancer (42). Moreover, the hypothesis that VEGF-NRP signaling sustains CSCs has significant implications for therapy because the most common anti-VEGF drug (bevacizumab) blocks the binding of VEGF to receptor tyrosine kinases but not to NRPs (2). This observation may explain, in part, the dismal efficacy of bevacizumab for many cancers (206, 207), and it highlights the potential benefit of targeting the NRPs directly. For this reason, understanding how VEGF-NRP signaling impacts CSCs is a timely and significant problem. Studies in this area have focused largely on breast cancer based, in part, on reports that enhanced TAZ activity is associated with high-grade breast tumors and the function of breast CSCs (111), and our finding that autocrine VEGF signaling mediated by NRP2 confers stem cell-like traits in breast cancer (68). In light of this information, we sought to identify the mechanism involved and discovered that autocrine VEGF-NRP2 signaling promotes the self-renewal of breast CSCs by sustaining TAZ activation (63). The significance of this observation is that it integrates VEGF signaling with TAZ activation as a mechanism that underlies CSC function. Our pursuit of how VEGF activates TAZ revealed a key role for the Rho GTPase Rac1. More specifically, we observed that VEGF-NRP2 signaling promotes focal adhesion kinase (FAK)-mediated Rac1 activation.

One mechanism by which Rac1 contributes to TAZ activation involves p21-activated kinase (PAK), a Rac-activated kinase, that phosphorylates Merlin, the protein encoded by the Neurofibromatosis Type 2 gene, on Ser518 (147-149). This phosphorylation inhibits LATS phosphorylation (89, 97-99) and, consequently, facilitates

YAP/TAZ activation (63, 208). Consistent with these findings, we found that either Rac inhibition or NRP2 depletion in CSCs reduced the abundance of Ser518-phosphorylated Merlin and LATS-mediated phosphorylation of TAZ at Ser89 (63). This information, combined with the studies discussed above, highlights a critical role of Rac1 in YAP/TAZ activation by potentially eliciting a "dual hit" on LATS, through its regulation of the cytoskeleton and facilitating Merlin phosphorylation.

By profiling the expression of Rac1 guanine nucleotide exchange factors (GEFs) and GTPase activating proteins (GAPs) in CSCs and non-CSCs, we found that the expression of the Rac-specific GAP β2-chimaerin was significantly reduced in CSCs compared to non-CSCs. This led to our hypothesis that β2-chimaerin repression is a consequence of TAZ-dependent gene regulation, which is sustained by upstream VEGF-NRP2-Rac1 signaling. The functional significance of β2-chimaerin repression was demonstrated by depleting β2-chimaerin in non-CSCs and observing enhanced TAZ activity and CSC properties. Importantly, we identified an inverse correlation in the expression of TAZ with β2-chimaerin and positive correlations in the expression of TAZ with VEGF and NRP2 in human breast tumors. Although β2-chimaerin has been identified as a tumor suppressor in breast cancer (153-155), mechanisms of its transcriptional regulation had not been reported. As a result, our study characterized a positive feedback loop in breast CSCs where Rac1 functions as a nexus that connects VEGF-NRP2 signaling to TAZ activation by a mechanism that involves TAZ-dependent repression of the Rac GAP β2-chimaerin.

Interestingly, VEGF-mediated YAP/TAZ activation in CSCs appears to be mediated by NRPs and it does not seem to involve VEGFRs (63, 209), which distinguishes it from VEGF activation of YAP/TAZ in endothelial cells described above. This conclusion is substantiated by other studies in breast and prostate cancer cells, which argued that VEGF-NRP-mediated Rac1 activation is VEGFR-independent (63, 64). Given that NRPs function as co-receptors and lack intrinsic signaling properties (56, 57, 210), the issue of how NRPs activate YAP/TAZ arises. One mechanism involves the ability of NRP2 to function as a co-receptor for the α6β1 integrin. We reported that this integrin associates with NRP2 in breast cancer cells and that this interaction facilitates the signaling potential of this integrin, including its ability to activate FAK (68, 73), which is consistent with the report that VEGF-NRP2 activates Rac1 in a FAK-dependent manner (63). A more recent study confirmed the importance of NRPs in regulating α6 integrin signaling in epidermal CSCs and the lack of VEGFR involvement (209). More work is needed, however, to exclude the involvement of VEGFRs in VEGF-mediated YAP/TAZ activation definitively, especially in light of their key role in YAP/TAZ activation in endothelial cells.

Other work by our group refined the role of α6β1 signaling in sustaining CSC function by demonstrating that a cytoplasmic domain splice variant of the α6β1 integrin, termed α6**B**β1, promotes breast CSC function through downstream TAZ activation (129). In contrast, the other splice variant, α6**A**β1, lacks this ability. We also showed that the engagement of α6**B**β1 with a specific laminin in the extracellular matrix, laminin 511, is required for its ability to activate TAZ. This finding raises the important issue of the role of the extracellular matrix (ECM) in VEGF-mediated YAP/TAZ activation. Given that

this activation appears to be dependent on cytoskeletal dynamics and mechanical tension, the ECM is likely to be critical, as is the involvement of specific integrins as we have shown for laminin 511-α6**B**β1. Indeed, the role of ECM and integrins in VEGF-mediated YAP/TAZ activation is an area that is ripe for investigation for angiogenesis and CSC function. In the latter case, the concept of a CSC niche has emerged comprised of non-CSCs and ECM proteins that supports CSC function (211, 212). In fact, we identified laminin 511 as a component of this niche in breast cancer (129). Much more work needs to be done, however, to understand how ECM-integrin signaling functions in concert with VEGF signaling to impact YAP/TAZ activation. More than likely, other surface receptors are also involved in this process.

Concluding Comments

The role of YAP/TAZ activation in executing the functional consequences of VEGF signaling in endothelial and CSCs that has become apparent is providing new insight into the mechanisms that underlie angiogenesis and the acquisition of stem-like traits. A central theme that has emerged from these studies is the critical role of the Rho family of small GTPases in mediating the signaling events initiated by VEGF to activate YAP/TAZ. These GTPases contribute to YAP/TAZ activation indirectly by altering cytoskeletal dynamics (mechanical tension) and directly by inhibiting LATS phosphorylation. The transcriptional alterations that result from YAP/TAZ activation can initiate a positive feedback loop that sustains Rho GTPase activation and mechanical tension. Although

aspects of this signaling network had been established previously, the novelty of the recent studies highlighted in this review is the ability of VEGF and VEGF receptors to orchestrate this network. This mode of YAP/TAZ regulation is significant because VEGF signaling itself is tightly regulated during development and aberrantly activated by the tumor microenvironment, which provides a pathophysiological context for YAP/TAZ activation.

Looking forward, a better understanding of how the different types of VEGF receptors (receptor tyrosine kinases and NRPs) contribute to YAP/TAZ activation and their interaction with other surface receptors is needed. These studies should consider the role of the ECM and tissue microenvironment in VEGF receptor signaling (**Figure 4.1**). Other areas ripe for investigation that are depicted in **Figure 4.1** include delineating the specific contributions of different Rho GTPase family members to YAP/TAZ activation in the context of VEGF signaling. Also, much more needs to be learned about how YAP and TAZ affect gene expression to execute VEGF-mediated functions in endothelial and tumor cells and how YAP and TAZ may differ in this regard. The impact of this work is likely to be substantial given the intense interest in targeting VEGF signaling as a therapeutic approach for inhibiting angiogenesis and CSC function.

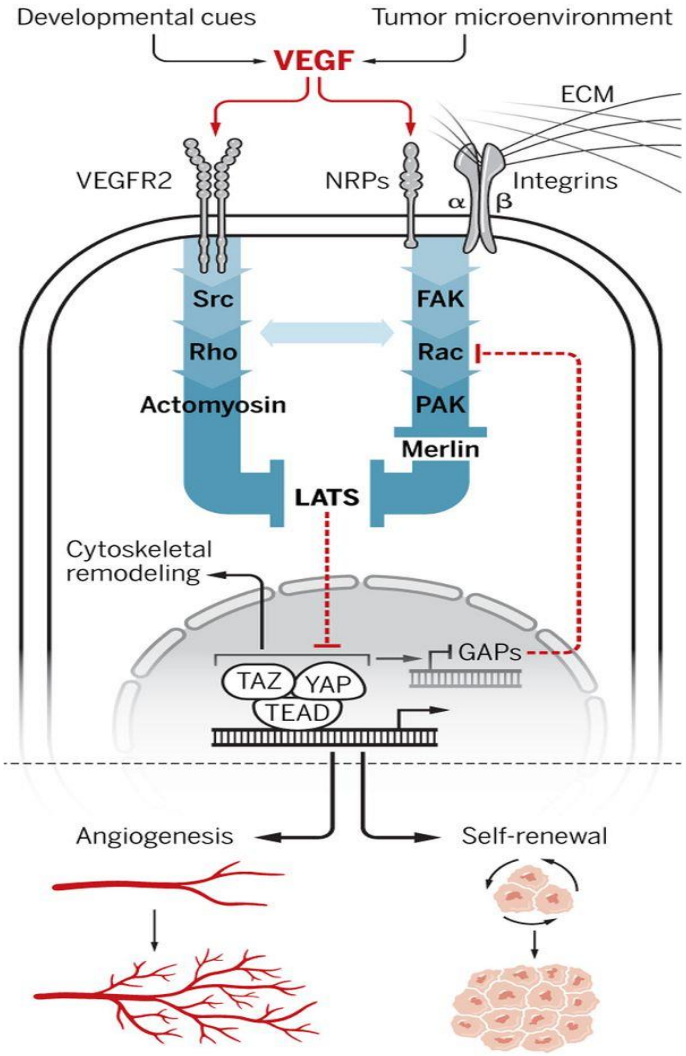

Figure 4.1. Schematic of VEGF and YAP/TAZ signaling thus far described in endothelial and tumor cells. Emerging studies suggest that VEGF signaling mediated by VEGFR2 and/or NRPs increases the activity of Rho family GTPases, resulting in LATS inhibition and YAP/TAZ activation, with consequent promotion of angiogenesis and stem cell maintenance. Integrins have a key role in this signaling by associating with NRPs and

engaging the extracellular matrix (ECM). VEGF signaling can involve Src-mediated Rho activation and the consequent activation of YAP/TAZ through cytoskeletal dynamics. It can also inhibit LATS by a Rac1-dependent mechanism that involves p21-activated kinase (PAK)–mediated inhibition of Merlin. An important question is whether these two mechanisms function in concert to promote YAP/TAZ activation in response to VEGF signaling. YAP/TAZ-mediated transcription can alter the expression of genes involved in cytoskeletal remodeling and in Rho and Rac1 activation, such as through the transcriptional repression of Rac GTPase activating proteins (GAPs) that normally turn off Rac, thereby establishing a positive feedback loop.

Role of the VEGF-NRP2-YAP/TAZ axis in DNA repair and therapy resistance

In the second study of this thesis, I established that autocrine VEGF-NRP2 signaling contributes to HR-directed repair in *BRCA*-wild type TNBC cells by contributing to the expression and function of the HR recombinase Rad51. Importantly, I identified Rad51 as a novel target gene of YAP/TAZ-TEAD-mediated transcriptional regulation. These findings are substantial because they integrate the VEGF-NRP2-YAP/TAZ signaling axis, discussed above, with HR-directed repair and therapy resistance. My findings implicating VEGF-NRP2-YAP/TAZ in DNA repair have potentially substantial implications for cancer biology and therapy.

Targeting VEGF-mediated signaling mechanisms in cancer is not a new idea. In fact, bevacizumab, the first VEGF inhibitor was approved by the Food and Drug Administration (FDA) for the treatment of breast cancer in 2004 (213). The rationale in inhibiting the function of VEGF was based on disrupting angiogenesis mediated by VEGF-VEGFR signaling in tumor-associated endothelial cells (214). By disrupting this key endothelial signaling axis, it was postulated that the reduction in oxygen and nutrient transportation to the tumor would contribute to inhibiting its growth. Following the approval of bevacizumab, several small molecule inhibitors of VEGFRs were developed that have shown favorable outcomes in several other tumor types including renal cell carcinoma, gastrointestinal tumors and hepatocellular carcinoma, among others (215). Surprisingly, although bevacizumab showed promise in the initial clinical trials that led to its approval, the FDA discontinued its label for the treatment of breast cancer in 2011 due to a lack of efficacy (1). This decision sparked intensive research into the mechanisms that

contribute to resistance to anti-angiogenic therapy and how this information can be incorporated into clinical decision making.

The seminal finding that my thesis builds on is that cancer cells express VEGF receptors, which can impact oncogenic processes independently of vascular biology. Given that cancer cells express NRPs in addition to VEGFRs, several studies have analyzed the potential contribution of autocrine and paracrine VEGF-NRP signaling in resistance to anti-angiogenic agents as well as other therapies. Consistent with my work that Rac1 is a key mediator of VEGF-NRP2 signaling in breast cancer cells, another study in prostate cancer demonstrated that VEGF-NRP2-Rac1 signaling promotes resistance to bevacizumab and VEGFR inhibitors (124). Specifically, prostate cancer cells selected for resistance to these agents exhibited CSC properties and up-regulation of VEGF and NRP expression, as well as enhanced Rac1 activity. The mechanism by which VEGF-NRP2 promotes resistance to anti-VEGF therapy is through downstream activation of extracellular regulated kinase (ERK), which subsequently facilitates expression of the Rac1 GEF P-rex1. This induction of P-rex1 occurs through ERK-mediated activation of Myc. Interestingly, P-rex1 is not expressed in TNBC (216), suggesting different mechanisms of VEGF-NRP2 activation of Rac1 that are tumor-type dependent. Nonetheless, these findings are significant because they directly implicate VEGF-NRP2-Rac1 signaling in resistance to anti-VEGF-VEGFR therapy and highlight this signaling axis as a potential therapeutic target in prostate cancer.

Consistent with the above report that NRP2 is upregulated in the adaptive resistance of tumor cells to therapy, another study demonstrated a key role for NRP1 in resistance to

targeted therapy (190). Specifically, NRP1 expression increases in melanoma cells resistant to BRAF inhibition and breast cancer cells resistant to HER2 inhibition. Enhanced NRP1 signaling contributed to c-jun N-terminal kinase (JNK) activation and subsequent upregulation of the epidermal growth factor receptor (EGFR) and insulin-like growth factor 1 receptor (IGF-1R), which sustained tumor cell growth and resistance.

The above studies characterizing NRPs in resistance to anti-VEGF and oncogene-targeted therapy provide important insight into their evolving role in tumor biology. However, VEGF-NRP signaling has not been implicated in resistance to DNA-damaging agents such as cytotoxic chemotherapy and radiation therapy, which are standards of care in most tumor types. It follows that determining mechanisms to overcome this resistance by targeting DNA damage pathways are being actively explored (217). My work implicating VEGF-NRP2 signaling in HR is novel and identifies this molecular association in resistance to commonly used anti-cancer therapies. This work provides rationale for further translational research integrating inhibitors of VEGF-NRP2 signaling with standard chemoradiation therapy regimens. This point is exemplified by my work in TNBC cells and organoids because efficient HR is a key determinant of TNBC patient therapeutic responses and disrupting VEGF-NRP2 signaling can sensitize to platinum chemotherapy, PARP inhibition and ionizing radiation.

Studies have reported that VEGF expression and secretion increases in the response of tumor cells to ionizing radiation and is associated with aggressive behavior (218, 219). My work establishing a function of autocrine VEGF-NRP2 signaling in HR has potentially important applications stemming from the observation that VEGF is upregulated in the

tumor microenvironment following radiation therapy. This is because enhanced VEGF-NRP2-mediated activation of YAP/TAZ and subsequent Rad51 expression in response to radiation is likely to promote resistance by stimulating HR. Therefore, regarding my point above about translational research integrating inhibitors of VEGF-NRP2 signaling with chemoradiation, it would be critical to study the kinetics of blocking NRP2 function. The reason for this is that combined inhibition of NRP2 with radiation and/or blocking NRP2 for a time period after radiation may lead to more favorable patient responses by disrupting the autocrine signaling mediated by enhanced VEGF in the tumor microenvironment.

Another major advance of my work is characterizing a role for YAP/TAZ in HR by regulating the expression of Rad51. Although YAP/TAZ have been implicated in the initiation and progression of breast and other cancers (110, 111), their contribution to DNA repair has not been previously reported, and my results and define a novel function of these transcriptional effectors. This finding is especially significant because YAP/TAZ have been implicated in therapy resistance, similar to VEGF-NRP2, but satisfying mechanisms have remained elusive (110). Given that YAP/TAZ confer CSC properties in TNBC, which have been implicated in tumor initiation, therapy resistance and recurrence (120-123), future work should focus on the role of Rad51 in CSCs and determining if CSCs exhibit more efficient HR than non-CSCs in response to therapy. This possibility is supported by my finding that YAP/TAZ contributes to Rad51 expression suggesting that breast CSCs, which are dependent on a YAP/TAZ transcriptional program, upregulate Rad51 as a mechanism of protecting themselves from genotoxic stress in order to preserve genomic integrity and facilitate long-term survival. These observations are consistent with

studies demonstrating that CSCs exhibit a more robust DNA damage response than non-CSCs in response to therapy (220). My findings integrating YAP/TAZ with Rad51 and HR provides a new dimension to our understanding of the critical role they play in breast cancer oncogenesis and, possibly, CSC survival and propagation following treatment with chemo- and radiation therapy.

Concluding remarks

My thesis work provides a mechanism by which autocrine VEGF signaling mediated by its non-canonical receptor NRP2 promotes CSC properties, DNA repair and therapy resistance in TNBC cells. Specifically, in the first part of my thesis, I characterized a previously unknown positive feedback circuit by which VEGF-NRP2 signaling converges on YAP/TAZ. In pursuit of this mechanism, I demonstrated a critical role for the Rac1 GTPase in mediating VEGF-NRP2 signaling to YAP/TAZ. Importantly, I discovered that the Rac GAP β2-chimaerin is a novel target gene that YAP/TAZ-TEAD represses to sustain enhanced Rac1 activity. These findings could have a profound impact in VEGF and YAP/TAZ biology by providing a targetable ligand-receptor association that contributes to enhanced YAP/TAZ activity. Additionally, subsequent studies have later revealed that Rho family GTPase GAPs can be regulated by and inhibit the functions of YAP/TAZ, which is consistent with my work that low β2-chimaerin expression is critical for YAP/TAZ activation (146).

The second part of my thesis extended the findings of Chapter II assessing the contribution of VEGF-NRP2-YAP/TAZ signaling in the response of TNBC cells to HR-inducing therapy. I identified novel functions of VEGF-NRP2 and YAP/TAZ in DNA

repair by demonstrating that they converge on Rad51 to promote efficient HR and therapy resistance in *BRCA*-wild type TNBC cells and organoids. This work also provides one of the first mechanisms governing Rad51 transcription, which is an area that is poorly understood. Together, my findings demonstrate a unified mechanism by which VEGF-NRP2-YAP/TAZ contributes to the aggressive behavior and therapy resistance of TNBC.

My findings have potentially substantial therapeutic implications. This is because targeting YAP/TAZ has been a challenge, and their inhibition has potential to disrupt physiological processes such as organ homeostasis. In addition, although Rad51 inhibitors exist, they can result in considerable toxicity because Rad51 has important housekeeping functions in DNA repair and replication. Given that NRP2 is preferentially expressed in tumors and contributes to hyper-activation of YAP/TAZ and high Rad51 expression, its inhibition may provide the selectivity needed to specifically disrupt the YAP/TAZ-Rad51 axis in cancer. Further translation research is of utmost importance to determine the viability of inhibiting NRP2 for TNBC patients.

APPENDIX

Real-time imaging of integrin β4 dynamics using a reporter cell line generated by Crispr/Cas9 genome editing

Ameer L. Elaimy, Ankur Sheel, Caitlin W. Brown, Melanie Walker, John J. Amante, Amanda Chan, Wen Xue, Christina Baer, Hira Lal Goel and Arthur M. Mercurio.

CONTRIBUTIONS:

Ameer L. Elaimy conceptualized the study, performed experiments, made the figures and wrote the manuscript. Ankur Sheel and Wen Xue contributed to the design of the Crispr constructs. Caitlin W. Brown and Melanie Walker contributed to image acquisition. John J. Amante contributed to flow cytometry experiments. Amanda Chan aided in the validation of the reporter cells. Christina Baer contributed to the set-up of live cell microscopy movies. Hira Lal Goel provided feedback on data and helped oversee the manuscript. Arthur M. Mercurio oversaw and conceptualized the study, provided feedback on experiments and wrote the manuscript.

Abstract

The ability to monitor changes in the expression and localization of specific integrins is essential for understanding their contribution to development, tissue homeostasis and disease. Here, we pioneered the use of Crispr/Cas9 genome editing to tag an allele of the β4 subunit of the α6β4 integrin. This integrin was chosen because of its diverse roles in epithelial and cancer biology. A tdTomato tag was inserted with a linker at the COOH-terminus of β4 in comma-d1 mouse mammary epithelial cells. Cells harboring this tagged allele were similar to wild-type cells with respect to the abundance of β4 on the cell surface, association of β4 with the α6 integrin subunit, as well as their ability to adhere to laminin and, consequently, activate Src. These β4 reporter cells were transformed with active YAP, which resulted in repression of β4 expression. The availability of control and YAP-transformed reporter cells enabled us to obtain novel insight into β4 dynamics in response to a migratory stimulus (scratch wound) by live-cell immunofluorescence video microscopy. Notably, an increase in β4 expression in cells proximal to the wound edge was evident and a population of β4 expressing cells that exhibited unusually rapid migration was identified. These findings that could shed insight into β4 dynamics during invasion and metastasis. Moreover, these β4 reporter cells should facilitate other studies on the contribution of this integrin to mammary gland biology and cancer.

Introduction

Changes in the expression and localization of specific integrins underlie the contribution of these receptors to a wide range of biological and pathological processes (221-224). The monitoring of these changes in real-time facilitates rigorous evaluation of their significance and functional contribution. The challenge to this approach, however, is preserving integrin function and cell homeostasis. For this reason, genome editing of integrins with Crispr/Cas9 technology has considerable potential. Although techniques describing integrin tagging have been previously described (225-228), Crispr/Cas9 genomic engineering to knock-in fluorescent tags has not been used for this purpose. This approach is ripe for employment because it allows direct visualization of the integrin transcribed from the endogenous gene and it circumvents the use of ectopic expression systems that have the potential for artifact. Given the challenges of monitoring integrins in real-time, the use of this technology to study their plasticity is timely and could be a useful resource for cell biologists.

A prime candidate for genome editing is the α6β4 integrin (referred to as 'β4' because there is only one β4 integrin). This integrin functions as a receptor for most laminins and it is expressed at the basal surface of many epithelial tissues (229, 230). The distinguishing structural feature of β4 is the atypical intracellular domain of the β4 subunit, which is distinct both in size (~1000aa) and structure from any other integrin subunit (231). A major function of this intracellular domain is to link β4 to intermediate filaments in stable adhesive structures termed hemidesmosomes (HDs) (232, 233). Our lab pioneered studies demonstrating that β4 has a more dynamic role in promoting cell migration and invasion

(234-236). Specifically, we discovered that β4 is mobilized from HDs in response to epithelial wounds or as a consequence of carcinoma progression and that it localizes in F-actin protrusions where it facilitates migration and invasion (237-242). Subsequent studies have confirmed and extended these findings e.g., (243, 244). These conclusions, however, were based primarily on immunofluorescence microscopy of fixed cells using β4-specific Abs and not real-time imaging of β4 in live cells. This consideration is significant because the published data suggest that rapid changes in β4 expression and localization may occur as cells acquire the ability to migrate.

In this Tools and Resources study, we used Crispr/Cas9-mediated homologous donor recombination (HDR) to knock-in a tdTomato tag to the cytoplasmic domain of the β4 integrin in mouse mammary epithelial cells. Oncogenic transformation of these cells with YAP enabled real-time monitoring and comparison of β4 expression and localization in live, normal and transformed epithelial cells in response to a scratch wound.

Results

Design and approach for Crispr/Cas9-mediated integrin β4 tagging:

We designed a strategy to knock-in a tdTomato tag connected by an 8 amino acid linker to the COOH-terminus of mouse integrin β4 using Crispr/Cas9-mediated homologous donor recombination (HDR). Our approach was based on limiting the likelihood of the endogenous tag altering β4 function, which includes laminin binding extracellularly and β4 signaling intracellularly. To accomplish this goal, we inserted the tdTomato tag connected by a linker at the COOH-terminus (cytoplasmic domain) near the last exon of

β4 because it ensures that the tag will not interfere with laminin binding extracellularly. The purpose of the linker was to provide space between β4 and the fluorescent tag to limit disruption of β4 interactions with cytoplasmic molecules.

Our initial step was to design, test the cutting efficiency and the effects on β4 expression of four sgRNAs targeting the region of the last exon of mouse integrin β4. Our goal in choosing a sgRNA and designing a corresponding donor plasmid was to identify a sgRNA that exhibits the greatest cutting efficiency and does not alter β4 expression. As shown in **Fig. A.1A**, none of the four sgRNAs we tested reduced β4 surface abundance when compared to a non-target sgRNA. This result can be explained because the sgRNAs we designed correspond to the region of the last exon of β4, as opposed to Crispr/Cas9 gene knockout which typically targets one of the first exons of a gene. We ultimately chose sgRNA #2 because it exhibited the greatest cutting efficiency by Tracking of Indels by Decomposition (TIDE) analysis (**Fig. A.1B**), which is a quantitative Sanger sequencing assessment that determines the nature and degree of targeted mutations (245). sgRNA #2 targets a component of the TGA stop codon and cuts 3 base pairs after the stop codon (**Fig. A.1C**). Therefore, one consideration in the design of the donor plasmid that corresponds to sgRNA #2 is to avoid Cas9 cutting the endogenous locus after HDR has occurred. To accomplish this goal, we introduced silent mutations in the component of the stop codon of the sgRNA (TGA to TAA) and the protospacer adjacent motif (PAM), which also consists of a component of the last codon (threonine) of β4 (ACC to ACG) (**Fig. A.1C**). We designed 900 base pair left and right homology arms in the donor plasmid based on a high recombination efficiency observed in prior studies (246). The linker sequence

(GGSGGSGG) was placed directly upstream of tdTomato, and we inserted a blasticidin resistance gene in the donor plasmid because the sgRNA #2/Cas9 plasmid contains a puromycin resistance gene.

Validation of the correct genomic insert in mammary epithelial cells:

Following the design of the donor plasmid that corresponds to sgRNA #2, we co-transfected circular donor and sgRNA/Cas9 plasmids into comma-d1 cells, which are mouse mammary epithelial cells (247, 248) that express β4. After 72 hours, we analyzed tdTomato expression by flow cytometry and observed that cells transfected with donor/sgRNA/Cas9 exhibited 1.2% tdTomato positive cells compared to control cells transfected with donor only (**Fig. A.1D**), which is a similar number of fluorescent cells observed using other Crispr/Cas9 knock-in strategies (249). Of note, we also transfected linearized donor plasmid with sgRNA/Cas9 but did not obtain any positive clones.

We subsequently performed a single-cell sort for tdTomato positive cells and grew surviving clones for the next 2-3 weeks to screen for the correct genomic insert. Clones were initially screened by polymerase chain reaction (PCR) amplification of the junction between β4 genomic DNA and the left homology arm using the donor plasmid as a negative control (**Fig. A.1E**). Amplification of the regions between the left homology arm and tdTomato, and the right homology arm and tdTomato was performed using the donor plasmid as a positive control (**Fig. A.1E**). The heterozygous tdTomato tagged β4 allele was verified by immunoblotting (**Fig. A.1F**). β4 reporter comma-d1 cells were 80% positive for tdTomato (**Fig. A.1G**), which is greater than other studies reporting between 22 and 76% positive cells using alternative Crispr/Cas9 knock-in strategies (249).

Integrin β4 reporter cells retain properties of parental cells:

After validation of the correct genomic insert, we evaluated the potential effect of the tdTomato tag on the function of β4. The comma-d1 reporter and parental cells exhibit similar levels of β4 at the cell surface indicating that the COOH-terminal tdTomato tag did not alter β4 trafficking and surface localization (**Fig. A.2A**). The tdTomato tag also did not interfere with integrin α6 pairing (**Fig. A.2B**). Importantly, the reporter and parental cells did not differ significantly in their ability to adhere to laminin111 (**Fig. A.2C**) and, consequently, activate Src (**Fig. A.2D**), which is an effector of β4-mediated signaling (250, 251).

Comma-d1 cells exhibit mammary progenitor potential (247, 252, 253), and we did not observe differences in the number of mammospheres between the reporter and parental cells indicating that progenitor properties are not altered in the β4 reporter cells (**Fig. A.2E**). Together, these data suggest that cyto-tagging β4 using Crispr/Cas9 does not alter its function. They also indicate that the resulting reporter cells are similar in nature to parental comma-d1 cells and that our strategy limited potential off-target effects related to Crispr/Cas9 genomic alterations.

Real-time visualization of the expression and localization of the β4 integrin in migrating cells:

The generation of a β4 reporter cell line provided an opportunity to visualize β4 expression and localization in real-time by immunofluorescence video microscopy. Given the established role of β4 in cell migration, a scratch wound was made in the monolayer immediately before filming. A burst of β4 expression was observed approximately 6 hours following wounding, especially in cells at the wound edge concomitant with an increase in

chemokinetic migration (**Fig. A.3; Movies 1,2).** However, there was little evidence of directional migration to heal the wound.

Based on the fact that the oncogenic transformation of epithelial cells stimulates their migration, we transformed our reporter cell line with YAP, which is a transcriptional effector of the Hippo tumor suppressor pathway that has been implicated in breast cancer progression, stemness, epithelial to mesenchymal transition (EMT) and drug resistance (110, 113, 254-257). More specifically, we used a constitutively active form of YAP (5SA) to transform the comma-d1 reporter cells. This transformation increased the expression of YAP target genes ANKRD1 and Cyr61 (**Fig. A.4A,B**), promoted soft agar colony growth (Fig. 4C) and increased mammosphere number (**Fig. A.4D**). Interestingly, YAP transformation decreased β4 mRNA expression (**Fig. A.4E**), and it reduced β4 surface abundance markedly (**Fig. A.4F**).

Immunofluorescence video microscopy of YAP-transformed reporter cells in response to a scratch wound revealed directional migration of cells into the scratch by 3 hours and restoration of the monolayer within 18 hrs of wounding (**Fig. 5; Movies 3-6**). We were able to detect several noteworthy aspects of β4 expression and localization because of our ability to visualize endogenous integrin in real-time. The most striking observation was an induction of the β4/tdTomato signal in cells proximal to the wound edge, which was evident within 3 hrs of wounding. Given that YAP transformation represses β4 (**Fig. A.4E, F**), this observation implies that that the migratory stimulus imposed by the wound is sufficient to induce expression of this integrin. It also appeared that the induction of β4 expression was coincident with the acquisition of motility in

multiple cells. As the wounds healed and the monolayer was restored, the β4/tdTomato signal diminished. Another key observation was the dynamic polarization of β4 signal at the leading edge of cells, which is consistent with its role in driving migration. Although it was not feasible to quantify the velocity of individual cells because of the heterogeneity of the population and the number of tdTomato-positive cells, it was evident from observing the videos that the tdTomato cells exhibited rapid directional migration and that some of these cells migrated across the monolayer extremely quickly relative to migrating neighboring cells (See arrows in **Fig. A.5; Movies 3-6**).

Discussion

The results of this study demonstrate the usefulness of Crispr/Cas9 genome editing to tag endogenous integrins for studies aimed at evaluating their expression, localization and function. We were able to engineer an allele of the β4 integrin subunit with a tdTomato tag at its COOH-terminus that retained the properties of the wild-type allele and generate reporter cells harboring this tagged allele. This resource, which enabled us to visualize β4 in real-time, has distinct advantages over the use of immunofluorescence microscopy because it does not require fixation and is independent of issues related to antibody specificity. Moreover, although the use of expression plasmids containing an epitope tag has proven useful for integrin studies, e.g., (225-228) , there are potential artifacts with this approach including the level of expression of the tagged integrin and competition with endogenous integrin that are obviated by the use of Crispr/Cas9 genome editing.

The most exciting and informative data we obtained was from our analysis of β4 expression and localization in response to a migratory stimulus (scratch wound). Although

previous studies by our group and others had implicated β4 in migration, the ability to visualize endogenous integrin in real-time proved to be quite powerful. This approach substantiated the dynamic nature of β4 during migration that we and others had observed based on more indirect approaches (235) but it also revealed novel insights. Specifically, we note the relatively rapid increase in β4 expression that appeared to be coincident with the acquisition of motility in YAP-transformed reporter cells at the wound edge. This finding provides visual evidence that supports previous work implicating β4 in migration (235). It also underscores the notion that β4 expression and localization can change rapidly in response to alterations in the microenvironment. This consideration should be a note of caution, for example, when interpreting data on the expression and localization of β4 in tumors based on the analysis of static images. We were also struck by the extremely rapid migration of some of the YAP-transformed, β4-expressing cells, which was unexpected. These cells would not have been detected without their ability to be imaged in real-time, and their nature clearly merits further investigation.

The β4 reporter cells that we have generated should be quite useful for studying other aspects of the contribution of this integrin to mammary gland biology and cancer. Comma-d1 cells are progenitor cells and capable of populating a mammary gland upon injection into the mammary fat pad of mice (247, 252, 253). Long-term intravital microscopy (258) of the β4-tagged comma-d1 cells could provide novel insight into β4 dynamics during mammary gland development. The same approach could be used to visualize β4 during tumor formation *in vivo* using the YAP-transformed reporter cells. Given that β4 has been implicated in metastasis (234, 259, 260), the presence of the

tdTomato tag could facilitate the isolation and characterization of circulating tumor cells from mice harboring tumors generated by orthotopic injection of the YAP-transformed reporter cells.

Materials and Methods

Antibodies, flow cytometry and cell culture

Immunoblotting antibodies were acquired as follows: Actin (4970S, Cell Signaling Technologies), β4 (ab29042, Abcam), red fluorescent protein that cross-reacts with tdTomato (ab62341, Abcam), Src (2108S, Cell Signaling Technologies), pY416 Src (2101S, Cell Signaling Technologies), α6 (provided by Dr. Anne Cress, University of Arizona) and Myc-tag (2278S, Cell Signaling Technologies). β4 antibody 34611A (ab25254, Abcam) was used for flow cytometry. Comma-d1 cells were provided by Dr. Nicholas Tonks (Cold Spring Harbor) and were cultured in Dulbecco's Modified Eagle Medium (DMEM)/F12 medium supplemented with 5% fetal bovine serum, insulin, epidermal growth factor (EGF) and HEPES.

Constructs, sgRNAs and transfection

We initially tested the cutting efficiency of 4 sgRNAs targeting the region of the last exon of mouse integrin β4 (sgRNA #1 = TGACCCAGGAATTCGTGACC; sgRNA #2 = CTGGGGCGCGGGGGAGGTTC; sgRNA #3 = GAGGAAGAAGGCGCTAGGAG; sgRNA #4 = GAGAGAGCCACTGGCCGTTA by cloning each sgRNA into lentiCrispr V2 vector. Cells were subsequently infected with lentivirus carrying each sgRNA and puromycin selected (2 μg/mL) for 2 days. TIDE

analysis (https://tide.nki.nl/) was performed to assess cutting efficiency of each sgRNA as well as flow cytometry to determine the effects on β4 surface abundance.

After selecting the sgRNA #2 sequence, VectorBuilder (https://en.vectorbuilder.com/) was used to construct puromycin resistant sgRNA #2/Cas9 plasmid (ID: VB180312-1135bvn) and the corresponding blasticidin resistant donor plasmid (ID: VB180312-1325zpa) to be transfected into comma-d1 cells. Approximately 75,000 cells were seeded in six-well plates. The next day cells were transfected with 800 nanograms sgRNA/Cas9 plasmid and 500 nanograms circular donor plasmid using lipofectamine 3000 (Thermo Fisher Scientific) and processed for single-cell sorting 72 hours later. Hygromycin resistant Myc-5SA-YAP was purchased from Addgene (plasmid #33093) and was used to transform the β4 reporter comma-d1 cells.

Polymerase chain reaction

For qPCR, RNA was isolated using an RNA extraction kit (BS88133, Bio Basic Inc) and cDNAs were produced using qScript cDNA kit (#95047, Quantabio). The qPCR master mix used was SYBR green (Applied Biosystems) and experiments were performed with three technical replicates and normalized to 18S. The Massachusetts General Hospital/Harvard Medical School PrimerBank (http://pga.mgh.harvard.edu/primerbank/) was used to obtain qPCR primer sequences.

To assess the correct insertion of tdTomato, genomic DNA was isolated using mammalian genomic DNA isolation kit (G1N70, Sigma) from comma-d1 cells that were grown from single cell clones. Primers were designed to amplify the junction between β4 genomic DNA and the left homology arm (Forward: 5'-AGGACCCCTCCAAATCAGTT-

3’; Reverse: 5’-CAGGTCACCAGGTAGCCAAG-3’), the left homology arm and tdTomato (Forward: 5’- GAGCTGGGACCTGTACTCCA-3’; Reverse: 5’-GCTTCTTGTAATCGGGGATG-3’) and tdTomato and the right homology arm (Forward: 5’- CCCGGCTACTACTACGTGGA-3’; Reverse: 5’-AGAACAAAAGGCTGGGGACT-3’).

Mammosphere and soft agar assays

UltraLow attachment 6 well plates were used for mammosphere experiments. Cells were plated in DMEM/F12 medium supplemented with B27, EGF and fibroblast growth factor as previously described (63, 130). Serial passaging was performed by pelleting and dissociating mammospheres with 0.05% Trypsin for 15 minutes at 37 degrees Celsius to obtain single cells, which were washed in 1X PBS, counted and re-plated in UltraLow attachment 6 well plates. Soft agar colony formation was performed as previously described (66).

Immunoblotting and co-immunoprecipitation

Immunoblotting was accomplished by washing cells in 1X PBS and scraping them on ice in RIPA buffer with EDTA and EGTA (BP-115DG, Boston Bioproducts) supplemented with protease and phosphatase inhibitors (Roche, 04693132001). Laemmli buffer (BP-111R, Boston Bioproducts) was added to each sample and the lysate was boiled and separated using sodium dodecyl polyacrylamide gel electrophoresis (SDS-PAGE). NP-40 lysis buffer (BP-119, Boston Bioproducts) containing protease and phosphatase inhibitors (Roche, 04693132001) was used to extract protein for co-immunoprecipitation. Protein A agarose beads were added to the lysate and incubated for one hour at 4º Celsius

for pre-clearing. Lysates were subsequently incubated with α6 antibody (555736, BD Biosciences) or IgG overnight at 4º Celsius. The next morning lysates were incubated again with protein A agarose beads at 4º Celsius for one hour to pull down the protein complexes, which were separated using SDS-PAGE and immunoblotted for α6 and β4.

Laminin attachment assay

Cell culture dishes were coated with laminin-111 (23017015, Thermo Fisher Scientific) and blocked in 1% bovine serum album at for one hour at 37 degrees Celsius. Cells were trypsinized, plated on the laminin-111 coated plates and allowed to attach for one hour. Subsequently, cells were lysed and immunoblotted for pY416 Src and Src or stained with crystal violet to measure the OD at 595 nm to determine adhesion.

Scratch wound assay

Cells were seeded on six-well plates and grown to confluency. A DeltaVision wide field deconvolution fluorescence microscope with temperature and CO_2 control was used to capture images at 20X magnification of migrating cells at 15-minute intervals for 18 hours or 72 hours following the introduction of a scratch with a pipet tip.

Figures

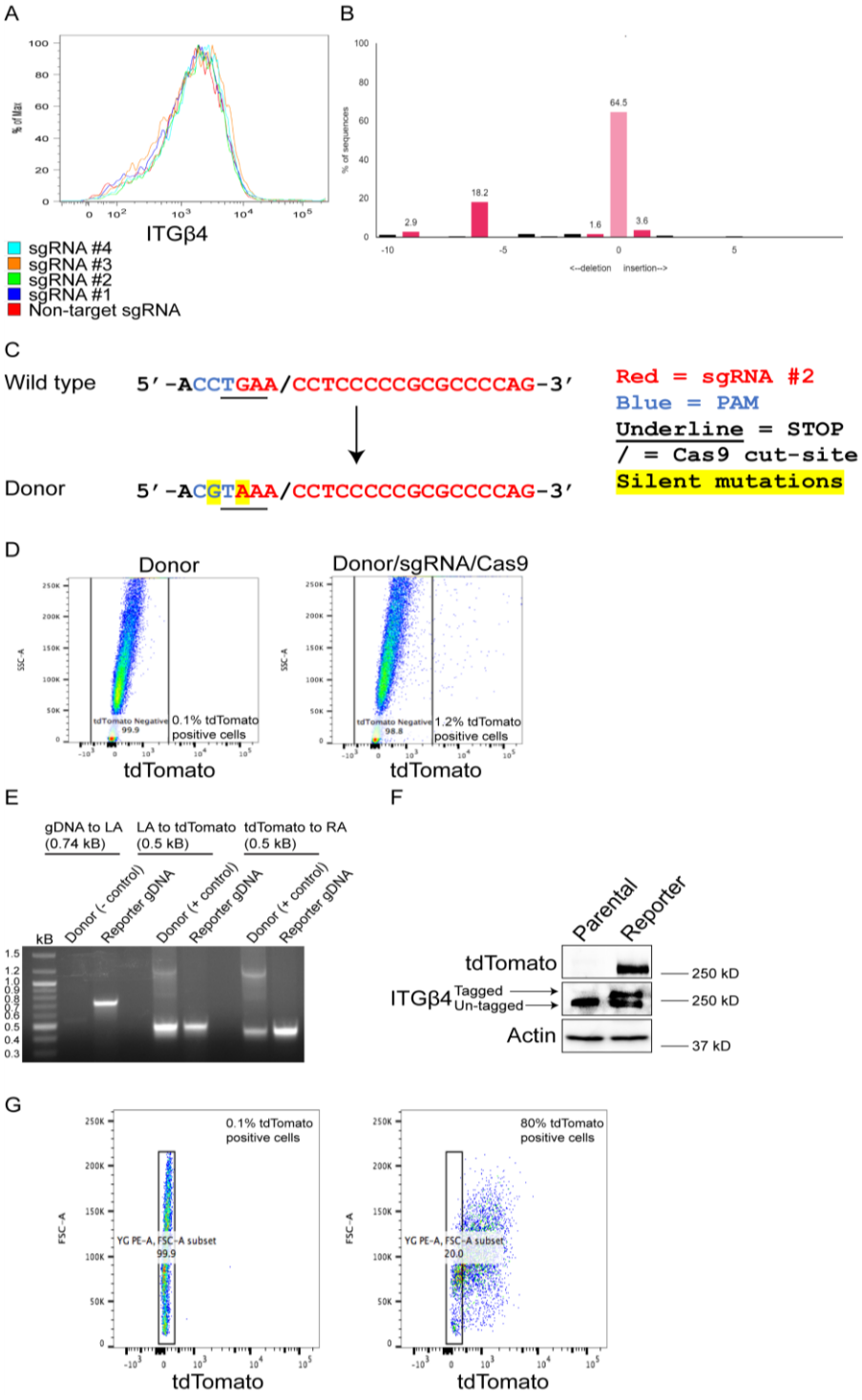
A
ITGβ4
sgRNA #4
sgRNA #3
sgRNA #2
sgRNA #1
Non-target sgRNA
B
% of sequences
64.5
18.2
2.9
1.6
3.6
<--deletion insertion-->
C
Wild type 5′-ACCTGAA/CCTCCCCCGCGCCCCAG-3′
Donor 5′-ACGTAAA/CCTCCCCCGCGCCCCAG-3′
Red = sgRNA #2
Blue = PAM
Underline = STOP
/ = Cas9 cut-site
Silent mutations
D
Donor
Donor/sgRNA/Cas9
tdTomato Negative 99.9
0.1% tdTomato positive cells
tdTomato Negative 98.8
1.2% tdTomato positive cells
tdTomato
E
gDNA to LA (0.74 kB)
LA to tdTomato (0.5 kB)
tdTomato to RA (0.5 kB)
kB
Donor (- control)
Reporter gDNA
Donor (+ control)
Reporter gDNA
Donor (+ control)
Reporter gDNA
F
Parental
Reporter
tdTomato
ITGβ4
Tagged
Un-tagged
Actin
250 kD
250 kD
37 kD
G
0.1% tdTomato positive cells
YG PE-A, FSC-A subset 99.9
80% tdTomato positive cells
YG PE-A, FSC-A subset 20.0
FSC-A
tdTomato

Fig. A.1. Design, approach and validation for Crispr/Cas9-mediated integrin β4 tagging. (A) Comma-d1 cells expressing either a non-target sgRNA or one of four sgRNAs targeting the region of the last exon of mouse integrin β4 were processed for flow cytometry to determine the effects on β4 surface abundance. (B) Genomic DNA was isolated from cells from (A) and was processed for TIDE analysis to quantify cutting efficiency of each sgRNA. (C) Depiction of the Crispr/Cas9 knock-in strategy and alterations that were engineered in the donor plasmid relative to the wild type β4 sequence. Mouse integrin β4 DNA sequence was downloaded from Ensembl genome browser (https://useast.ensembl.org/index.html). Note that the sgRNA used corresponds to the complementary DNA strand shown. (D) Comma-d1 cells were transfected with donor plasmid alone or donor plasmid and sgRNA #2/Cas9 plasmid and processed for flow cytometry to quantify tdTomato positive cells, which were subsequently processed for single-cell sorting. (E) Genomic DNA from clones described (D) was isolated and processed for PCR to determine the correct genomic insert of tdTomato. (F) Immunoblotting was performed to confirm expression of tdTomato and the heterozygous tdTomato tagged β4 allele. (G) Expression of tdTomato was quantified by flow cytometry to determine percentage of tdTomato positive cells.

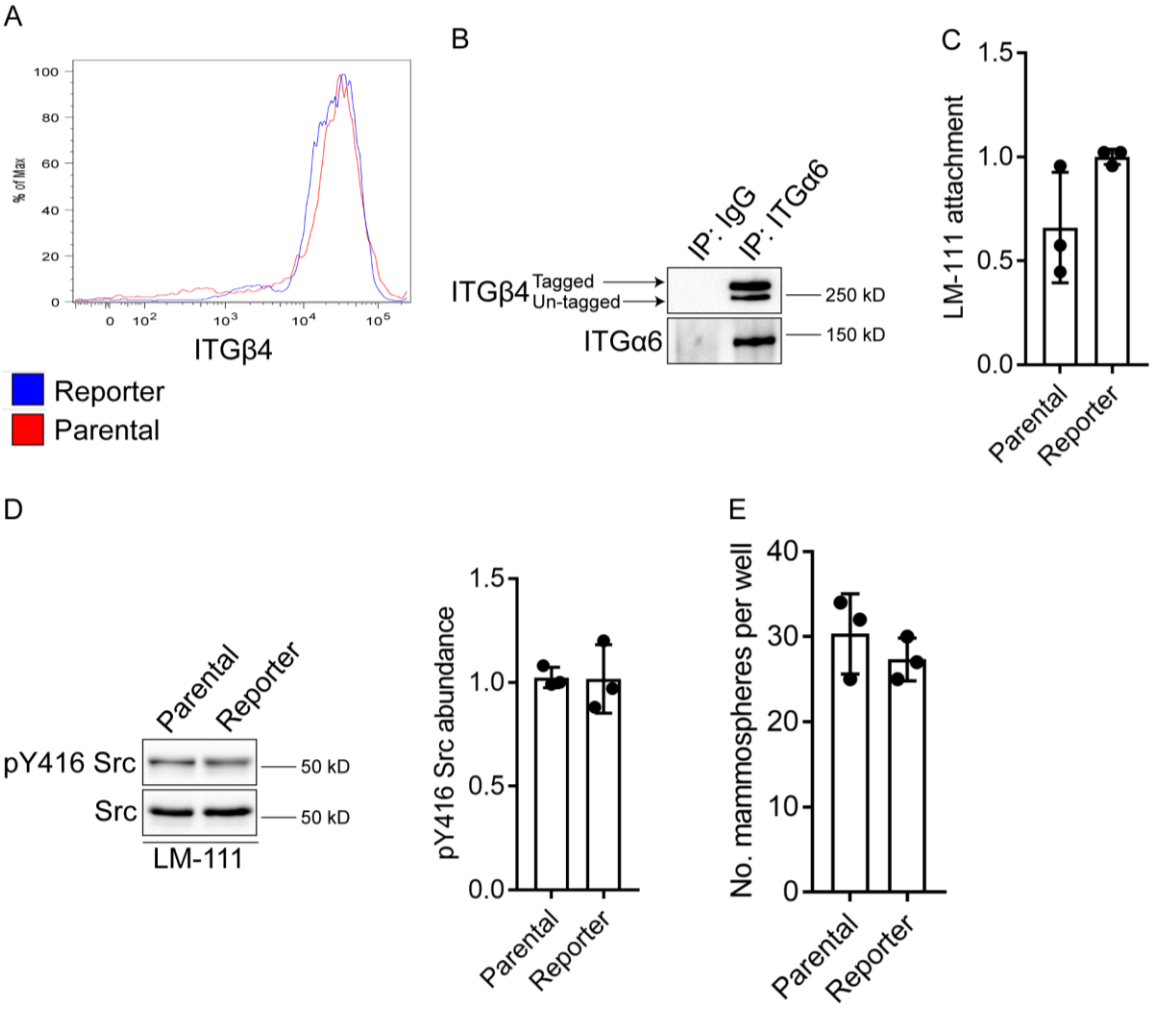

Fig. A.2. Integrin β4 reporter cells exhibit properties of parental cells. (A) Analysis of β4 surface expression by flow cytometry of β4 reporter (blue line) and parental (red line) comma-d1 cells. (B) Extracts of β4 reporter cells were immunoprecipitated using an integrin α6 Ab and then immunoblotted using an integrin β4 Ab. Note that both the tagged- and untagged β4 alleles associate with α6. (C) Cell culture dishes were coated with laminin-111 and β4 reporter and parental comma-d1 cells were allowed to attach for one hour. Subsequently, crystal violet staining was performed to compare laminin-111

attachment. (D) The cells in (C) were immunoblotted using a pY416 Src Ab to assess Src activation. Densitometry was performed on these immunoblots using ImageJ (right graph). (E) Mammosphere forming ability was assessed in β4 reporter and parental comma-d1 cells. Dot plots (mean ± standard deviation) are representative of three independent experiments. * $p \leq 0.05$ by two-tailed *t* test.

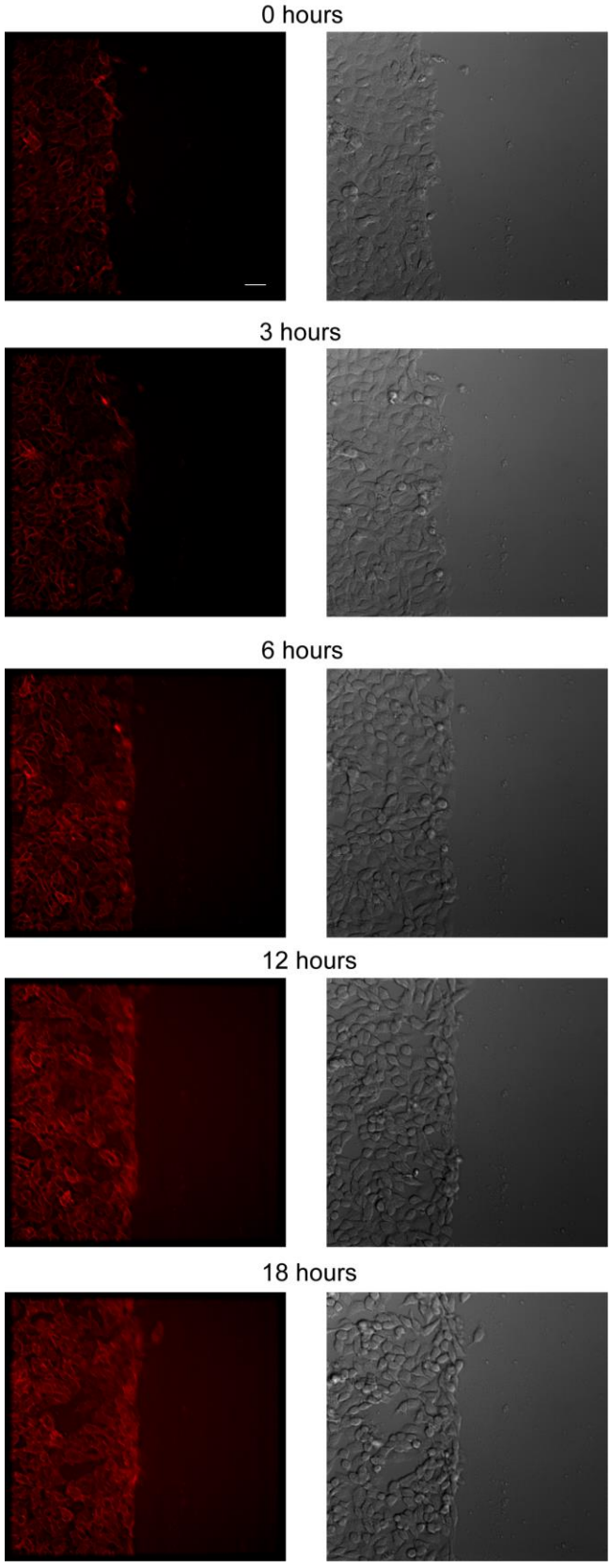
0 hours
3 hours
6 hours
12 hours
18 hours

Fig. A.3. Monitoring integrin β4 dynamics in non-transformed reporter cells in response to a scratch wound. A scratch wound was introduced in β4 reporter comma-d1 cells which were monitored for 18 hours. Representative still images are shown. Also seen Movies 1 and 2 for real-time immunofluorescence video microscopy. Scale bar represents 25 micrometers.

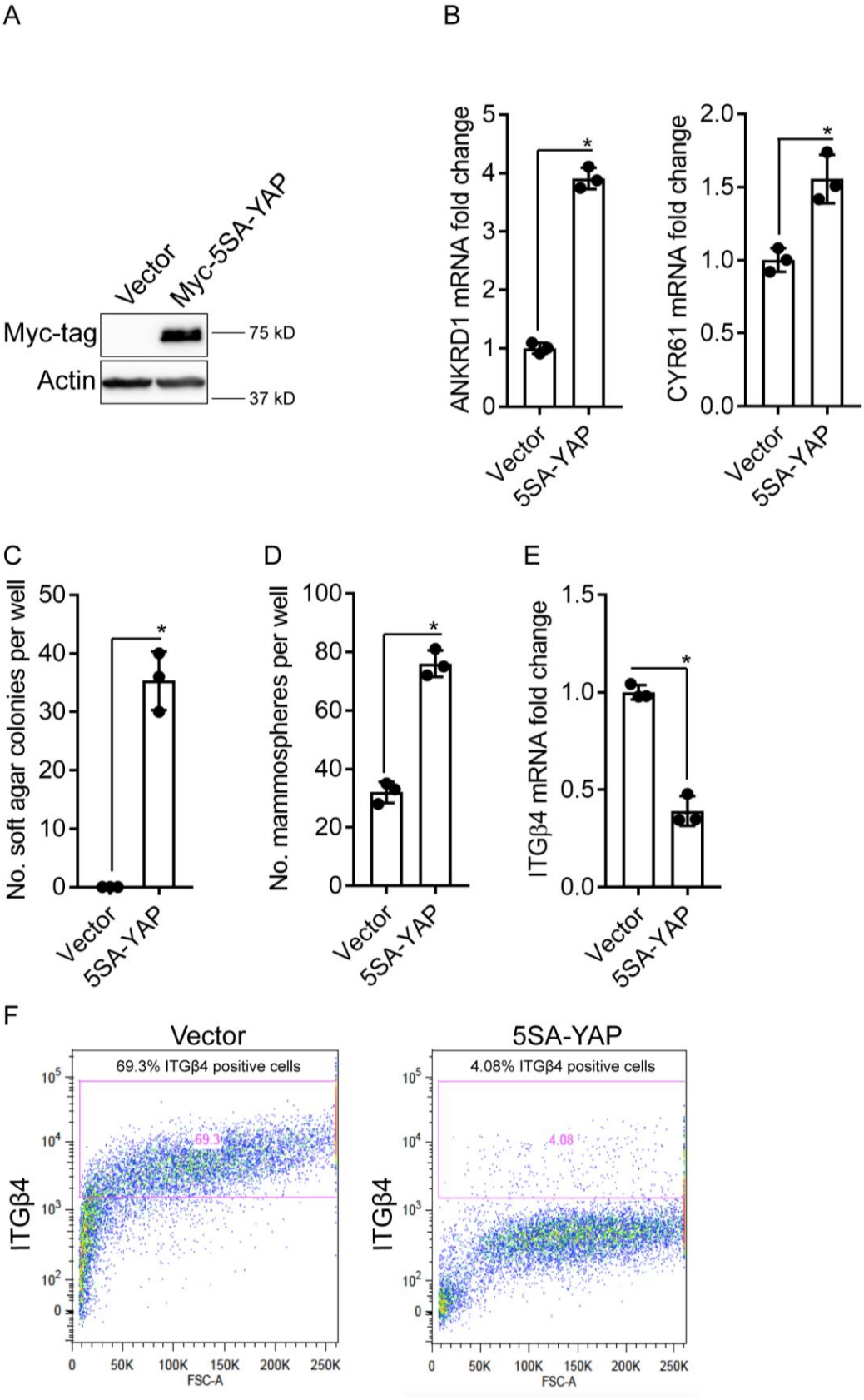
A
Vector
Myc-5SA-YAP
Myc-tag
75 kD
Actin
37 kD
B
ANKRD1 mRNA fold change
CYR61 mRNA fold change
Vector
5SA-YAP
C
No. soft agar colonies per well
D
No. mammospheres per well
E
ITGβ4 mRNA fold change
F
Vector
69.3% ITGβ4 positive cells
5SA-YAP
4.08% ITGβ4 positive cells
ITGβ4
FSC-A

Fig. A.4. YAP transformation of integrin β4 reporter cells. (A) Expression of Myc-5SA-YAP or empty vector in β4 reporter comma-d1 cells was evaluated by immunoblotting. (B) Expression of the YAP target genes ANKRD1 and Cyr61qPCR in both populations was quantified by qPCR. Soft agar colony (C) and mammosphere formation (D) was assessed in the control and YAP-transformed β4 reporter comma-d1 cells. (E) β4 mRNA expression was quantified in the control and YAP-transformed cells by qPCR. (F) Analysis of β4 surface expression by flow cytometry of β4 reporter cells expressing empty vector or 5SA-YAP. Dot plots (mean ± standard deviation) are representative of three independent experiments. * $p \leq 0.05$ by two-tailed *t* test.

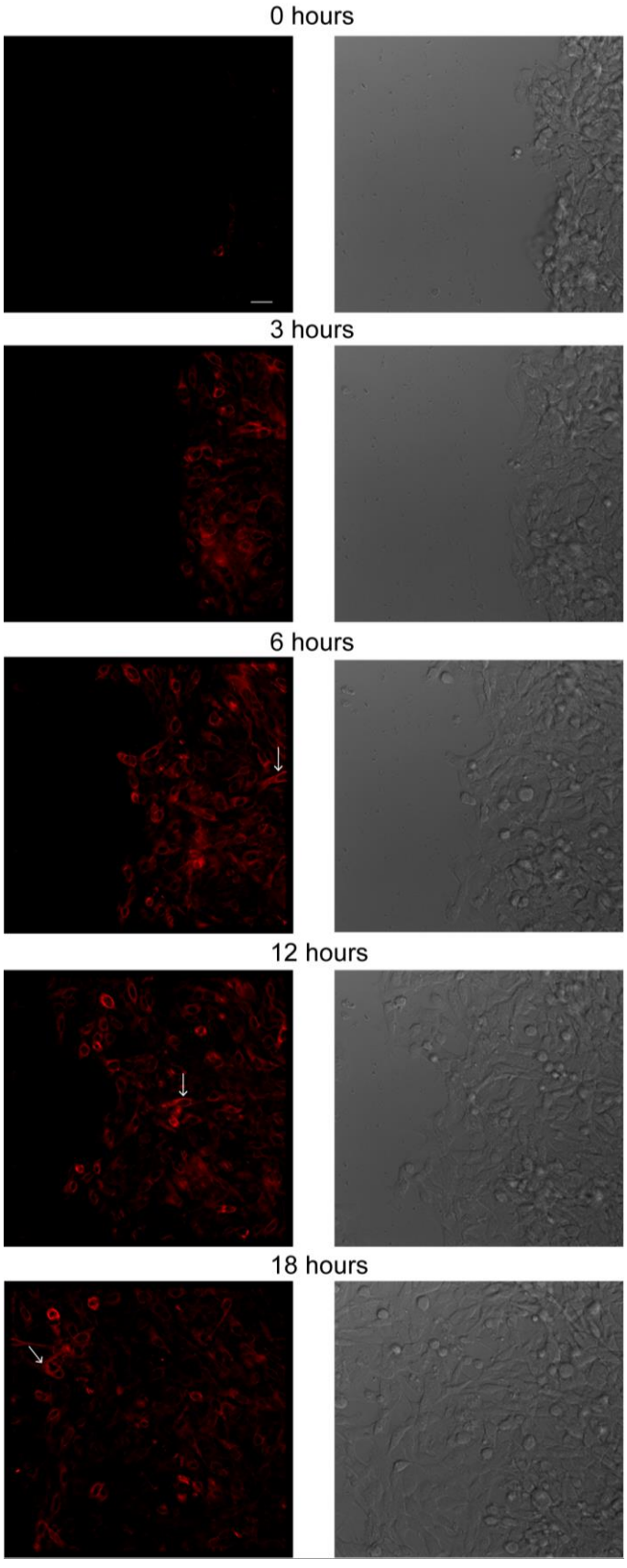
0 hours
3 hours
6 hours
12 hours
18 hours

Fig. A.5. Monitoring integrin β4 dynamics in YAP-transformed reporter cells in response to a scratch wound. A scratch wound was introduced in YAP-transformed β4 reporter comma-d1 cells which were monitored for 18 hours. Representative still images are shown. Arrow indicates an example of a β4 positive cell that migrated more rapidly than neighboring cells. Also see Movies 3-6 for real-time immunofluorescence video microscopy. Scale bar represents 25 micrometers.

Movie 1. 18-hour movie of control β4 reporter comma-d1 cells in response to a scratch wound using a green differential interference contrast (DIC) background. Scale bar represents 25 micrometers.

Movie 2. Movie 1 without a DIC background. Scale bar represents 25 micrometers.

Movie 3. An 18-hour movie of YAP-transformed β4 reporter comma-d1 cells in response to a scratch wound using a green DIC background. Scale bar represents 25 micrometers.

Movie 4. Movie 3 without a DIC background. Scale bar represents 25 micrometers.

Movie 5. 72-hour movie of YAP-transformed β4 reporter comma-d1 cells in response to a scratch wound using a green DIC background. Scale bar represents 25 micrometers.

Movie 6. Movie 5 without a DIC background. Scale bar represents 25 micrometers.

Bibliography

1. Tejpar S, Prenen H, & Mazzone M (2012) Overcoming resistance to antiangiogenic therapies. *Oncologist* 17(8):1039-1050.
2. Geretti E, *et al.* (2010) A mutated soluble neuropilin-2 B domain antagonizes vascular endothelial growth factor bioactivity and inhibits tumor progression. *Mol Cancer Res* 8(8):1063-1073.
3. Downs-Holmes C & Silverman P (2011) Breast cancer: overview & updates. *Nurse Pract* 36(12):20-26; quiz 27.
4. Bombonati A & Sgroi DC (2011) The molecular pathology of breast cancer progression. *J Pathol* 223(2):307-317.
5. Meisel JL, Venur VA, Gnant M, & Carey L (2018) Evolution of Targeted Therapy in Breast Cancer: Where Precision Medicine Began. *Am Soc Clin Oncol Educ Book* (38):78-86.
6. Waks AG & Winer EP (2019) Breast Cancer Treatment: A Review. *JAMA* 321(3):288-300.
7. Baselga J, Coleman RE, Cortes J, & Janni W (2017) Advances in the management of HER2-positive early breast cancer. *Crit Rev Oncol Hematol* 119:113-122.
8. Bianchini G, Balko JM, Mayer IA, Sanders ME, & Gianni L (2016) Triple-negative breast cancer: challenges and opportunities of a heterogeneous disease. *Nat Rev Clin Oncol* 13(11):674-690.
9. Russnes HG, Lingjaerde OC, Borresen-Dale AL, & Caldas C (2017) Breast Cancer Molecular Stratification: From Intrinsic Subtypes to Integrative Clusters. *Am J Pathol* 187(10):2152-2162.
10. Polyak K (2007) Breast cancer: origins and evolution. *J Clin Invest* 117(11):3155-3163.
11. McGranahan N & Swanton C (2017) Clonal Heterogeneity and Tumor Evolution: Past, Present, and the Future. *Cell* 168(4):613-628.
12. Meacham CE & Morrison SJ (2013) Tumour heterogeneity and cancer cell plasticity. *Nature* 501(7467):328-337.
13. Batlle E & Clevers H (2017) Cancer stem cells revisited. *Nat Med* 23(10):1124-1134.
14. Al-Hajj M, Wicha MS, Benito-Hernandez A, Morrison SJ, & Clarke MF (2003) Prospective identification of tumorigenic breast cancer cells. *Proc Natl Acad Sci U S A* 100(7):3983-3988.
15. Stingl J, *et al.* (2006) Purification and unique properties of mammary epithelial stem cells. *Nature* 439(7079):993-997.
16. Shibue T & Weinberg RA (2017) EMT, CSCs, and drug resistance: the mechanistic link and clinical implications. *Nat Rev Clin Oncol* 14(10):611-629.
17. Mani SA, *et al.* (2008) The epithelial-mesenchymal transition generates cells with properties of stem cells. *Cell* 133(4):704-715.
18. Pece S, *et al.* (2010) Biological and molecular heterogeneity of breast cancers correlates with their cancer stem cell content. *Cell* 140(1):62-73.

19. Zardavas D, Irrthum A, Swanton C, & Piccart M (2015) Clinical management of breast cancer heterogeneity. *Nat Rev Clin Oncol* 12(7):381-394.
20. Fleck O & Nielsen O (2004) DNA repair. *J Cell Sci* 117(Pt 4):515-517.
21. Ciccia A & Elledge SJ (2010) The DNA damage response: making it safe to play with knives. *Mol Cell* 40(2):179-204.
22. Chang HHY, Pannunzio NR, Adachi N, & Lieber MR (2017) Non-homologous DNA end joining and alternative pathways to double-strand break repair. *Nat Rev Mol Cell Biol* 18(8):495-506.
23. Sullivan MR & Bernstein KA (2018) RAD-ical New Insights into RAD51 Regulation. *Genes (Basel)* 9(12).
24. Bayraktar S, *et al.* (2011) Outcome of triple-negative breast cancer in patients with or without deleterious BRCA mutations. *Breast Cancer Res Treat* 130(1):145-153.
25. Sharma P, *et al.* (2014) Germline BRCA mutation evaluation in a prospective triple-negative breast cancer registry: implications for hereditary breast and/or ovarian cancer syndrome testing. *Breast Cancer Res Treat* 145(3):707-714.
26. Antoniou A, *et al.* (2003) Average risks of breast and ovarian cancer associated with BRCA1 or BRCA2 mutations detected in case Series unselected for family history: a combined analysis of 22 studies. *Am J Hum Genet* 72(5):1117-1130.
27. Couch FJ, *et al.* (2015) Inherited mutations in 17 breast cancer susceptibility genes among a large triple-negative breast cancer cohort unselected for family history of breast cancer. *J Clin Oncol* 33(4):304-311.
28. Telli ML, *et al.* (2016) Homologous Recombination Deficiency (HRD) Score Predicts Response to Platinum-Containing Neoadjuvant Chemotherapy in Patients with Triple-Negative Breast Cancer. *Clin Cancer Res* 22(15):3764-3773.
29. Kuchenbaecker KB, *et al.* (2017) Risks of Breast, Ovarian, and Contralateral Breast Cancer for BRCA1 and BRCA2 Mutation Carriers. *JAMA* 317(23):2402-2416.
30. Byrski T, *et al.* (2010) Pathologic complete response rates in young women with BRCA1-positive breast cancers after neoadjuvant chemotherapy. *J Clin Oncol* 28(3):375-379.
31. Isakoff SJ, *et al.* (2015) TBCRC009: A Multicenter Phase II Clinical Trial of Platinum Monotherapy With Biomarker Assessment in Metastatic Triple-Negative Breast Cancer. *J Clin Oncol* 33(17):1902-1909.
32. Silver DP, *et al.* (2010) Efficacy of neoadjuvant Cisplatin in triple-negative breast cancer. *J Clin Oncol* 28(7):1145-1153.
33. Tutt A, *et al.* (2018) Carboplatin in BRCA1/2-mutated and triple-negative breast cancer BRCAness subgroups: the TNT Trial. *Nat Med* 24(5):628-637.
34. Leung DW, Cachianes G, Kuang WJ, Goeddel DV, & Ferrara N (1989) Vascular endothelial growth factor is a secreted angiogenic mitogen. *Science* 246(4935):1306-1309.
35. Senger DR, *et al.* (1983) Tumor cells secrete a vascular permeability factor that promotes accumulation of ascites fluid. *Science* 219(4587):983-985.
36. Koch S & Claesson-Welsh L (2012) Signal transduction by vascular endothelial growth factor receptors. *Cold Spring Harb Perspect Med* 2(7):a006502.

37. Chung AS & Ferrara N (2011) Developmental and pathological angiogenesis. *Annu Rev Cell Dev Biol* 27:563-584.
38. Hoeben A, *et al.* (2004) Vascular endothelial growth factor and angiogenesis. *Pharmacol Rev* 56(4):549-580.
39. Carmeliet P (2005) Angiogenesis in life, disease and medicine. *Nature* 438(7070):932-936.
40. Carmeliet P (2005) VEGF as a key mediator of angiogenesis in cancer. *Oncology* 69 Suppl 3:4-10.
41. Ferrara N (2002) VEGF and the quest for tumour angiogenesis factors. *Nat Rev Cancer* 2(10):795-803.
42. Goel HL & Mercurio AM (2013) VEGF targets the tumour cell. *Nat Rev Cancer* 13(12):871-882.
43. McMahon G (2000) VEGF receptor signaling in tumor angiogenesis. *Oncologist* 5 Suppl 1:3-10.
44. Ferrara N (2005) VEGF as a therapeutic target in cancer. *Oncology* 69 Suppl 3:11-16.
45. Yaqoob U, *et al.* (2012) Neuropilin-1 stimulates tumor growth by increasing fibronectin fibril assembly in the tumor microenvironment. *Cancer Res* 72(16):4047-4059.
46. Hansen W, *et al.* (2012) Neuropilin 1 deficiency on CD4+Foxp3+ regulatory T cells impairs mouse melanoma growth. *J Exp Med* 209(11):2001-2016.
47. Kowanetz M & Ferrara N (2006) Vascular endothelial growth factor signaling pathways: therapeutic perspective. *Clin Cancer Res* 12(17):5018-5022.
48. Karkkainen MJ & Petrova TV (2000) Vascular endothelial growth factor receptors in the regulation of angiogenesis and lymphangiogenesis. *Oncogene* 19(49):5598-5605.
49. Waldner MJ, *et al.* (2010) VEGF receptor signaling links inflammation and tumorigenesis in colitis-associated cancer. *J Exp Med* 207(13):2855-2868.
50. Hamerlik P, *et al.* (2012) Autocrine VEGF-VEGFR2-Neuropilin-1 signaling promotes glioma stem-like cell viability and tumor growth. *J Exp Med* 209(3):507-520.
51. Soker S (2001) Neuropilin in the midst of cell migration and retraction. *Int J Biochem Cell Biol* 33(4):433-437.
52. Soker S, Takashima S, Miao HQ, Neufeld G, & Klagsbrun M (1998) Neuropilin-1 is expressed by endothelial and tumor cells as an isoform-specific receptor for vascular endothelial growth factor. *Cell* 92(6):735-745.
53. Kolodkin AL, *et al.* (1997) Neuropilin is a semaphorin III receptor. *Cell* 90(4):753-762.
54. Chen H, Chedotal A, He Z, Goodman CS, & Tessier-Lavigne M (1997) Neuropilin-2, a novel member of the neuropilin family, is a high affinity receptor for the semaphorins Sema E and Sema IV but not Sema III. *Neuron* 19(3):547-559.
55. Guo HF & Vander Kooi CW (2015) Neuropilin Functions as an Essential Cell Surface Receptor. *J Biol Chem* 290(49):29120-29126.

56. Geretti E, Shimizu A, & Klagsbrun M (2008) Neuropilin structure governs VEGF and semaphorin binding and regulates angiogenesis. *Angiogenesis* 11(1):31-39.
57. Parker MW, Xu P, Li X, & Vander Kooi CW (2012) Structural basis for selective vascular endothelial growth factor-A (VEGF-A) binding to neuropilin-1. *J Biol Chem* 287(14):11082-11089.
58. Rossignol M, Gagnon ML, & Klagsbrun M (2000) Genomic organization of human neuropilin-1 and neuropilin-2 genes: identification and distribution of splice variants and soluble isoforms. *Genomics* 70(2):211-222.
59. Prahst C, *et al.* (2008) Neuropilin-1-VEGFR-2 complexing requires the PDZ-binding domain of neuropilin-1. *J Biol Chem* 283(37):25110-25114.
60. Grun D, Adhikary G, & Eckert RL (2018) NRP-1 interacts with GIPC1 and alpha6/beta4-integrins to increase YAP1/Np63alpha-dependent epidermal cancer stem cell survival. *Oncogene* 37(34):4711-4722.
61. Gemmill RM, *et al.* (2017) The neuropilin 2 isoform NRP2b uniquely supports TGFbeta-mediated progression in lung cancer. *Sci Signal* 10(462).
62. Neufeld G, Kessler O, & Herzog Y (2002) The interaction of Neuropilin-1 and Neuropilin-2 with tyrosine-kinase receptors for VEGF. *Adv Exp Med Biol* 515:81-90.
63. Elaimy AL, *et al.* (2018) VEGF-neuropilin-2 signaling promotes stem-like traits in breast cancer cells by TAZ-mediated repression of the Rac GAP beta2-chimaerin. *Sci Signal* 11(528).
64. Goel HL, *et al.* (2016) P-Rex1 Promotes Resistance to VEGF/VEGFR-Targeted Therapy in Prostate Cancer. *Cell Rep* 14(9):2193-2208.
65. Caunt M, *et al.* (2008) Blocking neuropilin-2 function inhibits tumor cell metastasis. *Cancer Cell* 13(4):331-342.
66. Goel HL, *et al.* (2012) VEGF/neuropilin-2 regulation of Bmi-1 and consequent repression of IGF-IR define a novel mechanism of aggressive prostate cancer. *Cancer Discov* 2(10):906-921.
67. Gray MJ, *et al.* (2008) Therapeutic targeting of neuropilin-2 on colorectal carcinoma cells implanted in the murine liver. *J Natl Cancer Inst* 100(2):109-120.
68. Goel HL, *et al.* (2013) GLI1 regulates a novel neuropilin-2/alpha6beta1 integrin based autocrine pathway that contributes to breast cancer initiation. *EMBO Mol Med* 5(4):488-508.
69. Jamaspishvili T, *et al.* (2018) Clinical implications of PTEN loss in prostate cancer. *Nat Rev Urol* 15(4):222-234.
70. Qin J, *et al.* (2013) COUP-TFII inhibits TGF-beta-induced growth barrier to promote prostate tumorigenesis. *Nature* 493(7431):236-240.
71. Lin FJ, *et al.* (2010) Direct transcriptional regulation of neuropilin-2 by COUP-TFII modulates multiple steps in murine lymphatic vessel development. *J Clin Invest* 120(5):1694-1707.
72. Siegle JM, *et al.* (2014) SOX2 is a cancer-specific regulator of tumour initiating potential in cutaneous squamous cell carcinoma. *Nat Commun* 5:4511.

73. Goel HL, Pursell B, Standley C, Fogarty K, & Mercurio AM (2012) Neuropilin-2 regulates alpha6beta1 integrin in the formation of focal adhesions and signaling. *J Cell Sci* 125(Pt 2):497-506.
74. Liu S, *et al.* (2006) Hedgehog signaling and Bmi-1 regulate self-renewal of normal and malignant human mammary stem cells. *Cancer Res* 66(12):6063-6071.
75. Lukacs RU, Memarzadeh S, Wu H, & Witte ON (2010) Bmi-1 is a crucial regulator of prostate stem cell self-renewal and malignant transformation. *Cell Stem Cell* 7(6):682-693.
76. Zhang L, *et al.* (2017) VEGF-A/Neuropilin 1 Pathway Confers Cancer Stemness via Activating Wnt/beta-Catenin Axis in Breast Cancer Cells. *Cell Physiol Biochem* 44(3):1251-1262.
77. Bao S, *et al.* (2006) Glioma stem cells promote radioresistance by preferential activation of the DNA damage response. *Nature* 444(7120):756-760.
78. Wang CA, Harrell JC, Iwanaga R, Jedlicka P, & Ford HL (2014) Vascular endothelial growth factor C promotes breast cancer progression via a novel antioxidant mechanism that involves regulation of superoxide dismutase 3. *Breast Cancer Res* 16(5):462.
79. Shi X, Zhang Y, Zheng J, & Pan J (2012) Reactive oxygen species in cancer stem cells. *Antioxid Redox Signal* 16(11):1215-1228.
80. Xu T, Wang W, Zhang S, Stewart RA, & Yu W (1995) Identifying tumor suppressors in genetic mosaics: the Drosophila lats gene encodes a putative protein kinase. *Development* 121(4):1053-1063.
81. Justice RW, Zilian O, Woods DF, Noll M, & Bryant PJ (1995) The Drosophila tumor suppressor gene warts encodes a homolog of human myotonic dystrophy kinase and is required for the control of cell shape and proliferation. *Genes Dev* 9(5):534-546.
82. Tapon N, *et al.* (2002) salvador Promotes both cell cycle exit and apoptosis in Drosophila and is mutated in human cancer cell lines. *Cell* 110(4):467-478.
83. Harvey KF, Pfleger CM, & Hariharan IK (2003) The Drosophila Mst ortholog, hippo, restricts growth and cell proliferation and promotes apoptosis. *Cell* 114(4):457-467.
84. Wu S, Huang J, Dong J, & Pan D (2003) hippo encodes a Ste-20 family protein kinase that restricts cell proliferation and promotes apoptosis in conjunction with salvador and warts. *Cell* 114(4):445-456.
85. Li Q, *et al.* (2014) The conserved misshapen-warts-Yorkie pathway acts in enteroblasts to regulate intestinal stem cells in Drosophila. *Dev Cell* 31(3):291-304.
86. Li S, Cho YS, Yue T, Ip YT, & Jiang J (2015) Overlapping functions of the MAP4K family kinases Hppy and Msn in Hippo signaling. *Cell Discov* 1:15038.
87. Meng Z, *et al.* (2015) MAP4K family kinases act in parallel to MST1/2 to activate LATS1/2 in the Hippo pathway. *Nat Commun* 6:8357.
88. Zheng Y, *et al.* (2015) Identification of Happyhour/MAP4K as Alternative Hpo/Mst-like Kinases in the Hippo Kinase Cascade. *Dev Cell* 34(6):642-655.
89. Plouffe SW, *et al.* (2016) Characterization of Hippo Pathway Components by Gene Inactivation. *Mol Cell* 64(5):993-1008.

90. Huang J, Wu S, Barrera J, Matthews K, & Pan D (2005) The Hippo signaling pathway coordinately regulates cell proliferation and apoptosis by inactivating Yorkie, the Drosophila Homolog of YAP. *Cell* 122(3):421-434.
91. Kanai F, *et al.* (2000) TAZ: a novel transcriptional co-activator regulated by interactions with 14-3-3 and PDZ domain proteins. *EMBO J* 19(24):6778-6791.
92. Ren F, Zhang L, & Jiang J (2010) Hippo signaling regulates Yorkie nuclear localization and activity through 14-3-3 dependent and independent mechanisms. *Dev Biol* 337(2):303-312.
93. Goulev Y, *et al.* (2008) SCALLOPED interacts with YORKIE, the nuclear effector of the hippo tumor-suppressor pathway in Drosophila. *Curr Biol* 18(6):435-441.
94. Zhao B, *et al.* (2008) TEAD mediates YAP-dependent gene induction and growth control. *Genes Dev* 22(14):1962-1971.
95. Zhang H, *et al.* (2009) TEAD transcription factors mediate the function of TAZ in cell growth and epithelial-mesenchymal transition. *J Biol Chem* 284(20):13355-13362.
96. Totaro A, Panciera T, & Piccolo S (2018) YAP/TAZ upstream signals and downstream responses. *Nat Cell Biol* 20(8):888-899.
97. Yin F, *et al.* (2013) Spatial organization of Hippo signaling at the plasma membrane mediated by the tumor suppressor Merlin/NF2. *Cell* 154(6):1342-1355.
98. Li W, *et al.* (2014) Merlin/NF2 loss-driven tumorigenesis linked to CRL4(DCAF1)-mediated inhibition of the hippo pathway kinases Lats1 and 2 in the nucleus. *Cancer Cell* 26(1):48-60.
99. Li W, *et al.* (2010) Merlin/NF2 suppresses tumorigenesis by inhibiting the E3 ubiquitin ligase CRL4(DCAF1) in the nucleus. *Cell* 140(4):477-490.
100. Dupont S, *et al.* (2011) Role of YAP/TAZ in mechanotransduction. *Nature* 474(7350):179-183.
101. Lawson CD & Ridley AJ (2018) Rho GTPase signaling complexes in cell migration and invasion. *J Cell Biol* 217(2):447-457.
102. Park HW, *et al.* (2015) Alternative Wnt Signaling Activates YAP/TAZ. *Cell* 162(4):780-794.
103. Yu FX, *et al.* (2012) Regulation of the Hippo-YAP pathway by G-protein-coupled receptor signaling. *Cell* 150(4):780-791.
104. Varelas X, *et al.* (2008) TAZ controls Smad nucleocytoplasmic shuttling and regulates human embryonic stem-cell self-renewal. *Nat Cell Biol* 10(7):837-848.
105. Varelas X, *et al.* (2010) The Crumbs complex couples cell density sensing to Hippo-dependent control of the TGF-beta-SMAD pathway. *Dev Cell* 19(6):831-844.
106. Narimatsu M, Samavarchi-Tehrani P, Varelas X, & Wrana JL (2015) Distinct polarity cues direct Taz/Yap and TGFbeta receptor localization to differentially control TGFbeta-induced Smad signaling. *Dev Cell* 32(5):652-656.
107. Neto F, *et al.* (2018) YAP and TAZ regulate adherens junction dynamics and endothelial cell distribution during vascular development. *Elife* 7.
108. Hanahan D & Weinberg RA (2011) Hallmarks of cancer: the next generation. *Cell* 144(5):646-674.

109. Wang Y, *et al.* (2018) Comprehensive Molecular Characterization of the Hippo Signaling Pathway in Cancer. *Cell Rep* 25(5):1304-1317 e1305.
110. Zanconato F, Cordenonsi M, & Piccolo S (2016) YAP/TAZ at the Roots of Cancer. *Cancer Cell* 29(6):783-803.
111. Cordenonsi M, *et al.* (2011) The Hippo transducer TAZ confers cancer stem cell-related traits on breast cancer cells. *Cell* 147(4):759-772.
112. Lei QY, *et al.* (2008) TAZ promotes cell proliferation and epithelial-mesenchymal transition and is inhibited by the hippo pathway. *Mol Cell Biol* 28(7):2426-2436.
113. Zanconato F, *et al.* (2018) Transcriptional addiction in cancer cells is mediated by YAP/TAZ through BRD4. *Nat Med* 24(10):1599-1610.
114. Zhang H, *et al.* (2015) Tumor-selective proteotoxicity of verteporfin inhibits colon cancer progression independently of YAP1. *Sci Signal* 8(397):ra98.
115. Tischer E, *et al.* (1989) Vascular endothelial growth factor: a new member of the platelet-derived growth factor gene family. *Biochem Biophys Res Commun* 165(3):1198-1206.
116. Uniewicz KA & Fernig DG (2008) Neuropilins: a versatile partner of extracellular molecules that regulate development and disease. *Front Biosci* 13:4339-4360.
117. Sulpice E, *et al.* (2008) Neuropilin-1 and neuropilin-2 act as coreceptors, potentiating proangiogenic activity. *Blood* 111(4):2036-2045.
118. Koch S, *et al.* (2014) NRP1 presented in trans to the endothelium arrests VEGFR2 endocytosis, preventing angiogenic signaling and tumor initiation. *Dev Cell* 28(6):633-646.
119. Pan Q, *et al.* (2007) Blocking neuropilin-1 function has an additive effect with anti-VEGF to inhibit tumor growth. *Cancer Cell* 11(1):53-67.
120. Baccelli I & Trumpp A (2012) The evolving concept of cancer and metastasis stem cells. *J Cell Biol* 198(3):281-293.
121. Gupta PB, Chaffer CL, & Weinberg RA (2009) Cancer stem cells: mirage or reality? *Nat Med* 15(9):1010-1012.
122. Korkaya H, Liu S, & Wicha MS (2011) Breast cancer stem cells, cytokine networks, and the tumor microenvironment. *J Clin Invest* 121(10):3804-3809.
123. Liu S, *et al.* (2011) Breast cancer stem cells are regulated by mesenchymal stem cells through cytokine networks. *Cancer Res* 71(2):614-624.
124. Goel HL, *et al.* (2016) P-Rex1 Promotes Resistance to VEGF/VEGFR-Targeted Therapy in Prostate Cancer. *Cell Rep* 14(9):2193-2208.
125. Scheel C & Weinberg RA (2012) Cancer stem cells and epithelial-mesenchymal transition: concepts and molecular links. *Semin Cancer Biol* 22(5-6):396-403.
126. Yu FX & Guan KL (2013) The Hippo pathway: regulators and regulations. *Genes Dev* 27(4):355-371.
127. Varelas X (2014) The Hippo pathway effectors TAZ and YAP in development, homeostasis and disease. *Development* 141(8):1614-1626.
128. Iliopoulos D, Hirsch HA, Wang G, & Struhl K (2011) Inducible formation of breast cancer stem cells and their dynamic equilibrium with non-stem cancer cells via IL6 secretion. *Proc Natl Acad Sci U S A* 108(4):1397-1402.

129. Chang C, *et al.* (2015) A laminin 511 matrix is regulated by TAZ and functions as the ligand for the alpha6Bbeta1 integrin to sustain breast cancer stem cells. *Genes Dev* 29(1):1-6.
130. Goel HL, *et al.* (2014) Regulated splicing of the alpha6 integrin cytoplasmic domain determines the fate of breast cancer stem cells. *Cell Rep* 7(3):747-761.
131. Liu CY, *et al.* (2010) The hippo tumor pathway promotes TAZ degradation by phosphorylating a phosphodegron and recruiting the SCF{beta}-TrCP E3 ligase. *J Biol Chem* 285(48):37159-37169.
132. Liu BP & Strittmatter SM (2001) Semaphorin-mediated axonal guidance via Rho-related G proteins. *Curr Opin Cell Biol* 13(5):619-626.
133. Riccomagno MM, *et al.* (2012) The RacGAP beta2-Chimaerin selectively mediates axonal pruning in the hippocampus. *Cell* 149(7):1594-1606.
134. Tan W, *et al.* (2008) An essential role for Rac1 in endothelial cell function and vascular development. *FASEB J* 22(6):1829-1838.
135. Fryer BH & Field J (2005) Rho, Rac, Pak and angiogenesis: old roles and newly identified responsibilities in endothelial cells. *Cancer Lett* 229(1):13-23.
136. Feng X, *et al.* (2014) Hippo-independent activation of YAP by the GNAQ uveal melanoma oncogene through a trio-regulated rho GTPase signaling circuitry. *Cancer Cell* 25(6):831-845.
137. Jang JW, *et al.* (2017) RAC-LATS1/2 signaling regulates YAP activity by switching between the YAP-binding partners TEAD4 and RUNX3. *Oncogene* 36(7):999-1011.
138. Gargini R, *et al.* (2016) WIP Drives Tumor Progression through YAP/TAZ-Dependent Autonomous Cell Growth. *Cell Rep* 17(8):1962-1977.
139. Bachelder RE, *et al.* (2001) Vascular endothelial growth factor is an autocrine survival factor for neuropilin-expressing breast carcinoma cells. *Cancer Res* 61(15):5736-5740.
140. Chang F, Lemmon CA, Park D, & Romer LH (2007) FAK potentiates Rac1 activation and localization to matrix adhesion sites: a role for betaPIX. *Mol Biol Cell* 18(1):253-264.
141. Chiu YW, *et al.* (2016) Tyrosine 397 phosphorylation is critical for FAK-promoted Rac1 activation and invasive properties in oral squamous cell carcinoma cells. *Lab Invest* 96(3):296-306.
142. Pasapera AM, *et al.* (2015) Rac1-dependent phosphorylation and focal adhesion recruitment of myosin IIA regulates migration and mechanosensing. *Curr Biol* 25(2):175-186.
143. Kim NG & Gumbiner BM (2015) Adhesion to fibronectin regulates Hippo signaling via the FAK-Src-PI3K pathway. *J Cell Biol* 210(3):503-515.
144. Hu JK, *et al.* (2017) An FAK-YAP-mTOR Signaling Axis Regulates Stem Cell-Based Tissue Renewal in Mice. *Cell Stem Cell* 21(1):91-106 e106.
145. Chan EH, *et al.* (2005) The Ste20-like kinase Mst2 activates the human large tumor suppressor kinase Lats1. *Oncogene* 24(12):2076-2086.
146. Meng Z, Moroishi T, & Guan KL (2016) Mechanisms of Hippo pathway regulation. *Genes Dev* 30(1):1-17.

147. Shaw RJ, *et al.* (2001) The Nf2 tumor suppressor, merlin, functions in Rac-dependent signaling. *Dev Cell* 1(1):63-72.
148. Xiao GH, Beeser A, Chernoff J, & Testa JR (2002) p21-activated kinase links Rac/Cdc42 signaling to merlin. *J Biol Chem* 277(2):883-886.
149. Kissil JL, Johnson KC, Eckman MS, & Jacks T (2002) Merlin phosphorylation by p21-activated kinase 2 and effects of phosphorylation on merlin localization. *J Biol Chem* 277(12):10394-10399.
150. Kumar R, Gururaj AE, & Barnes CJ (2006) p21-activated kinases in cancer. *Nat Rev Cancer* 6(6):459-471.
151. Caloca MJ, Wang H, & Kazanietz MG (2003) Characterization of the Rac-GAP (Rac-GTPase-activating protein) activity of beta2-chimaerin, a 'non-protein kinase C' phorbol ester receptor. *Biochem J* 375(Pt 2):313-321.
152. Diekmann D, *et al.* (1991) Bcr encodes a GTPase-activating protein for p21rac. *Nature* 351(6325):400-402.
153. Yang C, Liu Y, Leskow FC, Weaver VM, & Kazanietz MG (2005) Rac-GAP-dependent inhibition of breast cancer cell proliferation by {beta}2-chimerin. *J Biol Chem* 280(26):24363-24370.
154. Casado-Medrano V, *et al.* (2016) A new role of the Rac-GAP beta2-chimaerin in cell adhesion reveals opposite functions in breast cancer initiation and tumor progression. *Oncotarget* 7(19):28301-28319.
155. Menna PL, *et al.* (2003) Inhibition of aggressiveness of metastatic mouse mammary carcinoma cells by the beta2-chimaerin GAP domain. *Cancer Res* 63(9):2284-2291.
156. Kim M, Kim T, Johnson RL, & Lim DS (2015) Transcriptional co-repressor function of the hippo pathway transducers YAP and TAZ. *Cell Rep* 11(2):270-282.
157. Valencia-Sama I, *et al.* (2015) Hippo Component TAZ Functions as a Co-repressor and Negatively Regulates DeltaNp63 Transcription through TEA Domain (TEAD) Transcription Factor. *J Biol Chem* 290(27):16906-16917.
158. Wang C, *et al.* (2015) The interplay between TEAD4 and KLF5 promotes breast cancer partially through inhibiting the transcription of p27Kip1. *Oncotarget* 6(19):17685-17697.
159. Adelaide J, *et al.* (2007) Integrated profiling of basal and luminal breast cancers. *Cancer Res* 67(24):11565-11575.
160. Liu X, *et al.* (2016) Tead and AP1 Coordinate Transcription and Motility. *Cell Rep* 14(5):1169-1180.
161. Ohgushi M, Minaguchi M, & Sasai Y (2015) Rho-Signaling-Directed YAP/TAZ Activity Underlies the Long-Term Survival and Expansion of Human Embryonic Stem Cells. *Cell Stem Cell* 17(4):448-461.
162. Cerami E, *et al.* (2012) The cBio cancer genomics portal: an open platform for exploring multidimensional cancer genomics data. *Cancer Discov* 2(5):401-404.
163. Gao J, *et al.* (2013) Integrative analysis of complex cancer genomics and clinical profiles using the cBioPortal. *Sci Signal* 6(269):pl1.
164. Bhat KP, *et al.* (2011) The transcriptional coactivator TAZ regulates mesenchymal differentiation in malignant glioma. *Genes Dev* 25(24):2594-2609.

165. Yuen HF, *et al.* (2013) TAZ expression as a prognostic indicator in colorectal cancer. *PLoS One* 8(1):e54211.
166. Chang C, Yang X, Pursell B, & Mercurio AM (2013) Id2 complexes with the SNAG domain of Snai1 inhibiting Snai1-mediated repression of integrin beta4. *Mol Cell Biol* 33(19):3795-3804.
167. Bachelder RE, *et al.* (2003) Competing autocrine pathways involving alternative neuropilin-1 ligands regulate chemotaxis of carcinoma cells. *Cancer Res* 63(17):5230-5233.
168. Lai YJ, *et al.* (2017) Small G protein Rac GTPases regulate the maintenance of glioblastoma stem-like cells in vitro and in vivo. *Oncotarget* 8(11):18031-18049.
169. Man J, *et al.* (2014) Sema3C promotes the survival and tumorigenicity of glioma stem cells through Rac1 activation. *Cell Rep* 9(5):1812-1826.
170. McCauley HA, Chevrier V, Birnbaum D, & Guasch G (2017) De-repression of the RAC activator ELMO1 in cancer stem cells drives progression of TGFbeta-deficient squamous cell carcinoma from transition zones. *Elife* 6.
171. Wang X, *et al.* (2017) YAP/TAZ Orchestrate VEGF Signaling during Developmental Angiogenesis. *Dev Cell* 42(5):462-478 e467.
172. Moriarty CH, Pursell B, & Mercurio AM (2010) miR-10b targets Tiam1: implications for Rac activation and carcinoma migration. *J Biol Chem* 285(27):20541-20546.
173. Benjamini Y, Hockberg, Y. (1995) Controlling the False Discovery Rate: A Practical and Powerful Approach to Multiple Testing *Journal of the Royal Statistical Society. Series B (Methodological)* Vol. 57(1):pp. 289-300.
174. Snuderl M, *et al.* (2013) Targeting placental growth factor/neuropilin 1 pathway inhibits growth and spread of medulloblastoma. *Cell* 152(5):1065-1076.
175. Helleday T (2010) Homologous recombination in cancer development, treatment and development of drug resistance. *Carcinogenesis* 31(6):955-960.
176. Godin SK, Sullivan MR, & Bernstein KA (2016) Novel insights into RAD51 activity and regulation during homologous recombination and DNA replication. *Biochem Cell Biol* 94(5):407-418.
177. Elstrodt F, *et al.* (2006) BRCA1 mutation analysis of 41 human breast cancer cell lines reveals three new deleterious mutants. *Cancer Res* 66(1):41-45.
178. Duarte AA, *et al.* (2018) BRCA-deficient mouse mammary tumor organoids to study cancer-drug resistance. *Nat Methods* 15(2):134-140.
179. Elaimy AL & Mercurio AM (2018) Convergence of VEGF and YAP/TAZ signaling: Implications for angiogenesis and cancer biology. *Sci Signal* 11(552).
180. Pierce AJ, Johnson RD, Thompson LH, & Jasin M (1999) XRCC3 promotes homology-directed repair of DNA damage in mammalian cells. *Genes Dev* 13(20):2633-2638.
181. Enzo E, *et al.* (2015) Aerobic glycolysis tunes YAP/TAZ transcriptional activity. *EMBO J* 34(10):1349-1370.
182. Liu Y, *et al.* (2017) RAD51 Mediates Resistance of Cancer Stem Cells to PARP Inhibition in Triple-Negative Breast Cancer. *Clin Cancer Res* 23(2):514-522.

183. Raderschall E, *et al.* (2002) Elevated levels of Rad51 recombination protein in tumor cells. *Cancer Res* 62(1):219-225.
184. Hine CM, *et al.* (2014) Regulation of Rad51 promoter. *Cell Cycle* 13(13):2038-2045.
185. Hine CM, Seluanov A, & Gorbunova V (2008) Use of the Rad51 promoter for targeted anti-cancer therapy. *Proc Natl Acad Sci U S A* 105(52):20810-20815.
186. Liu X, *et al.* (2016) Tead and AP1 Coordinate Transcription and Motility. *Cell Rep* 14(5):1169-1180.
187. Zhao W, *et al.* (2017) BRCA1-BARD1 promotes RAD51-mediated homologous DNA pairing. *Nature* 550(7676):360-365.
188. Alshareeda AT, *et al.* (2016) Clinical and biological significance of RAD51 expression in breast cancer: a key DNA damage response protein. *Breast Cancer Res Treat* 159(1):41-53.
189. Peng K, Bai Y, Zhu Q, Hu B, & Xu Y (2018) Targeting VEGF-neuropilin interactions: a promising antitumor strategy. *Drug Discov Today*.
190. Rizzolio S, *et al.* (2018) Neuropilin-1 upregulation elicits adaptive resistance to oncogene-targeted therapies. *J Clin Invest* 128(9):3976-3990.
191. Dutta S, *et al.* (2016) Neuropilin-2 Regulates Endosome Maturation and EGFR Trafficking to Support Cancer Cell Pathobiology. *Cancer Res* 76(2):418-428.
192. Budke B, *et al.* (2012) RI-1: a chemical inhibitor of RAD51 that disrupts homologous recombination in human cells. *Nucleic Acids Res* 40(15):7347-7357.
193. Ou J, Wang Y, Zhu LJ (2018) trackViewer: A R/Bioconductor package for drawing elegant interactive tracks or lollipop plot to facilitate integrated analysis of multi-omics data. *R package version 1.16.0.*
194. Davis S & Meltzer PS (2007) GEOquery: a bridge between the Gene Expression Omnibus (GEO) and BioConductor. *Bioinformatics* 23(14):1846-1847.
195. Ritchie ME, *et al.* (2015) limma powers differential expression analyses for RNA-sequencing and microarray studies. *Nucleic Acids Res* 43(7):e47.
196. Benjamini Y, Hochberg, Y (1995) Controlling the false discovery rate: a practical and powerful approach to multiple testing. *Journal of the Royal Statistical Society* 57(1):289-300.
197. Goel HL & Mercurio AM (2012) Enhancing integrin function by VEGF/neuropilin signaling: implications for tumor biology. *Cell Adh Migr* 6(6):554-560.
198. Piccolo S, Dupont S, & Cordenonsi M (2014) The biology of YAP/TAZ: hippo signaling and beyond. *Physiol Rev* 94(4):1287-1312.
199. Haigh JJ (2008) Role of VEGF in organogenesis. *Organogenesis* 4(4):247-256.
200. Tiwari A, Jung JJ, Inamdar SM, Nihalani D, & Choudhury A (2013) The myosin motor Myo1c is required for VEGFR2 delivery to the cell surface and for angiogenic signaling. *Am J Physiol Heart Circ Physiol* 304(5):H687-696.
201. Kim J, *et al.* (2017) YAP/TAZ regulates sprouting angiogenesis and vascular barrier maturation. *J Clin Invest* 127(9):3441-3461.
202. Sakabe M, *et al.* (2017) YAP/TAZ-CDC42 signaling regulates vascular tip cell migration. *Proc Natl Acad Sci U S A* 114(41):10918-10923.

203. He J, *et al.* (2018) Yes-Associated Protein Promotes Angiogenesis via Signal Transducer and Activator of Transcription 3 in Endothelial Cells. *Circ Res* 122(4):591-605.
204. Azad T, *et al.* (2018) A LATS biosensor screen identifies VEGFR as a regulator of the Hippo pathway in angiogenesis. *Nat Commun* 9(1):1061.
205. Park JA & Kwon YG (2018) Hippo-YAP/TAZ signaling in angiogenesis. *BMB Rep* 51(3):157-162.
206. Bergers G & Hanahan D (2008) Modes of resistance to anti-angiogenic therapy. *Nat Rev Cancer* 8(8):592-603.
207. Lambrechts D, Lenz HJ, de Haas S, Carmeliet P, & Scherer SJ (2013) Markers of response for the antiangiogenic agent bevacizumab. *J Clin Oncol* 31(9):1219-1230.
208. Sabra H, *et al.* (2017) beta1 integrin-dependent Rac/group I PAK signaling mediates YAP activation of Yes-associated protein 1 (YAP1) via NF2/merlin. *J Biol Chem* 292(47):19179-19197.
209. Grun D, Adhikary G, & Eckert RL (2018) NRP-1 interacts with GIPC1 and alpha6/beta4-integrins to increase YAP1/Np63alpha-dependent epidermal cancer stem cell survival. *Oncogene*.
210. Parker MW, Guo HF, Li X, Linkugel AD, & Vander Kooi CW (2012) Function of members of the neuropilin family as essential pleiotropic cell surface receptors. *Biochemistry* 51(47):9437-9446.
211. Qin Y, Rodin S, Simonson OE, & Hollande F (2017) Laminins and cancer stem cells: Partners in crime? *Semin Cancer Biol* 45:3-12.
212. Plaks V, Kong N, & Werb Z (2015) The cancer stem cell niche: how essential is the niche in regulating stemness of tumor cells? *Cell Stem Cell* 16(3):225-238.
213. Rosen LS (2005) VEGF-targeted therapy: therapeutic potential and recent advances. *Oncologist* 10(6):382-391.
214. Rosen LS (2002) Clinical experience with angiogenesis signaling inhibitors: focus on vascular endothelial growth factor (VEGF) blockers. *Cancer Control* 9(2 Suppl):36-44.
215. Ivy SP, Wick JY, & Kaufman BM (2009) An overview of small-molecule inhibitors of VEGFR signaling. *Nat Rev Clin Oncol* 6(10):569-579.
216. Sosa MS, *et al.* (2010) Identification of the Rac-GEF P-Rex1 as an essential mediator of ErbB signaling in breast cancer. *Mol Cell* 40(6):877-892.
217. Morgan MA & Lawrence TS (2015) Molecular Pathways: Overcoming Radiation Resistance by Targeting DNA Damage Response Pathways. *Clin Cancer Res* 21(13):2898-2904.
218. Kil WJ, Tofilon PJ, & Camphausen K (2012) Post-radiation increase in VEGF enhances glioma cell motility in vitro. *Radiat Oncol* 7:25.
219. Hovinga KE, *et al.* (2005) Radiation-enhanced vascular endothelial growth factor (VEGF) secretion in glioblastoma multiforme cell lines--a clue to radioresistance? *J Neurooncol* 74(2):99-103.
220. Vitale I, Manic G, De Maria R, Kroemer G, & Galluzzi L (2017) DNA Damage in Stem Cells. *Mol Cell* 66(3):306-319.

221. Hynes RO (2002) Integrins: bidirectional, allosteric signaling machines. *Cell* 110(6):673-687.
222. Bridgewater RE, Norman JC, & Caswell PT (2012) Integrin trafficking at a glance. *J Cell Sci* 125(Pt 16):3695-3701.
223. Desgrosellier JS & Cheresh DA (2010) Integrins in cancer: biological implications and therapeutic opportunities. *Nat Rev Cancer* 10(1):9-22.
224. Longmate W & DiPersio CM (2017) Beyond adhesion: emerging roles for integrins in control of the tumor microenvironment. *F1000Res* 6:1612.
225. Huet-Calderwood C, *et al.* (2017) Novel ecto-tagged integrins reveal their trafficking in live cells. *Nat Commun* 8(1):570.
226. De Franceschi N, *et al.* (2016) Selective integrin endocytosis is driven by interactions between the integrin alpha-chain and AP2. *Nat Struct Mol Biol* 23(2):172-179.
227. Nader GP, Ezratty EJ, & Gundersen GG (2016) FAK, talin and PIPKIgamma regulate endocytosed integrin activation to polarize focal adhesion assembly. *Nat Cell Biol* 18(5):491-503.
228. Wang Y, *et al.* (2015) Formin-like 2 Promotes beta1-Integrin Trafficking and Invasive Motility Downstream of PKCalpha. *Dev Cell* 34(4):475-483.
229. Giancotti FG (2007) Targeting integrin beta4 for cancer and anti-angiogenic therapy. *Trends Pharmacol Sci* 28(10):506-511.
230. Mercurio AM (1995) Laminin receptors: achieving specificity through cooperation. *Trends Cell Biol* 5(11):419-423.
231. Tamura RN, *et al.* (1990) Epithelial integrin alpha 6 beta 4: complete primary structure of alpha 6 and variant forms of beta 4. *J Cell Biol* 111(4):1593-1604.
232. Borradori L & Sonnenberg A (1999) Structure and function of hemidesmosomes: more than simple adhesion complexes. *J Invest Dermatol* 112(4):411-418.
233. Green KJ & Jones JC (1996) Desmosomes and hemidesmosomes: structure and function of molecular components. *FASEB J* 10(8):871-881.
234. Lipscomb EA & Mercurio AM (2005) Mobilization and activation of a signaling competent alpha6beta4integrin underlies its contribution to carcinoma progression. *Cancer Metastasis Rev* 24(3):413-423.
235. Mercurio AM, Rabinovitz I, & Shaw LM (2001) The alpha 6 beta 4 integrin and epithelial cell migration. *Curr Opin Cell Biol* 13(5):541-545.
236. Mercurio AM & Rabinovitz I (2001) Towards a mechanistic understanding of tumor invasion--lessons from the alpha6beta 4 integrin. *Semin Cancer Biol* 11(2):129-141.
237. O'Connor KL, Nguyen BK, & Mercurio AM (2000) RhoA function in lamellae formation and migration is regulated by the alpha6beta4 integrin and cAMP metabolism. *J Cell Biol* 148(2):253-258.
238. Rabinovitz I, Toker A, & Mercurio AM (1999) Protein kinase C-dependent mobilization of the alpha6beta4 integrin from hemidesmosomes and its association with actin-rich cell protrusions drive the chemotactic migration of carcinoma cells. *J Cell Biol* 146(5):1147-1160.

239. O'Connor KL, Shaw LM, & Mercurio AM (1998) Release of cAMP gating by the alpha6beta4 integrin stimulates lamellae formation and the chemotactic migration of invasive carcinoma cells. *J Cell Biol* 143(6):1749-1760.
240. Lotz MM, *et al.* (1997) Intestinal epithelial restitution. Involvement of specific laminin isoforms and integrin laminin receptors in wound closure of a transformed model epithelium. *Am J Pathol* 150(2):747-760.
241. Rabinovitz I & Mercurio AM (1997) The integrin alpha6beta4 functions in carcinoma cell migration on laminin-1 by mediating the formation and stabilization of actin-containing motility structures. *J Cell Biol* 139(7):1873-1884.
242. Shaw LM, Rabinovitz I, Wang HH, Toker A, & Mercurio AM (1997) Activation of phosphoinositide 3-OH kinase by the alpha6beta4 integrin promotes carcinoma invasion. *Cell* 91(7):949-960.
243. Colburn ZT & Jones JCR (2018) Complexes of alpha6beta4 integrin and vimentin act as signaling hubs to regulate epithelial cell migration. *J Cell Sci* 131(14).
244. Santoro MM, Gaudino G, & Marchisio PC (2003) The MSP receptor regulates alpha6beta4 and alpha3beta1 integrins via 14-3-3 proteins in keratinocyte migration. *Dev Cell* 5(2):257-271.
245. Brinkman EK, Chen T, Amendola M, & van Steensel B (2014) Easy quantitative assessment of genome editing by sequence trace decomposition. *Nucleic Acids Res* 42(22):e168.
246. Zhang JP, *et al.* (2017) Efficient precise knockin with a double cut HDR donor after CRISPR/Cas9-mediated double-stranded DNA cleavage. *Genome Biol* 18(1):35.
247. Deugnier MA, *et al.* (2002) EGF controls the in vivo developmental potential of a mammary epithelial cell line possessing progenitor properties. *J Cell Biol* 159(3):453-463.
248. Danielson KG, Oborn CJ, Durban EM, Butel JS, & Medina D (1984) Epithelial mouse mammary cell line exhibiting normal morphogenesis in vivo and functional differentiation in vitro. *Proc Natl Acad Sci U S A* 81(12):3756-3760.
249. Lackner DH, *et al.* (2015) A generic strategy for CRISPR-Cas9-mediated gene tagging. *Nat Commun* 6:10237.
250. Merdek KD, Yang X, Taglienti CA, Shaw LM, & Mercurio AM (2007) Intrinsic signaling functions of the beta4 integrin intracellular domain. *J Biol Chem* 282(41):30322-30330.
251. Brown CW, Amante JJ, Goel HL, & Mercurio AM (2017) The alpha6beta4 integrin promotes resistance to ferroptosis. *J Cell Biol* 216(12):4287-4297.
252. Deugnier MA, *et al.* (2006) Isolation of mouse mammary epithelial progenitor cells with basal characteristics from the Comma-Dbeta cell line. *Dev Biol* 293(2):414-425.
253. Taddei I, *et al.* (2008) Beta1 integrin deletion from the basal compartment of the mammary epithelium affects stem cells. *Nat Cell Biol* 10(6):716-722.
254. Di Agostino S, *et al.* (2016) YAP enhances the pro-proliferative transcriptional activity of mutant p53 proteins. *EMBO Rep* 17(2):188-201.
255. Zanconato F, *et al.* (2015) Genome-wide association between YAP/TAZ/TEAD and AP-1 at enhancers drives oncogenic growth. *Nat Cell Biol* 17(9):1218-1227.

256. Zanconato F & Piccolo S (2016) Eradicating tumor drug resistance at its YAP-biomechanical roots. *EMBO J* 35(5):459-461.
257. Sorrentino G, *et al.* (2017) Glucocorticoid receptor signalling activates YAP in breast cancer. *Nat Commun* 8:14073.
258. Ewald AJ, Werb Z, & Egeblad M (2011) Preparation of mice for long-term intravital imaging of the mammary gland. *Cold Spring Harb Protoc* 2011(2):pdb prot5562.
259. Hoshino A, *et al.* (2015) Tumour exosome integrins determine organotropic metastasis. *Nature* 527(7578):329-335.
260. Falcioni R, Kennel SJ, Giacomini P, Zupi G, & Sacchi A (1986) Expression of tumor antigen correlated with metastatic potential of Lewis lung carcinoma and B16 melanoma clones in mice. *Cancer Res* 46(11):5772-5778.